

(NASA-TM-84245) AN EXPERIMENTAL STUDY OF
DYNAMIC STALL ON ADVANCED AIRFOIL SECTIONS.
VOLUME 1: SUMMARY OF THE EXPERIMENT (NASA)
102 p HC AC6/ME AC1 CSCL 01A

82-32314

Unclas
G3/C2 26944

An Experimental Study of Dynamic Stall on Advanced Airfoil Sections Volume 1. Summary of the Experiment

✓ W. J. McCroskey, K. W. McAlister, L. W. Carr, and
S. L. Pucci

July 1982



NASA
National Aeronautics and
Space Administration

United States Army
Aviation Research
and Development
Command



An Experimental Study of Dynamic Stall on Advanced Airfoil Sections

Volume 1. Summary of the Experiment

W. J. McCroskey

K. W. McAlister

L. W. Carr

S. L. Pucci. Aeromechanics Laboratory
AVRADCOM Research and Technology Laboratories
Ames Research Center, Moffett Field, California

NASA

National Aeronautics and
Space Administration

Ames Research Center
Moffett Field, California 94035

United States Army
Aviation Research and
Development Command
St. Louis, Missouri 63166



TABLE OF CONTENTS

	<u>Page</u>
LIST OF TABLES	v
LIST OF FIGURES	vii
SYMBOLS	ix
SUMMARY	1
1. INTRODUCTION	1
2. DESCRIPTION OF THE EXPERIMENT	2
Test Apparatus	2
Instrumentation	3
Data Analysis and Measurement Accuracy	4
Test Conditions	7
3. GUIDE TO THE DATA	8
4. RESULTS AND DISCUSSION	10
Static Data	10
Dynamic Data	12
Comments on Wind-Tunnel Effects	14
5. SUMMARY AND CONCLUSIONS	14
REFERENCES	16
TABLES	19
FIGURES	55

PRECEDING PAGE BLANK NOT FILMED

LIST OF TABLES

	<u>Page</u>
1 Harmonic Coefficients of the Oscillation Mechanism	19
2 Airfoil Coordinates: NACA 0012 and Ames A-01 Airfoils	20
3 Airfoil Coordinates: Wortmann FX-098 and Sikorsky SC-1095 Airfoils	21
4 Airfoil Coordinates: Hughes HH-02 (-5° Tab) and Vertol VR-7 (-3° Tab) Airfoils	22
5 Airfoil Coordinates: NLR-1 and NLR-7301 Airfoils	23
6 Transducer Locations on the Airfoils	24
7 Static Drag Coefficients at $M_{\infty} = 0.30$ based on Wake Surveys	25
8 Summary of the Measured Static Airfoil Characteristics at $M_{\infty} = 0.30$, including Wind Tunnel Wall Corrections	25
9 List of Test Points with Unusual Zero Drift of Pressure Transducers.	26
10 Coefficients of Linear Curve-Fit of Static Lift Data, without Wind-Tunnel Corrections	27
11 List of Data Frames	28
12 List of Static Data	44
13 Mach Number Sweep at $\alpha = 15^{\circ} + 10^{\circ} \sin \omega t$, $k = 0.10$	45
14 Frequency Sweep at $M_{\infty} = 0.29$, $\alpha = 15^{\circ} + 10^{\circ} \sin \omega t$	45
15 Frequency Sweep at $M_{\infty} = 0.30$, $\alpha = 10^{\circ} + 10^{\circ} \sin \omega t$	46
16 Frequency Sweep at $M_{\infty} = 0.30$, $\alpha = 15^{\circ} + 5^{\circ} \sin \omega t$	46
17 Frequency Sweep at $M_{\infty} = 0.30$, $\alpha = 10^{\circ} + 5^{\circ} \sin \omega t$	46
18 Stall Onset at $M_{\infty} = 0.30$, $\alpha = \alpha_0 + 10^{\circ} \sin \omega t$, $k = 0.10$	47
19 Stall Suppression at $M_{\infty} = 0.30$, $\alpha = \alpha_0 + 10^{\circ} \sin \omega t$	47
20 Stall Suppression at $M_{\infty} = 0.18$, $\alpha = \alpha_0 + 10^{\circ} \sin \omega t$	47
21 Pitch Damping Studies at $M_{\infty} = 0.30$, $\alpha = \alpha_0 + 2^{\circ} \sin \omega t$	48
22 No Separation: $M_{\infty} = 0.30$, $\alpha = 5^{\circ} + 5^{\circ} \sin \omega t$	50
23 Dynamic Boundary-Layer Trip Data	50

	<u>Page</u>
24 Miscellaneous Dynamic Data	51
25 Test Cases for Numerical Analysis (ref. 1)	54

LIST OF I JRÉS

	<u>Page</u>
1 Airfoils tested in the experiment	55
2 Model installation in the test section	56
3 Photograph of the oscillation mechanism	57
4 Sketch of the wooden model shells surrounding the steel spar	58
5 Pressure transducer and hot-wire installation: view from inside the upper-surface shell	59
6 Coordinate axes for the airfoils	59
7 Sketch of the shadowgraph system for visualizing the leading- edge region	60
8 Representative shadowgraphs before (upper) and during (lower) dynamic stall: Sikorsky SC-1095 airfoil, $M_\infty = 0.30$, $\alpha = 10^\circ + 10^\circ \sin \omega t$, $k = 0.10$	61
9 Static lift and moment data on the NACA 0012 airfoil at $M_\infty = 0.3$; shaded bands represent uncertainty limits of data corrected for wind-tunnel-wall effects	62
10 Static lift and moment data on the Wortmann FX-098 airfoil at $M_\infty = 0.11$	63
11 Static lift and moment data on the Vertol VR-7 airfoil at $M_\infty = 0.30$	64
12 Comparison of measured lift-drag polars for the NACA 0012 airfoil at $M_\infty = 0.30$, including wind-tunnel-wall corrections	65
13 Comparison of lift-curve slopes on the NACA 0012 and SC-1095 airfoils, including wind-tunnel-wall corrections	65
14 Typical data presentation from volume 2; no wall corrections	66
15 Typical data presentation from volume 3	67
16 Static characteristics of the NACA 0012 airfoil at $M_\infty = 0.30$, including wind-tunnel-wall corrections	67
17 Static characteristics of the Ames A-01 airfoil at $M_\infty = 0.30$, including wind-tunnel-wall corrections	69
18 Static characteristics of the Wortmann FX-098 airfoil at $M_\infty = 0.30$, including wind-tunnel-wall corrections	71

	<u>Page</u>
19 Static characteristics of the Sikorsky SC-1095 airfoil at $M_\infty = 0.30$, including wind-tunnel-wall corrections	73
20 Static characteristics of the Hughes HH-02 airfoil at $M_\infty = 0.30$, including wind-tunnel-wall corrections	75
21 Static characteristics of the Vertol VR-7 airfoil at $M_\infty = 0.30$, including wind-tunnel-wall corrections	77
22 Static characteristics of the NLR-1 airfoil at $M_\infty = 0.30$, including wind-tunnel-wall corrections	79
23 Static characteristics of the NLR-7301 airfoil at $M_\infty = 0.30$, including wind-tunnel-wall corrections	81
24 Comparison of maximum static lift on the NACA 0012 airfoil	83
25 Comparison of maximum static lift on the Ames A-01 airfoil	83
26 Comparison of maximum static lift on the Wortmann FX-098 airfoil	84
27 Comparison of maximum static lift on the Sikorsky SC-1095 airfoil	84
28 Comparison of maximum static lift on the Hughes HH-02 airfoil	85
29 Comparison of maximum static lift on the Vertol VR-7 airfoil	85
30 Comparison of maximum static lift on the NLR-1 airfoil	86
31 Comparison of maximum static lift on the NLR-7301 airfoil	86
32 Maximum unsteady lift on the eight airfoils: solid symbols = stall onset; open symbols = deep stall	87
33 Comparison of maximum lift on the eight airfoils at $M_\infty = 0.30$	88
34 Comparison of maximum lift on the NACA 0012 airfoil under deep-dynamic-stall conditions: $\alpha = 15^\circ + 10^\circ \sin \omega t$, $k = 0.10$	89
35 Comparison of the lift hysteresis on the NACA 0012 airfoil: $M_\infty \cong 0.1$, $\alpha = 15^\circ + 10^\circ \sin \omega t$, $k = 0.10$	89
36 Comparison of maximum airloads on the NACA 0012 airfoil at $M_\infty = 0.30$ and $\alpha_1 k^2 \cong \text{constant}$	90
37 Comparison of maximum airloads on the Sikorsky SC-1095 airfoil at $M_\infty = 0.30$ and $\alpha_1 k^2 \cong \text{constant}$	91
38 Comparison of maximum airloads on the NLR-1 airfoil at $M_\infty = 0.3$ and $\alpha_{\text{max}} = 20^\circ$	92

SYMBOLS

A	static lift coefficient at $\alpha = 0$ (see table 10)
B	static $C_{L\alpha} \sqrt{1 - M_\infty^2}$ (see table 10)
C_C	chord force coefficient
C_D	form drag coefficient derived from surface pressure measurements
C_{DW}	total drag coefficient derived from wake survey (see table 7)
C_L	lift coefficient
$C_{L\alpha}$	lift-curve slope at low α , per deg
C_M	quarter-chord pitching moment coefficient
C_{M_0}	static pitching-moment coefficient at zero angle of attack
C_N	normal force coefficient
C_p	pressure coefficient
c	airfoil chord, m
k	reduced frequency, $\omega c/2U_\infty$
L/D	ratio of lift to drag
M_∞	free-stream Mach number (also M in table 11 and fig. 14)
M_{\max}	maximum local Mach number on the airfoil
q_∞	free-stream dynamic pressure, N/m^2 (also Q, psi, in table 11)
Re	Reynolds number based on chord and free-stream conditions
r_0	leading-edge radius, m
t	time, sec
U_∞	free-stream velocity, m/sec
$X_{a.c.}$	chordwise location of the aerodynamic center of pressure at zero lift
x	chordwise coordinate, m (see fig. 6)
y	normal coordinate, m (see fig. 6)
α	angle of attack, deg
$\alpha_{C_{\min}}$	angle of attack for maximum negative chordwise force, deg

- $\alpha_{L_{max}}$ angle of attack for maximum lift, deg
 $\alpha_{M_{max}}$ angle of attack for maximum local Mach number, deg
 α_0 mean angle, deg (also A0 in computer printouts); also angle for zero lift in table 8 and figs. 9-11
 α_{ss} static-stall angle, corresponding to $C_{L_{max}}$, deg
 α_1 amplitude, deg (also A1 in table 11 and fig 14)
 α_2 magnitude of second harmonic of α , deg
 β $\sqrt{1 - M_\infty^2}$
 ζ aerodynamic pitch damping coefficient, $-\frac{1}{4\alpha_1^2} \oint C_M d\alpha$
 ϕ_2 phase of second harmonic component of α , deg
 ω circular frequency, rad/sec

AN EXPERIMENTAL STUDY OF DYNAMIC STALL ON ADVANCED AIRFOIL SECTIONS

VOLUME 1. SUMMARY OF THE EXPERIMENT

W. J. McCroskey, K. W. McAlister, L. W. Carr, and S. L. Pucci

U.S. Army Aeromechanics Laboratory (AVRADCOM), Ames Research Center

SUMMARY

The static and dynamic characteristics of seven helicopter sections and a fixed-wing supercritical airfoil were investigated over a wide range of nominally two-dimensional flow conditions, at Mach numbers up to 0.30 and Reynolds numbers up to 4×10^6 . Details of the experiment, estimates of measurement accuracy, and test conditions are described in this volume (the first of three volumes). Representative results are also presented and comparisons are made with data from other sources. The complete results for pressure distributions, forces, pitching moments, and boundary-layer separation and reattachment characteristics are available in graphical form in volumes 2 and 3.

The results of the experiment show important differences between airfoils, which would otherwise tend to be masked by differences in wind tunnels, particularly in steady cases. All of the airfoils tested provide significant advantages over the conventional NACA 0012 profile. In general, however, the parameters of the unsteady motion appear to be more important than airfoil shape in determining the dynamic-stall airloads.

1. INTRODUCTION

Retreating-blade stall limits the high-speed performance of most modern helicopters. In the past decade, numerous new airfoils have been designed in attempts to improve the stall characteristics of rotors without compromising the advancing-blade performance. Only a few of these have been tested under unsteady conditions, and some have not been tested at all. Furthermore, there is almost no overlap between the existing data sets with regard to the important parameters of oscillatory motion.

The motivation of the present experimental investigation was the obvious need for a standard data base for a series of modern rotor-blade sections. The primary objective was to measure the unsteady airloads, over an extensive matrix of test conditions, on the eight profiles shown in figure 1. Other investigations were also overlapped as much as possible. The NACA 0012 served primarily as a standard reference section; the six modern helicopter sections were chosen as representative of contemporary designs from several different companies and research organizations. A modern fixed-wing supercritical profile was also included to extend the range of leading-edge geometries and to provide a basis for comparison with oscillating-airfoil results obtained in other wind tunnels.

Secondary objectives were to investigate the type of stall and boundary-layer separation characteristics for each profile, to provide guidelines for estimating the dynamic-stall characteristics of new airfoils in the future, to supplement the conventional lift and pitching-moment measurements with unsteady drag data and

stall-flutter boundaries, and to determine the effects of leading-edge roughness that is comparable to the erosion of blades in service or in incipient icing conditions.

Dynamic stall depends on a large number of parameters. Consequently, a very large number of unsteady test points (more than 600) plus 44 sets of static data were required to fulfill the objectives of this investigation. As a result, the complete report consists of three volumes. The present volume summarizes the experiment and some of the principal results, including comparisons with data from other sources. It also contains a comprehensive index of the individual unsteady data points. Volume 2 (Pressure and Force Data) contains the pressure, force, and moment data in graphical form. These data are also available upon request on digital computer tapes, one tape for each airfoil, as explained in volume 2. In addition, there is a single tape containing only the 10 test cases that were discussed in reference 1 for the NACA 0012, Vertol VR-7, and NLR-7301 airfoils. Boundary-layer transition, flow reversal, and reattachment results appear in volume 3 (Hot-Wire and Hot-Film Measurements).

This report is primarily intended to assist the users of the data; therefore, the results are not discussed at length. The principal results have been published in references 1 and 2.

2. DESCRIPTION OF THE EXPERIMENT

Test Apparatus

The experiment was performed in the 2- by 3-m atmospheric-pressure, solid-wall Wind Tunnel at the U.S. Army Aeromechanics Laboratory. The tests were conducted in essentially the same manner as those in a previous experiment (refs. 3,4), except that the free-stream Mach number was extended to 0.3, the model chord c was reduced to 0.61 m (except for the Hughes HH-02 airfoil, $c = 0.69$ m), the frequency of oscillation was extended to 11 Hz, and the data processing was refined considerably. The models spanned the 2.13-m vertical dimension of the wind tunnel, as indicated in figure 2, and were oscillated sinusoidally in pitch about the quarter chord. A gap of approximately 2 mm existed between the ends of the model and the wind-tunnel walls.

The drive mechanism used (fig. 3) was the same one described in references 3 and 4, with some notable improvements. In some cases, the connecting push rod was fitted with a remotely controlled jackscrew mechanism that allowed the mean angle, α_0 , to be varied continuously while the tunnel was operating. Discrete amplitudes of oscillation of 2°, 5°, 6°, 8°, 10°, or 14° could be set between runs. The motion of the airfoils was given by $\alpha \approx \alpha_0 + \alpha_1 \sin \omega t$, with maximum higher harmonic distortion approximately 2% of α_1 . Table 1 gives the harmonic content of the mechanism for various values of α_0 and α_1 . The frequency of oscillation could be varied between approximately 0.02 and 12 Hz.

The models of the eight airfoils (fig. 1) consisted of interchangeable shells constructed of wood and fiberglass. These shells surrounded a stainless steel spar that contained the instrumentation and wiring, as indicated schematically in figures 2 and 4. The shells contained special fittings for the pressure transducers and hot-wire or hot-film sensors (fig. 5) that facilitated model changes without disconnecting the instrumentation.

Each set of shells was precision-machined, while mounted on the spar, to a design accuracy of ± 0.1 mm. However, measurements after the test revealed that the rms standard deviation of the coordinates from the design values was about 0.4 mm, or 0.06% of chord, and that the maximum error was about 0.8 mm. The nominal design coordinates of the airfoils are given in tables 2-5, referred to the standard coordinate system sketched in figure 6. The coordinates were taken originally from references 5-9 and from Amer (K. Amer, private communication, 1977).

A limited amount of static and dynamic data were obtained on each airfoil at $M_\infty = 0.185$ and 0.29 with a boundary-layer trip, consisting of a 3-mm-wide band of 0.10-mm-diam glass spheres glued to the leading edge. The purpose of the trip was to eliminate the laminar separation bubble that would normally form near the leading edge as the stall angle was approached. It also approximately simulated surface abrasion on helicopter blades operating under severe field conditions, as well as roughness caused by incipient icing conditions.

Instrumentation

The primary data were obtained from 26 Kulite differential pressure transducers, types YCQH-250-1 and YCQL-093-15. Those of the latter type were used in the leading- and trailing-edge regions, because of their smaller size. The locations of the transducers for each airfoil are given in table 6. The back side of each transducer was referenced to the total pressure of the wind tunnel; total pressure was measured about 1.5 m upstream of the model. The measuring side of the transducers mated with the fittings shown in figure 5, which had 0.79-mm-diam orifices. The transducers thus installed had flat amplitude versus frequency responses of 250 Hz or better and typical cavity resonance frequencies of about 850 Hz.

Special on-line analog computers that calculated and displayed the instantaneous normal force, pitching moment, pitch damping, and pressure distributions proved to be extremely valuable in assessing the dynamic-stall behavior, as well as the performance of the instrumentation, while the tests were in progress. These devices also enabled the unsteady parameters to be adjusted until some desired result was obtained, such as the maximum lift condition in the absence of moment stall or neutral aerodynamic damping in pitch.

Boundary-layer transition, flow reversal, separation, and reattachment were studied with a variety of surface hot films and hot-wire sensors (single-, double-, and triple-element probes), using the techniques described in references 4, 10, and 11. Six sensors were used on the upper surface of each airfoil, at the locations given in table 6. In addition, a hot-wire probe protruding just outside the boundary layer was mounted near the leading edge of the NLR-1 profile to aid in diagnosing the local supersonic zone that was frequently inferred at high incidence.

The leading-edge region was also examined with a shadowgraph flow visualization system (fig. 7). The high-intensity strobe light was fired at selected phase angles during the oscillation, and the pattern that developed on the Scotchlite high-gain reflective sheeting on the floor of the tunnel was photographed by the pulse camera above the test section. A representative photograph is shown in figure 8.

Finally, a traversing pitot-static probe was used to survey the wake behind each airfoil under steady-flow conditions. The steady drag of the airfoils at $M_\infty = 0.30$ was derived from these measurements; these drag coefficients are listed in table 7.

Data Analysis and Measurement Accuracy

For quantitative purposes, the pressure transducer and hot-wire signals were amplified and recorded on a 32-channel analog tape recorder with 2500-Hz flat frequency response. In addition, the average free-stream dynamic pressure, the instantaneous angle of attack of the model, and 1/cycle and 200/cycle timing indicators were recorded simultaneously. Calibrations of the pressure transducers were recorded at the beginning and end of each analog tape. The unsteady data tapes were digitized and ensemble-averaged off line. At least 50 cycles of data were normally sampled 200 times per cycle; however, for the NACA-0012 airfoil at very low frequencies, that is, $k < 0.002$, only about 10 cycles were recorded. Reference and calibration signals and the steady pressure data were acquired with the same system and were digitally sampled 100 times over a 5-sec interval. The averaged pressure data were then processed and integrated numerically by trapezoidal rule to determine the unsteady lift, moment, and pressure drag.

End-to-end checks of the data acquisition and processing system indicated that the pressure signals were reproduced to within an rms error of approximately 70 N/m^2 (0.01 psi), and that the transducer calibrations were reliable to better than $\pm 150 \text{ N/m}^2$ (0.02 psi) or $\pm 3\%$ of the reading, whichever was greater, over the range of tunnel speeds and temperatures. The model temperature, measured inside the shells, was closely monitored and not allowed to vary more than 3°C between records of no-flow pressure readings. Transducer zero drift was normally controlled to within the greater value of either $\pm 150 \text{ N/m}^2$ (0.02 psi) or $\pm 5\%$ of free-stream dynamic pressure. However, some exceptions are noted later in this section.

The hot-wire and hot-film signals were recorded as consecutive, separate data frames, and individual cycles of the analog records were examined to determine the boundary-layer characteristics, as discussed in references 4, 10, and 11. For these data, the results from three to eight cycles were averaged to obtain the relative times within the cycle, ωt , at which the various boundary-layer events occurred.

The instantaneous angle of attack was measured with a potentiometer attached to the tubular portion of the model spar (fig. 3). The angle-of-attack signal was calibrated for each data point based on the value of α_1 , which was set by the oscillation linkage, and physical measurements of α_{max} and α_{min} that were obtained from the trailing-edge position relative to the centerline of the tunnel with the wind off. The maximum absolute error in α was estimated to be $\pm 0.2^\circ$, with a relative uncertainty of $\pm 0.05^\circ$ over the cycle. The maximum torsional deflection of the model at the centerline was calculated to be $\pm 0.3^\circ$. Table 1 gives the amplitude and phase of the second harmonic component of α for various nominal values of α_1 . The frequency of the oscillation was maintained and measured to an estimated accuracy of $\pm 0.03 \text{ Hz}$.

The tunnel dynamic pressure was measured with a conventional pitot-static probe mounted approximately 1.5 m upstream of the model and connected to a pressure transducer and amplifier system with a net accuracy of approximately $\pm 14 \text{ N/m}^2$ (0.002 psi) under steady conditions. The measured values ranged from 90 N/m^2 (0.013 psi) at $M_\infty = 0.04$ to 6200 N/m^2 (0.90 psi) at $M_\infty = 0.3$. The output of this transducer was recorded by hand and on the 32-channel analog tape recorder. An average of these two values, which rarely differed by more than 2%, was used to compute q_∞ , except in a few cases in the early stages of the test program in which the tape-recorded value was obviously in error and was therefore ignored. The 25-mm-thick ground plane shown in figure 2 caused a 1% reduction in tunnel cross-sectional area between the pitot-static tube and the model; this was ignored except as noted in connection with the steady lift results presented in section 4 under the heading Static Data.

A detailed examination of the digitized data revealed that the 200/cycle sampling of the analog signals was not always synchronized perfectly with the 200/cycle timing indicators. That is, the effective time base of the digitized data was in error, the cumulative effect of which was either to leave a small gap in the data at the end of the cycle or to overlap the 200th sample of a given cycle with the first sample of the next cycle. Consequently, a corrected time base for the digital data arrays was obtained by least-squares curve-fitting a first- and second-harmonic sine wave to the angle-of-attack signal, α . All of the pressure data were then linearly interpolated onto the new time base at 200 even intervals per cycle and stored in new arrays, with the first data point in each array corresponding to $\omega t = 0$. The end result is that the final data appear at the desired times, but suffer an effective "smearing" that would be, at worst, equivalent to sampling at a rate of 100 points per cycle instead of 200 per cycle.

Experimental uncertainty of the airloads- For the purposes of comparing the static and dynamic-stall characteristics of the eight airfoil sections, the absolute accuracy of the measurements and the consequences of wind-tunnel blockage, circulation interference, and sidewall boundary-layer interference are less important than the random experimental errors outlined above. However, an attempt was made to assess all of these, as described below.

The total measurement uncertainty in the pressure, force, and moment coefficients depends on the operating conditions. For example, the probable error in C_p based on the instrumentation characteristics quoted above varies from less than ± 0.07 at $M_\infty = 0.3$ and $\alpha = 0$ to about ± 0.4 near the leading edge at $M_\infty = 0.11$ and α approaching the stall angle. For most of the static data at $M_\infty = 0.3$, the measurement uncertainty is estimated at ± 0.03 for C_{Lmax} , ± 0.005 for C_M , and ± 0.0005 for C_D derived from the wake measurements. However, the uncertainty in the SC-1095 lift and moment data is thought to be at least twice as large, because of some unresolved difficulties with the pressure measurements. These values increase with decreasing Mach number, rising by a factor of about 5 in the extreme case $M_\infty = 0.035$, where the pressure signals were very small.

Some representative examples of static C_L and C_M versus α are given in figures 9-11, and the primary characteristics of each airfoil at $M_\infty = 0.30$ are presented in table 8. The symbols in the figures indicate the individual uncorrected data points, as presented in volume 2 of this report; the shaded bands denote the estimated bounds of the airfoil characteristics. The bounds of the airfoil characteristic include static wind-tunnel-wall corrections according to Allen and Vincenti (ref. 12) and a 1% correction due to the reduction in test-section area at the model caused by the steel plate on the floor of the tunnel (fig. 2). (This wall correction method is only valid below stall, where the corrections are about 1% for α and 1.5% for C_L .) These boundaries were derived based on the measurement uncertainties described above, on data that were obtained with the on-line analog computers, and on the dynamic data obtained at $k \leq 0.01$. It should be noted that the scatter in the data and the uncertainty bounds increase considerably for conditions above the stall angle. The last line in table 8 indicates the experimental uncertainties for the various quantities listed. The static data are discussed further in section 4.

A novel feature of the present experiment was the determination of unsteady pressure drag, $C_D = C_C \cos \alpha + C_N \sin \alpha$, where C_C and C_N are the chordwise and normal force coefficients derived from the upper and lower surface-pressure distributions. The two terms in this expression for C_D are approximately equal and opposite at high angles of attack below stall, so that the probable percentage errors of

C_D are much greater than for C_C , C_N , C_L , or C_M . Figure 12 shows a typical static lift-drag polar based on pressure measurements and on the more accurate wake survey of the total drag (table 7). The measured pressure drag, which neglects the contribution due to skin friction, is less than the total drag at low lift coefficients, but it incorrectly exceeds the wake measurements by as much as 0.02 near the stall angle, that is, by as much as 100%. (It may be noted that Woodward (ref. 13) reported similar, unexplained discrepancies between measured pressure drag and C_D based on wake surveys.) However, the percentage errors are much less in the stall regime, where the magnitude of C_C decreases considerably and the maximum drag coefficient becomes of the order of $C_L \tan \alpha$ (i.e., of the order of unity) for the deep-dynamic-stall cases studied.

The measurement uncertainty of the unsteady data is probably comparable to that of the static data, but fewer independent checks were available to assess the random experimental errors and the wind-tunnel interference, especially in the post-stall regime. Fromme and Golberg (ref. 14) have indicated that unsteady wall corrections can be greater than the corresponding static corrections, but it is not clear to what extent their potential flow analysis can be applied to the present measurements. Likewise, it is not possible to estimate reliably the post-stall tunnel sidewall effects nor how these vary from one airfoil to another, but tuft flow visualization and experience suggested that these problems became less important as the frequency of oscillation is increased. It is the authors' judgment that for $M_\infty \geq 0.2$, the unsteady data in the deep-dynamic-stall regime should be in error by no more than ± 0.2 for C_L , ± 0.05 for C_M , and ± 0.10 for C_D , except as noted in the next section. The results are thought to be about twice this accurate below stall and in light stall, whereas the accuracy was seriously degraded for $M_\infty < 0.1$ because of the small values of the pressure signals.

Special cases of questionable accuracy- Despite efforts to monitor the performance of the pressure instrumentation during the test and to control and minimize the measurement uncertainties, various problems sometimes arose that only became evident during the post-test reduction and analysis of the data. In most cases, it was possible to correct these problems on an individual basis, using redundant information or by interpolating in time or space between neighboring values, without significantly compromising the accuracy of the results. In other instances, the measurements appeared to be qualitatively correct, but the experimental uncertainty was likely to have been outside the normal bounds discussed in the previous section. These cases are identified below by data-point or "frame" number.

Frame 10202 for the NACA 0012 airfoil had an unusually large number of random irregularities, a total of 44 in the 5,200 pressure data samples. These were eliminated by linearly interpolating between data at preceding and succeeding time increments. Because some of these irregularities occurred during rapid fluctuations of the flow, the time-histories of part of the pressure data for this particular frame may have been degraded. However, the effect on the integrated force and moment coefficients was probably small.

Table 9 lists the frames for which the "zero" drift of one or more of the transducers appeared to have exceeded by a significant amount the nominal values quoted in the previous section. Also included are the low Mach-number cases for which the no-flow pressure readings taken before and after recording data varied by more than 50% of free-stream dynamic pressure, even though this drift amounted to less than the nominal measurement uncertainty of 150 N/m^2 (0.02 psi). It should be mentioned that in all cases the differences between these pretest and post-test zeros were linearly interpolated with respect to elapsed time to obtain effective zeros for the individual

data frames. In principle, this should have reduced the effects of the transducer drift; however, the actual improvement in the measurement accuracy because of this technique remains unknown.

For the Hughes HH-02 airfoil, the responses of pressure transducers No. 1 (leading edge) and No. 25 ($x/c = 0.0081$, lower surface) were rather sluggish, possibly because the orifices were partially clogged. Therefore, the unsteady data from these two transducers are suspect. In calculating the force and moment data for this airfoil, transducer No. 25 was ignored and the pressure integrals

$$C_N = -\oint C_p dx/c \quad \text{etc.}$$

were replaced by

$$C_N = -2 \oint C_p \xi d\xi \quad \text{etc.}$$

where $\xi = \sqrt{x/c}$, thereby eliminating the influence of transducer No. 1, since $C_{p_1} \sqrt{x_1} = 0$. Another problem with the HH-02 force and moment data is that the trailing-edge transducers were at $x/c = 0.925$ instead of 0.98, so that the error in extrapolating to $x/c = 1.0$ is greater for this airfoil. The net effect of these modifications is difficult to assess, but it probably increased the experimental uncertainties for the lift, pressure drag, and pitching moment data by no more than 50%.

The NLR-7301 airfoil had a large amount of concave curvature on the lower surface downstream of $x/c = 0.5$, which produced larger pressure gradients there than existed on the other airfoils. Therefore, the relatively sparse distribution of pressure transducers in that region may have led to larger errors in determining the forces and moments than the nominal values quoted in the preceding section.

The reduced data for the Sikorsky SC-1095 airfoil under static conditions and at low frequencies consistently exhibited values of maximum lift coefficient and lift-curve slope that appeared to be about 5% too large, based on comparisons with the other airfoils and with the results obtained from the special on-line analog computer described above under Instrumentation. In particular, the comparison with the present NACA 0012 data (fig. 13) contrasts significantly with the steady results of Noonam and Bingham (ref. 15) and Jepson (ref. 16), who found C_{L_α} to be approximately the same for both airfoils. A detailed examination of the present data and the transducer calibrations revealed somewhat erratic performance in a few cases, but no systematic behavior emerged that could explain the apparent problem. Therefore, the conclusion is that the SC-1095 results should be viewed with caution, even though they appear to be qualitatively correct.

Test Conditions

The primary reference conditions for the initial comparisons of the various airfoils were static and deep-dynamic stall at $M_\infty = 0.3$, with the nominal unsteady motion given by $\alpha = 10^\circ + 10^\circ \sin \omega t$ and $k = \omega c / 2U_\infty = 0.10$. Limited but systematic variations in Mach number and the unsteady parameters were explored for all airfoils as indicated below and in section 3, where the specific test points are indexed and cross-referenced.

Static data- Pressure measurements were recorded at discrete values of α between -5° and 20° for $M_\infty = 0.11, 0.185, 0.25,$ and 0.30 for all airfoils except the NACA 0012. In the latter case, static data were recorded only at $M_\infty = 0.30$; quasi-steady data were obtained for a continuous range of $\alpha = \alpha_0 + 10^\circ \sin \omega t$ for $k \approx 0.001$ for nine values of M_∞ between 0.035 and 0.30 . A number of the static conditions were repeated with a boundary-layer trip at the leading edge. Wake surveys for static drag were obtained at $M_\infty = 0.3$ for α between -5° and the static stall angle.

Unsteady data- The parameters that were varied under dynamic-stall conditions were Mach number, reduced frequency, mean angle, and amplitude of the oscillation. The effect of Mach number was studied between $M_\infty = 0.035$ and 0.30 , primarily in the deep-stall regime for $\alpha = 15^\circ + 10^\circ \sin \omega t$ and $k = 0.10$. In these cases, the Reynolds number also varied, proportional to Mach number, according to the relation $Re \approx 14 \times 10^6 M_\infty$.

The principal ranges of reduced frequency, mean angle, and amplitude were $0.01 \leq k \leq 0.20$, $\alpha_0 = 10^\circ$ and 15° , and $\alpha_1 = 2^\circ, 5^\circ,$ and 10° , respectively; the effects of these parameters were studied primarily at $M_\infty = 0.30$. Additional variations in k and α_0 were effected to achieve specific dynamic effects, such as no stall, stall onset, stall suppression because of unsteady effects, and neutral aerodynamic damping in pitch.

Finally, additional test points were selected that duplicated some of the conditions of references 3 and 17-19 as closely as possible. A complete list of the unsteady test conditions and descriptions of the parametric variations are given in the following section.

3. GUIDE TO THE DATA

A very large data base was generated in this investigation. As mentioned in the Introduction, summary graphs of the pressure, force, and moment coefficients and selected results from the boundary-layer studies are contained in separate volumes. The airloads data are also stored on digital computer tapes, one for each airfoil, as explained in volume 2. This section describes briefly the data presentations to be found in the subsequent volumes and indicates by test point, or "frame number," the various types of data that are available.

Figure 14 illustrates the format of volume 2 for the unsteady pressure, force, and moment coefficient data, that is, $C_L, C_M,$ and C_D versus α and ωt , and the upper-surface pressure distributions throughout the cycle. Additional information is listed at the top of the graphs. Following the airfoil name is the identification number for each test point. As explained in volume 2, these frame numbers comprise data at a single angle of attack for the steady data, and data at 200 evenly spaced time intervals throughout the cycle for the unsteady cases. The quantities A_0 and A_1 are the mean value and the first-harmonic amplitude, respectively, of the instantaneous angle of attack, α ; M_{\max} is the estimated maximum value of the local Mach number at any time in the cycle, calculated from the classical gas-dynamic equations for steady isentropic flow and the measured pressure coefficient, $-C_{p_{\min}}$ (cf. ref. 2); $\alpha_{l_{\max}}, \alpha_{C_{\min}},$ and $\alpha_{M_{\max}}$ are the angles of attack corresponding to maximum lift, minimum chord force (cf. ref. 3), and M_{\max} , respectively; and ζ is

the aerodynamic damping in pitch. The asterisk on the ordinate of the pressure-coefficient graph represents sonic conditions.

The dotted line in the C_L vs α curve in figure 14 is an approximation to the quasi-static lift behavior for this flow condition, according to the relation

$$C_L = A + \frac{B\alpha}{\sqrt{1 - M_\infty^2}}$$

where α is in degrees and A and B were obtained from the relevant steady and very low-frequency data, that is, for $k \leq 0.01$. The values of A and B are given in table 10. Finally, it should be mentioned that in contrast to the data in table 8 and the static results presented in section 4 under the heading Static Data, wind-tunnel wall corrections have not been applied to A and B, to the data in volume 2, nor to the numerical data tapes.

Figure 15 shows two representative examples of the boundary-layer "flow reversal" information contained in volume 3. The abscissa in the figures show the position on the airfoil where the surface instrumentation first indicated a breakdown of the attached boundary-layer flow at the beginning of dynamic stall, as explained and discussed in volume 3 and in references 4, 10, and 11. This event either signifies or is closely associated with the separation that accompanies the beginning stages of dynamic stall. The ordinate indicates the nondimensional time in the cycle, ωt , at which this event occurred.

Tables 11-24 provide a comprehensive summary and index of the entire experimental program. Table 11 lists the frame numbers of all the pressure data, in the sequence in which they appear on the data tapes. The airfoil and pertinent test conditions are also listed, and the conditions for which boundary-layer data were recorded are indicated in the last column. The letter "Y" in the "TRIP" column indicates the use of the boundary-layer trip; "N" denotes the standard smooth condition. The notations "ST" and "US" denote steady and unsteady data, respectively, and the frequency of oscillation in Hertz is given in the column labeled "FREQ."

Table 12 is an index of the steady-data sets, arranged by airfoil and Mach number. The use of a boundary-layer trip is indicated by the letter "T." The notation "Quasi-steady" indicates the data that were acquired on the NACA 0012 airfoil as unsteady data, but at very low frequency, $k \leq 0.002$.

A cross-reference index that groups the unsteady data by types for each of the eight airfoils is given in tables 13-24. There are some duplicate entries in these tables, in order to facilitate the identification of data sets with variations in the individual parameters of the unsteady motion. There are also blank entries, since not all conditions were recorded for all airfoils. The principal types of unsteady conditions are outlined below.

Variations in Mach number- Table 13 lists the test points concerned with the effect of Mach number on deep dynamic stall, for $\alpha = 15^\circ + 10^\circ \sin \omega t$ and $k = 0.10$. Although the NLR-7301 airfoil was only tested at three values of M_∞ with $\alpha_0 = 15^\circ$, it was also tested with $\alpha_0 = 10^\circ$ at $M_\infty = 0.11, 0.18, 0.22,$ and 0.30 ; these frames are given in table 24. Stall-suppression conditions, tables 19 and 20, and the effects of leading-edge trips, table 23, were studied at $M_\infty = 0.18$ and 0.30 for various values of α_0 and k . As stated in section 2 under Test Conditions, the variation of Reynolds number with Mach number was $Re = 14 \times 10^6 M_\infty$.

Reduced frequency sweeps- The test points concerned with the effect of frequency on dynamic stall are given in tables 14-17. These data cover the range $0.01 \leq k \leq 0.20$ at $M_\infty = 0.3$, with mean angles of 10° and 15° and amplitudes of 5° and 10° . In addition, the NACA 0012 airfoil was tested over an extensive range of other values of α_0 (table 24).

Stall onset- This condition, defined in references 1 and 2 as obtaining the maximum possible lift without moment stall occurring at any time throughout the cycle of oscillation, was studied at $M_\infty = 0.30$, $k = 0.10$, $\alpha_1 = 10^\circ$, and variable mean angle, as indicated in table 18.

Stall suppression caused by unsteady effects- With α_1 fixed at 10° , α_0 was varied so that α_{\max} was slightly greater than the static-stall angle. Data were then recorded (tables 19 and 20) at various reduced frequencies to study whether stall would diminish or increase with increasing k .

Pitch damping boundaries- Stall conditions relevant to small-amplitude flutter boundaries are listed in table 21, at $\alpha_1 = 2^\circ$ and $M_\infty = 0.30$. Mean angle and reduced frequency were varied to obtain approximate boundaries of neutral aerodynamic damping in pitch and to obtain the maximum negative value of pitch damping, $-\zeta_{\min}$. However, no data of this type were recorded for the NACA 0012 airfoil.

No separation- A limited number of test points were recorded at $M_\infty = 0.30$ and $\alpha = 5^\circ + 5^\circ \sin \omega t$, as indicated in table 22. Some additional conditions for the NLR-1 and NLR-7301 profiles without separation are given in table 24.

Boundary-layer trip- Data with the leading-edge trip were obtained statically for α between 0° and 20° and dynamically for $\alpha = 15^\circ + 10^\circ \sin \omega t$ at two values of Mach number, 0.18 and 0.30. The values of k for the dynamic data are given in table 23; the static data with trip are so indicated in table 12. An exception was the NLR-7301 section at $M_\infty = 0.30$, for which $\alpha = 10^\circ + 5^\circ \sin \omega t$ (table 24). In addition, the NLR-1 section with trip was studied with $\alpha_0 = 2.5^\circ$ (table 24).

Miscellaneous- These test points are included in table 24. In addition to the cases mentioned above, the unsteady test conditions of references 3 and 17 for the NACA 0012, of reference 18 for the Sikorsky SC-1095, and of reference 19 for the NLR-1 airfoil were reproduced insofar as possible. Also, for the Vertol VR-7 airfoil, k was varied from 0.01 to 0.25 at $M_\infty = 0.18$ with $\alpha_0 = 10^\circ$ and 15° and $\alpha_1 = 10^\circ$. Finally, dynamic stall on the NLR-1 profile at negative incidence was studied at $M_\infty = 0.30$ for $\alpha = -2^\circ + 10^\circ \sin \omega t$ and $0.01 \leq k \leq 0.10$.

Selected test cases- Finally, table 25 lists the unsteady data that were proposed in reference 1 as specific test cases for evaluating unsteady viscous flow theories and computational methods. These data were obtained on the NACA 0012, Vertol VR-7, and NLR-7301 airfoils. They include conditions of no-stall, stall-onset, light-stall, and deep-dynamic-stall, all at $M_\infty = 0.3$.

4. RESULTS AND DISCUSSION

Static Data

The measurements performed under steady or quasi-static flow conditions provide a frame of reference for the dynamic-stall results and a basis for comparison with

data from other wind tunnels. Some of the highlights of the static data are presented below, with particular reference to the force and moment coefficients at $M_\infty = 0.3$. With the exception of the drag data listed in table 7, wind-tunnel-wall corrections have been applied to all of the static results presented in this section, using the formulae of reference 12.

As noted earlier, table 8 gives a summary of the primary static characteristics of each airfoil at $M_\infty = 0.30$, and figures 16-23 show the basic variations of lift, pitching moment, and drag coefficients for the eight sections. The dashed lines in the "a" parts of figures 17-23 represent curve-fits of the lift data in the linear $C_L - \alpha$ regime. The drag data derived from the wake surveys are listed in table 7. In the following discussions, some comparisons are made for each airfoil between the present measurements and data obtained elsewhere.

NACA 0012 airfoil- This profile has been tested by many investigators, with a wide range of results. Figure 24 shows the variation in $C_{L_{max}}$ with Mach number, including results reported or summarized in references 3, 5, 15-17, and 20-24 over a wide range of Reynolds numbers. The present values of $C_{L_{max}}$ increase with increasing Mach number for $M_\infty < 0.22$, probably because of the effects of increasing Reynolds number, whereas compressibility effects are thought to be responsible for the decrease in $C_{L_{max}}$ for $M_\infty > 0.22$. The boundary-layer trip was found to be relatively unimportant for this airfoil at the Mach and Reynolds numbers of the test.

The present $C_{L_{max}}$ data tend to lie near the upper range of the values from other sources. The same is true for the lift-curve slopes in the linear regime, C_{L_α} , which is not shown.

Ames A-01 airfoil- Figure 25 compares the data from the present test with measurements made in a transonic wind tunnel at somewhat lower Reynolds numbers (ref. 6) for the A-01 airfoil. Although the lift-curve slopes for $C_L < 1.0$ were not significantly different in the two tests, the airfoil stalled at lower angles of attack in the transonic tunnel. Consequently, lower values of maximum lift coefficient were measured and reported in reference 6 at $M_\infty = 0.2$ and 0.3, which was near the lower operating limit of that facility.

Wortmann FX-098 airfoil- Maximum-lift data from several investigations (refs. 8, 24-26) are compared with the present data in figure 26 for the FX-098 airfoil. All of the data agree reasonably well over the Mach-number range of the present test. However, there are marked differences at higher Mach numbers.

Sikorsky SC-1095 airfoil- Steady results for this section are shown in figure 27, where the comparison is generally unfavorable. The suspicious nature of the present lift data was mentioned earlier in section 2 under Data Analysis and Measurement Accuracy; here the open circles indicate the present data analyzed in the normal way and the solid symbols represent what are thought to be the true values. The latter, somewhat lower, values are based primarily on the on-line measurements. It should be mentioned that the data of Noonan and Bingham (ref. 15) were obtained on a modified profile with a reflex trailing edge that reduced C_{M_0} to approximately zero, compared with the present value of -0.027 at $M_\infty = 0.3$ (cf. table 8). Also, the data of Jepson (ref. 16) in figure 27 came from a slotted-wall tunnel with 12.5% porosity, which was thought to yield somewhat lower values of C_L than comparable tests in solid-wall tunnels. Furthermore, the Reynolds numbers in references 15 and 16 were

lower than those of the present tests. Nevertheless, the discrepancies in figure 27 seem to be too large to be attributed to these factors or to measurement uncertainties. It will be shown later that dynamic data on the SC-1095 section are generally in better agreement.

Hughes HH-02 airfoil- Figure 28 shows the measured maximum lift coefficients for the present HH-02 airfoil, in comparison with data from a section that is almost identical except for a slightly smaller leading-edge radius (ref. 27). Although the Mach number range does not overlap, the two sets of results seem consistent.

Vertol VR-7 airfoil- Results from four sources are plotted in figure 29 for the VR-7 profile. The present data are somewhat higher than those of Coulomb (ref. 28), primarily because the stall occurred at slightly higher angles of attack, but the lift-curve slopes (not shown) and the effect of a boundary-layer trip were approximately the same. The value of $C_{L_{max}}$ at $M_\infty = 0.3$ is slightly lower than that of Dadone (ref. 5), whose measurements at higher Mach numbers exceed considerably those of Bingham et al. (ref. 29).

NLR-1 airfoil- Figure 30 shows the good agreement of the present measurements with those of Dadone (ref. 19) for the NLR-1 airfoil. It should be mentioned, however, that the details of the pitching-moment behavior in the vicinity of $C_{L_{max}}$ (not shown) were somewhat different. As in the previous example, the data of Noonan and Bingham (ref. 24) for $C_{L_{max}}$ at $M_\infty \geq 0.35$ tend to be lower than the data of Dadone (ref. 19). This airfoil appears to be more sensitive to Mach number than any of the other modern helicopter sections.

NLR-7301 airfoil- As shown in figure 31, the maximum static lift for the NLR-7301 airfoil exceeded that of the other sections by a considerable margin; however, C_{M_0} was -0.083 (cf. table 8). The values of $C_{L_{max}}$ shown are also greater than those obtained at NLR under virtually identical conditions (ref. 30). This was obtained at a significantly larger stall angle, more than 1° larger at $M_\infty = 0.18$, than in the NLR experiments, apparently because of different boundary-layer separation characteristics and sidewall interferences.

Dynamic Data

Although the static data described above comprised an essential part of the investigation, the primary objective was to obtain a common data base of unsteady characteristics for helicopter applications. In this section some representative examples are presented and comparisons made with other investigations. More complete discussions of the basic phenomena and of the results obtained are given in references 1 and 2.

The unsteady stall-onset and dynamic-stall counterparts of the static $C_{L_{max}}$ results discussed above are shown in figures 32 and 33, reproduced from reference 2 with some minor corrections. The dashed lines in figure 33 indicate the estimated deep-stall $C_{L_{max}}$ for the NLR-7301 airfoil; data were not obtained for this condition for $M_\infty > 0.25$. These results have not been corrected for wind-tunnel-wall interference.

Figures 32 and 33 illustrate an important general result of the investigation: the parameters of the unsteady motion tend to be more important than the airfoil geometry. For example, the differences in the values of $C_{L_{max}}$ for the Wortmann, Sikorsky, and Hughes airfoils can hardly be discerned within the experimental uncertainty, but the unsteady stall-onset and deep-stall results are much higher than the static values shown in figures 26-28 and 33. It is also interesting to note that at least for $M \leq 0.25$, the deep-stall $C_{L_{max}}$ values for the NLR-1 and NLR-7301 airfoils are almost identical. In contrast, the static and unsteady stall-onset results for these two very different profiles are considerably different and represent the lower and upper bounds, respectively, of all the airfoils tested.

In view of the aforementioned scatter in the static results from different wind tunnels, it is logical to inquire how different sets of dynamic data might compare. Because of the large number of parameters that affect dynamic stall and the tendency for past investigators to select different combinations of these parameters, the possibilities for direct comparison of unsteady results are much more limited. However, some examples are given below.

NACA 0012 airfoil- The first comparison for this profile is shown in figures 34 and 35, where data from reference 3 were obtained in the same wind tunnel as the present results, but with a model whose chord was twice as large. Figure 34 shows that the large values of $C_{L_{max}}$ reported in reference 3 were not realized in the present experiment. Figure 35 shows C_L versus α , where the two results are seen to differ by approximately 10% during the portion of the cycle when α is increasing but before dynamic stall begins. This is approximately the same as the difference in the lift-curve slopes for the corresponding static data, and it is consistent with the differences that would be predicted for static wind-tunnel-wall corrections (ref. 12) for the two chord-to-height ratios. However, it can be inferred from the differences in the peaks of the lift curves in figure 35 that the organized vortex-shedding phenomenon was more pronounced on the larger model after stall began. Also, reattachment of the boundary layer on the downstroke occurred earlier. These do not seem to be solely Reynolds-number effects; rather, it is suspected that in the earlier tests there was excessive interference between the boundary layers on the upper and lower walls of the tunnel and the unsteady viscous flow on the ends of the vertically mounted airfoil.

St. Hilaire and Carta (ref. 17) have reported on dynamic-stall tests of the NACA 0012 airfoil at UTRC under conditions similar to those in the present experiment. Figure 36 compares some of the data from the two investigations. The format and choice of unsteady parameters is based on an extension of the observation in reference 2, that for sinusoidal pitching oscillations the values of α_{max} and the product $\alpha_1 k^2$ seem to be particularly important in determining the detailed time-history of the unsteady airloads during dynamic stall. In order to compare as many test points as possible, data were selected that satisfied the criterion $0.0014 < \alpha_1 k^2 < 0.0022$, where α_1 is in radians. The variations in $C_{L_{max}}$ and $C_{M_{min}}$ in figure 36 are seen to correlate reasonably well on this basis, and the results from the two sources are in fairly good agreement. Some of the $C_{L_{max}}$ data from the UTRC wind tunnel are slightly higher than the present measurements.

SC-1095 airfoil- Gangwani (ref. 18) has reported data that were obtained on the SC-1095 section in the same facility that was used by St. Hilaire and Carta (ref. 17) to obtain the NACA 0012 data described in the preceding paragraph. The results are

compared with the present data in figure 37, following the same format as above. Fewer data points are available, but the degree of correlation is approximately comparable to that of the NACA 0012 results in figure 36. In contrast with that figure, however, the present values of $C_{L_{max}}$ tend to be slightly higher than the UTRC data (ref. 18). In any case, the discrepancies generally appear to be within the measurement uncertainty, and the agreement is better than for the static results (fig. 27).

NLR-1 airfoil- This profile was tested by Dadone (ref. 19) over a wide range of Mach numbers, mean angles, and amplitudes. Based on the considerations outlined above regarding α_{max} and $\alpha_1 k^2$, his results are compared with the present data in figure 38 as functions of $\alpha_1 k^2$ at a constant value $\alpha_{max} = 20^\circ$, where α_1 is also in degrees. The lift data are in better agreement than in the previous examples, but more scatter appears in the pitching-moment results than before.

No unsteady results from other sources are presently available from other sources for comparison with the data obtained on the Wortmann-FX-098, Ames A-01, Hughes HH-02, Vertol VR-7, and NLR 7301 airfoils.

Comments on Wind-Tunnel Effects

It is well known that testing the same airfoil in different wind tunnels often gives different results, especially for the static-stall characteristics. This is borne out in figures 24-31. In fact, if the results from these eight figures were overlaid, the real differences between the individual airfoils would be almost completely obscured by the differences attributable to the test facilities.

Although more limited in scope, the comparisons of dynamic-stall data shown in figures 36-38 are more encouraging than the static results. Since all of these data came from tests with either high aspect-ratio models or sidewall boundary-layer control, this suggests that the present dynamic data may be relatively free of wind-tunnel-wall contamination and other three-dimensional effects. A detailed examination of the complete time-histories of the unsteady airloads and further studies on models of various aspect ratios would be required to confirm this speculation.

A special feature of the present experiment is that a large number of airfoils were studied over a wide range of unsteady flow conditions in the same facility. This provides the basis for meaningful comparisons, even though wind-tunnel interference effects were not completely negligible. However, as stated in reference 1, it is recommended that the wind-tunnel walls be included or considered in any quantitative uses of the data.

5. SUMMARY AND CONCLUSIONS

A large amount of steady and unsteady data has been obtained on eight airfoil sections over a wide range of test conditions, at Mach numbers up to 0.30. The details of the experimental arrangements, estimates of the measurement accuracy, and the test conditions are described in this volume. Some comparisons are also made with data from other sources. Volume 2 (Pressure and Force Data) presents the results in graphical form and describes the digital computer tapes that contain the extensive numerical data. Volume 3 (Hot-Wire and Hot-Film Measurements) describes the boundary-layer studies performed with surface-mounted hot wires and hot films.

The results of the experiment show important differences between airfoils, differences that would otherwise tend to be masked by differences in wind tunnels, particularly in steady cases. All of the airfoils tested offer significant advantages over the standard NACA 0012 profile. In general, however, the parameters of the unsteady motion appear to be more important than airfoil shape in determining the dynamic-stall airloads.

REFERENCES

1. McCroskey, W. J.; and Pucci, S. L.: Viscous-Inviscid Interaction on Oscillating Airfoils in Subsonic Flow. AIAA J., vol. 20, no. 2, Feb. 1982, pp. 167-174.
2. McCroskey, W. J.; McAlister, K. W.; et al.: Dynamic Stall on Advanced Airfoil Sections. J. American Helicopter Soc., vol. 26, no. 3, July 1981, pp. 40-50.
3. McAlister, K. W.; Carr, L. W.; and McCroskey, W. J.: Dynamic Stall Experiments on the NACA 0012 Airfoil. NASA TP-1100, 1978.
4. Carr, L. W.; McAlister, K. W.; and McCroskey, W. J.: Analysis of the Development of Dynamic Stall Based on Oscillating Airfoil Experiments. NASA TN D-8382, 1977.
5. Dadone, L. U.: U.S. Army Helicopter Design Datcom. Vol. I - Airfoils. NASA CR-153247, 1976.
6. Hicks, R. M.; and McCroskey, W. J.: An Experimental Evaluation of a Helicopter Rotor Section Design by Numerical Optimization. NASA TM-78622, 1980.
7. Balch, D. T.: Helicopter Blade. U.S. Patent 3,728,045, 1973.
8. Kemp, L. D.: An Analytical Study for the Design of Advanced Rotor Airfoils. NASA CR-112297, 1973.
9. Barche, J., ed.: Experimental Data Base for Computer Program Assessment. AGARD Advisory Report 138, Advisory Group for Aerospace Research and Development, Neuilly-sur-Seine, France, 1979.
10. Carr, L. W.; and McCroskey, W. J.: A Directionally Sensitive Hot-Wire Probe for Detection of Flow Reversal in Highly Unsteady Flows. International Congress on Instrumentation in Aerospace Facilities, 1979 Record, Sept. 1979, pp. 154-162.
11. McCroskey, W. J.; McAlister, K. W.; and Carr, L. W.: Dynamic Stall Experiments on Oscillating Airfoils. AIAA J., vol. 14, no. 1, Jan. 1976, pp. 57-63.
12. Allen, H. J.; and Vincenti, W. G.: Wall Interference in a Two-Dimensional Flow Wind Tunnel with Consideration of the Effect of Compressibility. NACA Report 782, 1944.
13. Woodward, D. S.: The Twodimensional Characteristics of a 12.2% Thick R.A.E. Aerofoil Section. RAE Technical Report 68303, Royal Aircraft Establishment, Farnborough Hants, England, Jan. 1969.
14. Fromme, J. A.; and Golberg, M. A.: Unsteady Two-Dimensional Airloads Acting on Oscillating Airfoils in Subsonic Ventilated Wind Tunnels. NASA CR-2914, 1977.
15. Noonan, K. W.; and Bingham, G. J.: Aerodynamic Characteristics of Three Helicopter Rotor Airfoil Sections at Reynolds Numbers from Model Scale to Full Scale at Mach Numbers from 0.35 to 0.90. NASA TP-1701, 1980.

16. Jepson, W. D.: Two Dimensional Test of Four Airfoil Configurations with an Aspect Ratio of 7.5 and a 16 Inch Chord up to a Mach Number of 1.1. Report SER-50977, Sikorsky Aircraft, Stratford, Conn., Apr. 1977.
17. St. Hilaire, A. L.; and Carta, F. O.: The Influence of Sweep on the Aerodynamic Loading of an Oscillating NACA 0012 Airfoil. Vol. II - Data Report. NASA CR-145350, 1979.
18. Gangwani, S. T.: Prediction of Dynamic Stall and Unsteady Airloads for Rotor Blades. American Helicopter Society Paper 81-01, May 1981.
19. Dadone, L. U.: Two-Dimensional Wind Tunnel Test of an Oscillating Rotor Airfoil. NASA CR-2915, 1977.
20. Lizak, A. A.: Two-Dimensional Wind Tunnel Tests of an H-34 Main Rotor Airfoil Section. TREC Technical Report 60-53, U.S. Army Transportation Research Command, Ft. Eustis, VA, 1960.
21. Prouty, R. W.: A State-of-the-Art Survey of Two-Dimensional Airfoil Data. J. American Helicopter Soc., vol. 20, no. 4, Oct. 1975, pp. 14-25.
22. Bevert, A.: Essais Comparatifs en Courant Plan des Profils "G.1" et NACA 0012. ONERA Doc. No. 76/1157.AN, Office National d'Etudes et de Recherches Aérospatiales, Châtillon, France, Mar. 1970.
23. Harris, C. D.: Two-Dimensional Aerodynamic Characteristics of the NACA 0012 Airfoil in the Langley 8-Foot Transonic Pressure Tunnel. NASA TM-81927, 1981.
24. Noonan, K. W.; and Bingham, G. J.: Two-Dimensional Aerodynamic Characteristics of Several Rotorcraft Airfoils at Mach Numbers from 0.35 to 0.90. NASA TM X-73990, Jan. 1977.
25. Bingham, G. J.; and Noonan, K. W.: Low-Speed Aerodynamic Characteristics of Five Helicopter Blade Sections at Reynolds Numbers from 2.4×10^6 to 8.4×10^6 . NASA TM X-2467, 1972.
26. Wortmann, F. X.: Design of Airfoils with High Lift at Low and Medium Subsonic Mach Numbers. Paper No. 7, AGARD Conference Proceedings CP-102, Advisory Group for Aerospace Research and Development, Neuilly-sur-Seine, France, 1972.
27. Prouty, R. W.: Airfoil Section Data Report. Report No. 150-A-1012, Hughes Helicopters, Culver City, Calif., Mar. 1978.
28. Coulomb, J.: Caractéristiques Stationnaires du Profil VR 7. Procès-verbal No. 102 B/SC, Centre d'Essais Aéroronautique de Toulouse, Toulouse, France, June 1979.
29. Bingham, G. J.; Noonan, K. W.; and Jones, H. E.: Results of an Investigation of Several New Rotorcraft Airfoils as Related to Airfoil Requirements. Paper No. 8, NASA Conference Publication 2046, Mar. 1978.

30. Joosen, C. J. J.; and Kho, C. G.: Two Dimensional Low-Speed Wind Tunnel Investigation on a NLR 73-108-10 Airfoil with Fowler Type Flap, Part 1: Text, Tables, and Figures. NLR TR 74058 C, National Lucht- en Ruimtevaartlaboratorium, Amsterdam, The Netherlands, Sept. 1975.

TABLE 1.- HARMONIC COEFFICIENTS
OF THE OSCILLATION MECHANISM

$$\alpha = \alpha_0 + \alpha_1 \sin \omega t + \alpha_2 \sin(\omega t + \phi_2)$$

α_0	Nominal α_1	α_1	α_2	ϕ_2
5	5	5.00	0.05	(a)
10	5	4.90	.05	(a)
0	10	10.20	.20	(a)
5	10	10.05	.20	(a)
10	10	9.90	.20	260°
15	10	9.90	.20	(a)
15	14	14.10	.38	200°

^aNot measured.

TABLE 2. - AIRFOIL COORDINATES: NACA 0012 AND AMES A-01 AIRFOILS

x/c	NACA 0012, y/c		AMES A-01, y/c	
	upper	lower	upper	lower
0.0000	0.00000	0.00000	0.00000	0.00000
0.0005	0.00395	-0.00395	0.00377	-0.00338
0.0010	0.00556	-0.00556	0.00541	-0.00472
0.0020	0.00781	-0.00781	0.00766	-0.00651
0.0035	0.01027	-0.01027	0.01013	-0.00844
0.0050	0.01221	-0.01221	0.01214	-0.00994
0.0065	0.01386	-0.01386	0.01388	-0.01120
0.0080	0.01531	-0.01531	0.01543	-0.01227
0.0100	0.01704	-0.01704	0.01732	-0.01350
0.0125	0.01894	-0.01894	0.01945	-0.01481
0.0160	0.02127	-0.02127	0.02214	-0.01634
0.0200	0.02360	-0.02360	0.02490	-0.01777
0.0250	0.02615	-0.02615	0.02801	-0.01922
0.0350	0.03043	-0.03043	0.03335	-0.02137
0.0500	0.03555	-0.03555	0.03991	-0.02365
0.0650	0.03966	-0.03966	0.04523	-0.02549
0.0800	0.04307	-0.04307	0.04961	-0.02710
0.1000	0.04683	-0.04683	0.05421	-0.02902
0.1250	0.05055	-0.05055	0.05829	-0.03104
0.1500	0.05345	-0.05345	0.06098	-0.03277
0.2000	0.05737	-0.05737	0.06344	-0.03551
0.2500	0.05941	-0.05941	0.06431	-0.03727
0.3000	0.06002	-0.06002	0.06446	-0.03828
0.3500	0.05949	-0.05949	0.06409	-0.03866
0.4000	0.05803	-0.05803	0.06316	-0.03848
0.4500	0.05581	-0.05581	0.06154	-0.03782
0.5000	0.05294	-0.05294	0.05924	-0.03665
0.5500	0.04952	-0.04952	0.05623	-0.03501
0.6000	0.04563	-0.04563	0.05249	-0.03297
0.6500	0.04132	-0.04132	0.04792	-0.03056
0.7000	0.03664	-0.03664	0.04246	-0.02785
0.7500	0.03160	-0.03160	0.03600	-0.02486
0.8000	0.02623	-0.02623	0.02860	-0.02153
0.8500	0.02053	-0.02053	0.02064	-0.01786
0.9000	0.01448	-0.01448	0.01260	-0.01374
0.9250	0.01132	-0.01132	0.00899	-0.01144
0.9500	0.00807	-0.00807	0.00598	-0.00888
0.9750	0.00472	-0.00472	0.00392	-0.00603
0.9900	0.00265	-0.00265	0.00322	-0.00421
1.0000	0.00126	-0.00126	0.00299	-0.00300
	$r_o/c = 0.0158$		$r_o/c = 0.012$	

TABLE 3. - AIRFOIL COORDINATES: WORTMANN FX-098 AND SIKORSKY SC-1095 AIRFOILS

x/c	WORTMANN FX-098, y/c		SIKORSKY SC-1095, y/c	
	upper	lower	upper	lower
0.0000	0.00000	0.00000	0.00000	0.00000
0.0005	0.00293	-0.00249	0.00307	-0.00257
0.0010	0.00426	-0.00343	0.00443	-0.00368
0.0020	0.00619	-0.00471	0.00640	-0.00535
0.0035	0.00837	-0.00609	0.00865	-0.00724
0.0050	0.01017	-0.00717	0.01054	-0.00880
0.0065	0.01175	-0.00807	0.01221	-0.01016
0.0080	0.01319	-0.00886	0.01374	-0.01138
0.0100	0.01494	-0.00978	0.01560	-0.01285
0.0125	0.01692	-0.01079	0.01771	-0.01450
0.0160	0.01944	-0.01202	0.02041	-0.01657
0.0200	0.02204	-0.01321	0.02320	-0.01865
0.0250	0.02501	-0.01451	0.02635	-0.02092
0.0350	0.03021	-0.01664	0.03140	-0.02454
0.0500	0.03681	-0.01913	0.03677	-0.02842
0.0650	0.04234	-0.02111	0.04070	-0.03108
0.0800	0.04705	-0.02277	0.04374	-0.03295
0.1000	0.05222	-0.02464	0.04680	-0.03464
0.1250	0.05714	-0.02658	0.04963	-0.03619
0.1500	0.06073	-0.02819	0.05174	-0.03739
0.2000	0.06491	-0.03059	0.05447	-0.03884
0.2500	0.06650	-0.03198	0.05548	-0.03933
0.3000	0.06630	-0.03251	0.05524	-0.03918
0.3500	0.06515	-0.03242	0.05437	-0.03858
0.4000	0.06336	-0.03184	0.05299	-0.03760
0.4500	0.06097	-0.03096	0.05105	-0.03622
0.5000	0.05798	-0.02982	0.04854	-0.03446
0.5500	0.05445	-0.02843	0.04555	-0.03234
0.6000	0.05040	-0.02678	0.04212	-0.02985
0.6500	0.04586	-0.02487	0.03819	-0.02702
0.7000	0.04085	-0.02273	0.03375	-0.02384
0.7500	0.03543	-0.02034	0.02887	-0.02034
0.8000	0.02962	-0.01768	0.02362	-0.01658
0.8500	0.02337	-0.01473	0.01808	-0.01265
0.9000	0.01642	-0.01134	0.01235	-0.00865
0.9250	0.01253	-0.00932	0.00943	-0.00664
0.9500	0.00856	-0.00702	0.00642	-0.00454
0.9750	0.00476	-0.00423	0.00328	-0.00233
0.9900	0.00255	-0.00237	0.00132	-0.00093
1.0000	0.00110	-0.00110	0.00000	0.00000
	$r_o/c = 0.007$		$r_o/c = 0.008$	

TABLE 4. - AIRFOIL COORDINATES: HUGHES HH-02 (-5° TAB) AND VERTOL VR-7 (-3° TAB) AIRFOILS

x/c	HUGHES HH-02, y/c		VERTOL VR-7, y/c	
	upper	lower	upper	lower
0.0000	0.00000	0.00000	0.00000	0.00000
0.0005	0.00283	-0.00284	0.00337	-0.00330
0.0010	0.00405	-0.00388	0.00483	-0.00460
0.0020	0.00594	-0.00532	0.00696	-0.00633
0.0035	0.00819	-0.00683	0.00943	-0.00800
0.0050	0.01009	-0.00800	0.01149	-0.00919
0.0065	0.01176	-0.00895	0.01330	-0.01010
0.0080	0.01327	-0.00978	0.01494	-0.01086
0.0100	0.01510	-0.01072	0.01695	-0.01172
0.0125	0.01717	-0.01172	0.01923	-0.01263
0.0160	0.01975	-0.01290	0.02213	-0.01367
0.0200	0.02237	-0.01404	0.02512	-0.01467
0.0250	0.02531	-0.01524	0.02846	-0.01575
0.0350	0.03029	-0.01714	0.03423	-0.01751
0.0500	0.03640	-0.01943	0.04144	-0.01966
0.0650	0.04137	-0.02127	0.04759	-0.02154
0.0800	0.04553	-0.02276	0.05299	-0.02320
0.1000	0.05012	-0.02432	0.05922	-0.02516
0.1250	0.05468	-0.02575	0.06565	-0.02709
0.1500	0.05828	-0.02675	0.07091	-0.02855
0.2000	0.06328	-0.02793	0.07887	-0.03055
0.2500	0.06608	-0.02843	0.08378	-0.03186
0.3000	0.06738	-0.02834	0.08592	-0.03273
0.3500	0.06750	-0.02755	0.08574	-0.03308
0.4000	0.06640	-0.02500	0.08365	-0.03271
0.4500	0.06391	-0.02377	0.07984	-0.03148
0.5000	0.06008	-0.02104	0.07451	-0.02952
0.5500	0.05504	-0.01797	0.06781	-0.02712
0.6000	0.04891	-0.01482	0.05996	-0.02464
0.6500	0.04174	-0.01176	0.05171	-0.02207
0.7000	0.03344	-0.00952	0.04322	-0.01929
0.7500	0.02403	-0.00751	0.03442	-0.01639
0.8000	0.01436	-0.00889	0.02527	-0.01346
0.8500	0.00481	-0.00984	0.01575	-0.01050
0.9000	-0.00431	-0.01041	0.00558	-0.00744
0.9250	-0.00394	-0.00777	0.00117	-0.00609
0.9500	-0.00203	-0.00583	-0.00016	-0.00512
0.9750	-0.00006	-0.00387	0.00115	-0.00380
0.9900	0.00112	-0.00269	0.00194	-0.00300
1.0000	0.00190	-0.00190	0.00247	-0.00247
	$r_o/c = 0.008$		$r_o/c = 0.011$	

TABLE 5. - AIRFOIL COORDINATES: NLR-1 AND NLR-7301 AIRFOILS

x/c	NLR-1, y/c		NLR-7301, y/c	
	upper	lower	upper	lower
0.0000	0.00000	0.00000	0.00000	0.00000
0.0005	0.00359	-0.00288	0.00730	-0.00748
0.0010	0.00499	-0.00388	0.01051	-0.01020
0.0020	0.00687	-0.00518	0.01518	-0.01373
0.0035	0.00890	-0.00643	0.02030	-0.01735
0.0050	0.01053	-0.00730	0.02424	-0.02016
0.0065	0.01194	-0.00799	0.02756	-0.02252
0.0080	0.01321	-0.00858	0.03043	-0.02455
0.0100	0.01475	-0.00929	0.03375	-0.02688
0.0125	0.01648	-0.01006	0.03729	-0.02935
0.0160	0.01868	-0.01101	0.04140	-0.03225
0.0200	0.02097	-0.01196	0.04514	-0.03502
0.0250	0.02358	-0.01301	0.04873	-0.03794
0.0350	0.02799	-0.01477	0.05372	-0.04264
0.0500	0.03328	-0.01688	0.05920	-0.04806
0.0650	0.03750	-0.01859	0.06321	-0.05229
0.0800	0.04093	-0.02007	0.06636	-0.05576
0.1000	0.04435	-0.02179	0.06985	-0.05962
0.1250	0.04701	-0.02363	0.07347	-0.06358
0.1500	0.04905	-0.02522	0.07648	-0.06689
0.2000	0.05200	-0.02775	0.08115	-0.07194
0.2500	0.05386	-0.02958	0.08441	-0.07527
0.3000	0.05489	-0.03082	0.08649	-0.07713
0.3500	0.05528	-0.03154	0.08755	-0.07763
0.4000	0.05511	-0.03185	0.08764	-0.07672
0.4500	0.05443	-0.03176	0.08678	-0.07412
0.5000	0.05327	-0.03126	0.08495	-0.06934
0.5500	0.05164	-0.03025	0.08206	-0.06237
0.6000	0.04948	-0.02882	0.07789	-0.05386
0.6500	0.04677	-0.02707	0.07212	-0.04397
0.7000	0.04348	-0.02503	0.06458	-0.03316
0.7500	0.03892	-0.02276	0.05551	-0.02227
0.8000	0.03172	-0.02028	0.04523	-0.01221
0.8500	0.02368	-0.01756	0.03415	-0.00409
0.9000	0.01562	-0.01427	0.02269	0.00108
0.9250	0.01179	-0.01199	0.01696	0.00228
0.9500	0.00811	-0.00903	0.01129	0.00246
0.9750	0.00454	-0.00511	0.00577	0.00153
0.9900	0.00244	-0.00253	0.00258	0.00042
1.0000	0.00103	-0.00103	0.00055	-0.00055
	$r_o/c = 0.007$		$r_o/c = 0.055$	

TABLE 6.- TRANSDUCER LOCATIONS ON THE AIRFOILS

Transducer Number ^a	Nominal ^b x/c		Actual pressure transducer location									
	Pressure	Hot wire	0012	A-01	FX-098	SC-1095	VR-7	NLR-1	NLR-7301	HH-02		
1 LE	0.		0.	0.	0.0002U	0.	0.	0.	0.0015U	0.		
2 U	.005 (.004)		.0060	.0054	.0038	.0040	.0044	.0054	.0101	.0050		
3	.010 (.010)		.0103	.010	.0067	.0110	.0083	.0108	.0165	.0087		
4	.025 (.030)	0.025 (.025)	.0242	.024	.0196	.0275	.0225	.028	.0335	.0326		
5	.050 (.06)		.052	.050	.051	.053	.050	.051	.0512	.0581		
6	.100 (.12)	.10 (.12)	.102	.100	.101	.1025	.100	.101	.102	.1167		
7	.175 (.18)		.176	.175	.177	.178	.175	.177	.177	.183		
8	.25 (.25)		.252	.250	.252	.252	.250	.250	.252	.250		
9	.325 (.32)		.326	.325	.326	.325	.325	.325	.326	.317		
10	.40 (.38)	.40 (.38)	.40	.40	.40	.40	.40	.40	.40	.383		
11	.50 (.48)		.50	.50	.50	.50	.50	.50	.50	.472		
12	.60 (.56)	.60 (.56)	.60	.60	.60	.60	.60	.60	.60	.561		
13	.70 (.65)		.70	.70	.70	.70	.70	.70	.70	.650		
14	.80 (.74)	.80 (.74)	.80	.80	.80	.80	.80	.80	.80	.739		
15	.90 (.84)		.899	.90	.90	.90	.90	.90	.90	.840		
16 U	.98 (.93)		.98	.98	.98	.98	.98	.98	.98	.925		
17 L	.98 (.93)		.979	.98	.98	.98	.98	.98	.98	.925		
18	.90 (.84)		.90	.90	.90	.90	.90	.90	.90	.840		
19	.70 (.65)		.70	.70	.70	.70	.70	.70	.70	.650		
20	.50 (.48)		.50	.50	.50	.50	.50	.50	.50	.472		
21	.30 (.29)		.30	.30	.30	.30	.30	.30	.30	.294		
22	.15 (.16)		.153	.150	.153	.150	.150	.150	.155	.161		
23	.05 (.072)		.0504	.050	.051	.052	.050	.051	.0517	.0730		
24	.025 (.030)		.023	.026	.027	.028	.0246	.0220	.0194	.0293		
25	.010 (.010)		.0093	.0130	.0125	.009	.0094	.0108	.0051	.0081		
26 L	.005 (.004)		.0049	.0073	.0061	.005	.0040	.0062	.0021	.0044		

^aLE = leading edge; U = upper surface; L = lower surface.

^bLocations for HH-02, for which c = 68.6 cm, are shown in parentheses; for all other airfoils shown, c = 61.0 cm.

TABLE 7. - STATIC DRAG COEFFICIENTS AT $M = 0.30$ BASED ON WAKE SURVEYS

α , deg	N-0012	AMES-01	W-098	SC-1095	HH-02	VR-7	NLR-1	NLR-7301
-5.0	0.00843	0.00851	0.00886	0.00739	0.00846	0.00899	0.02602	0.00952
-2.0	0.00729	0.00832	0.00771	0.00713	0.00719	0.00759	0.00743	0.00780
0.0	0.00711	0.00794	0.00683	0.00708	0.00679	0.00723	0.00710	0.00968
2.0	0.00718	0.00662	0.00664	0.00670	0.00655	0.00707	0.00745	0.00891
5.0	0.00865	0.00767	0.00755	0.00807	0.00816	0.00800	0.00831	0.01011
8.0	0.01031	0.00965	0.01142	0.01013	0.01112	0.01059	0.01086	0.01305
10.0	0.01190	0.01248	0.01405	0.01127	0.01382	0.01353	0.01322	0.01569
12.0	0.01711	0.01600	0.01773	0.01586	0.01849	0.02156	0.02006	0.02022
13.0	--	--	--	0.02015	0.02236	--	--	--
14.0	0.02901	--	0.08922	--	--	--	--	--
-4.0	--	--	--	--	--	--	0.00773	0.00843
-1.75	--	--	--	--	--	--	--	0.00874
-1.0	--	--	--	--	--	--	--	0.00962
1.0	--	0.00738	--	--	--	--	--	0.00973
1.5	--	--	--	--	--	--	--	0.00910
2.5	--	--	--	--	--	--	--	0.00896
3.0	--	0.00702	--	--	--	--	--	--
4.0	--	0.00712	--	--	--	--	--	--
6.0	--	0.00791	--	--	--	--	--	--
9.9	--	0.01218	--	--	--	--	--	--

TABLE 8. - SUMMARY OF THE MEASURED STATIC AIRFOIL CHARACTERISTICS AT $M_\infty = 0.30$, INCLUDING WIND TUNNEL WALL CORRECTIONS

Airfoil	C_{L_α}	α_0	C_{M_0}	$C_{D_{min}}$	$X_{a.c.}$	$C_{L_{max}}$	α_{ss}	$(L/D)_{max}$
NACA 0012	0.109	-0.1°	-0.007	0.0072	0.24	1.33	13.7°	90
Ames-01	.111	-.6	-.005	.0070	.25	1.45	13.6	100
FX-098	.109	-1.3	-.026	.0066	.24	1.43	13.1	94
SC-1095	(.110) ^a	-.9	-.027	.0073	.245	(1.46) ^a	13.5	(98) ^a
HH-02	.114	-.6	-.002	.0066	.255	1.42	13.2	92
VR-7	.117	-1.6	-.016	.0071	.26	1.51	12.6	107
NLR-1	.102	-1.0	-.025	.0071	.22	1.29	12.4	87
NLR-7301	.117	-1.9	-.083	.0078	.25	(1.83) ^a	(17.2) ^a	89
Nominal uncertainty	±.003	.2	.005	.0005	.005	.03	.3	5

^aUncertainty larger than nominal value in table.

TABLE 9.- LIST OF TEST POINTS WITH UNUSUAL ZERO DRIFT OF PRESSURE TRANSDUCERS

Airfoil	Frame	M_∞	Type ^a	Problem transducers	Airfoil	Frame	M_∞	Type ^a	Problem transducers									
NACA 0012	8019	0.035	U	All	↓	Wortmann FX-098	↓	S	↓									
	8021																	
	8023																	
	8102																	
	8104																	
	8106																	
	8114																	
	8116																	
	8118																	
	8210																	
	12118																	
	13107																	
	13115																	
	13120																	
	13205																	
	13217																	
	14104																	
	14106																	
	14108																	
Ames A-01	26306	↓	↓	↓	↓	S	↓	↓	↓									
	26307																	
	28019																	
	28021																	
	28023																	
	28101																	
	28106																	
	28107																	
	28109																	
	28110																	
	28115																	
	28116																	
	28117																	
	28119																	
	28120																	
	29317																	
	Wortmann FX-098									16019	↓	↓	↓	↓	U	↓	↓	↓
										16200								
										17220								
18102																		
18106																		
18108																		
18410																		
18411																		
18413																		
Sikorsky SC-1095		33022	↓	↓	↓	↓	U	↓	↓	↓								
	33106																	
	33110																	
	34409																	
	35021																	
	35023																	
	35100																	
	35102																	
	35103																	
	36209																	
Hughes HH-02	42309	↓	↓	↓	↓	U	↓	↓	↓									
	42313																	
	43308																	
	43309																	
	Vertol VR-7									47213	↓	↓	↓	↓	↓	↓	↓	↓
47217																		
47301																		
47305																		
62020																		
63018																		
63019																		
63020																		
63021																		
65207																		
NLR-7301	66616	↓	↓	↓	↓	S	↓	↓	↓									
	66617																	
	NLR-7301									66617	↓	↓	↓	↓	S	↓	↓	↓
66616																		
66617																		

^aS = steady; U = unsteady; Q = quasi-steady, $k \leq 0.002$.

TABLE 10.- COEFFICIENTS OF LINEAR CURVE-FIT OF STATIC LIFT DATA
WITHOUT WIND-TUNNEL CORRECTIONS

$$C_L = A + \frac{B\alpha}{\sqrt{1 - M_\infty^2}}$$

Airfoil	A = C _L (0)	B = βC _{Lα}
NACA 0012	0	0.110
Ames 01	.15	.108
Wortmann FX-098	.07	.111
Sikorsky SC-1095	.11	.110
Hughes HH-02	.07	.116
Vertol VR-7	.19	.117
NLR-1	.11	.102
NLR-7301	.24	.116

ORIGINAL PAGE IS
OF POOR QUALITY

TABLE 11.- Continued.
(a) Concluded.

A	FRAME	TRIP	TYPE	AD	A1	Q	M	RE	K	FREQ	B	FRAME
10105	N	US	12.0	8.0	878	302	3684271.	0.968	5.36	13316		
10108	N	US	12.0	8.0	847	295	3635889.	1.253	6.81	13205		
10113	N	US	15.0	5.0	876	302	3896846.	0.098	1.53	14020		
10114	N	US	15.0	5.0	841	295	3801337.	0.252	1.34	14100		
10118	N	US	15.0	5.0	823	291	3749526.	1.020	5.36	14109		
10120	N	US	15.0	5.0	845	294	3785165.	1.511	8.04	14118		
10123	N	US	15.0	5.0	832	293	3758528.	2.024	10.72	14120		
10202	N	US	10.0	5.0	877	301	3658103.	0.098	5.4	14201		
10203	N	US	10.0	5.0	877	301	3627481.	0.246	1.34	14209		
10204	N	US	10.0	5.0	870	300	3824514.	0.493	2.68	14211		
10207	N	US	10.0	5.0	877	302	3832529.	0.740	4.02	14221		
10208	N	US	10.0	5.0	870	300	3854785.	0.990	5.36	14222		
10211	N	US	10.0	5.0	870	300	3852253.	1.486	8.04	14223		
10212	N	US	10.0	5.0	870	300	3850737.	1.979	10.72	14224		
10218	N	US	5.0	5.0	890	300	3933484.	0.098	5.36	14225		
10221	N	US	5.0	5.0	878	301	3920397.	0.993	10.72	14226		
10222	N	US	5.0	5.0	878	301	3912114.	1.983	10.72	14227		
10303	N	US	5.0	10.0	877	301	3910580.	0.991	5.36	14228		
10309	N	US	5.0	10.0	877	301	3911328.	0.991	5.36	14229		
10309	N	US	3.8	10.0	877	301	3863661.	0.989	5.36	14230		
12020	N	US	20.0	10.0	718	270	3490909.	0.010	0.5	12023		
12102	N	US	5.0	10.0	682	302	3880000.	0.009	0.5	12105		
12109	N	US	6.0	10.0	756	279	3485785.	0.010	0.5	12112		
12118	N	US	20.0	10.0	676	262	3246704.	0.010	0.5	12121		
12203	N	US	20.0	10.0	531	231	2887477.	0.011	0.5	12212		
12208	N	US	7.0	10.0	587	244	3268975.	0.010	0.5	12301		
12300	N	US	20.0	10.0	421	204	2706734.	0.011	0.4	12306		
12305	N	US	20.0	10.0	292	169	2252844.	0.011	0.3	13104		
13021	N	US	7.0	10.0	350	186	2469266.	0.010	0.3	13108		
13107	N	US	20.0	10.0	113	105	1421201.	0.017	0.3	13116		
13115	N	US	20.0	10.0	048	068	913563.	0.027	0.3	13202		
13120	N	US	5.0	10.0	053	072	962303.	0.025	0.3	13213		
13205	N	US	5.0	10.0	014	035	489772.	0.035	0.2	13316		
13217	N	US	20.0	10.0	013	036	4856631.	0.026	0.5	14020		
13222	N	US	20.0	10.0	749	276	3656957.	0.010	0.5	14100		
13303	N	US	7.0	10.0	603	247	3298109.	0.010	0.5	14109		
13308	N	US	7.0	10.0	461	215	2884310.	0.010	0.4	14118		
13310	N	US	7.0	10.0	466	216	2884723.	0.010	0.4	14120		
13313	Y	US	7.0	10.0	332	181	2404940.	0.010	0.3	14201		
14019	Y	US	15.0	10.0	339	183	3740354.	0.009	1.65	14202		
14021	Y	US	15.0	10.0	336	182	2453690.	0.499	3.30	14100		
14023	Y	US	15.0	10.0	335	182	243182.	1.001	4.95	14109		
14104	Y	US	15.0	10.0	338	183	2426579.	1.504	4.95	14118		
14106	Y	US	15.0	10.0	340	184	2449389.	0.499	1.65	14120		
14108	Y	US	15.0	10.0	339	183	2443079.	0.994	3.30	14201		
14117	Y	US	15.0	10.0	337	293	3843264.	1.493	4.95	14209		
14119	Y	US	15.0	10.0	336	293	3843264.	0.257	1.35	14211		
14200	Y	US	15.0	10.0	836	293	3519432.	0.509	2.68	14221		
14202	Y	US	15.0	10.0	843	294	382179.	0.253	1.34	14222		
14208	Y	US	15.0	10.0	839	293	3792702.	0.506	2.68	14223		
14210	Y	US	15.0	10.0	828	291	3763396.	1.019	5.36	14224		
14218	N	US	15.0	10.0	832	292	3760353.	1.014	5.36	14225		
14219	N	US	15.0	10.0	830	292	3762798.	0.254	1.34	14226		
14220	N	US	15.0	10.0	824	291	3735990.	0.509	2.68	14227		
15218	N	US	15.0	10.0	805	287	368317.	1.031	5.36	14228		
10117	N	US	15.0	10.0	818	290	3678973.	0.994	5.24	14229		
7202	N	US	12.0	5.0	843	295	3803563.	0.504	2.68	7201		
7222	N	US	10.0	5.0	877	302	3861194.	0.496	2.70	7223		
					876	298	3975490.	0.509	2.70			

ORIGINAL PAGE IS
OF POOR QUALITY

TABLE 11.- Continued.

(b) Concluded.

A	FRAME	TRIP	TYPE	AC	A1	Q	M	RE	K	FREQ	B
25102	N	US	10.0	10.0	881	302	3831527.	0489	2.68	29100	
25104	N	US	10.0	10.0	880	302	3816708.	0978	5.36	29102	
25109	N	US	10.0	10.0	879	302	3810775.	1468	8.04	29107	
25117	N	US	5.0	5.0	894	303	3928075.	0244	1.34	29116	
25118	N	US	5.0	5.0	879	302	3803407.	0489	2.68	29118	
25119	N	US	5.0	5.0	883	303	3805390.	0975	5.36	29121	
25121	N	US	10.0	5.0	881	302	3813088.	1465	8.04	29206	
25122	N	US	10.0	5.0	884	303	3819823.	1462	8.04	29210	
25123	N	US	10.0	5.0	845	403	3816927.	1947	10.72	30202	
25223	Y	US	15.0	10.0	825	291	3797799.	0248	1.34	30216	
25101	Y	US	15.0	10.0	805	288	3614634.	0500	2.62	30221	
25106	Y	US	15.0	10.0	806	288	3646183.	1001	5.24	30228	
25115	Y	US	15.0	10.0	340	194	2418121.	0494	1.65	30238	
25119	Y	US	15.0	10.0	341	184	2418248.	0387	3.30	30246	
25205	N	US	5.0	10.0	341	194	2417060.	1481	4.95	30254	
25207	N	US	5.0	10.0	876	301	3947215.	0098	5.53	30262	
25211	N	US	5.0	10.0	877	301	3918856.	0496	8.04	30270	
25215	N	US	5.0	10.0	877	301	3922857.	0991	5.36	30278	
25223	N	US	5.0	10.0	879	301	3868095.	1483	8.04	30286	
25304	N	US	15.0	2.0	879	301	3891313.	1481	8.04	30294	
25309	N	US	15.0	2.0	876	301	3511877.	1765	10.72	30302	
30019	N	US	15.0	2.0	870	300	3777473.	1967	10.72	30310	
30020	N	US	15.0	2.0	852	296	3727411.	1936	10.72	30318	
30105	N	US	15.0	2.0	852	296	472349.	1021	6.53	30326	
30114	N	US	15.0	2.0	865	298	3856941.	0097	5.2	30334	
30201	N	US	15.0	2.0	865	298	3828146.	0096	5.2	30342	
30206	N	US	15.0	2.0	864	298	3844592.	0097	5.3	30350	
30215	N	US	15.0	2.0	850	301	3817844.	0697	5.3	30358	
31102	N	US	10.0	10.0	877	300	3819252.	0097	5.3	30366	
31104	N	US	10.0	10.0	877	301	3814196.	0099	5.3	30374	
31110	N	US	10.0	10.0	875	301	3818950.	0097	5.3	30382	
31112	N	US	10.0	10.0	878	302	3815733.	0099	5.3	30390	
31119	N	US	10.0	10.0	878	302	3880209.	0247	1.34	30398	
31121	N	US	10.0	10.0	850	302	3651535.	0492	2.68	30406	
31123	N	US	10.0	10.0	850	302	3641535.	1471	8.04	30414	
31201	N	US	5.0	10.0	884	303	3833051.	1469	8.04	30422	
31209	N	US	5.0	10.0	884	303	3856266.	0245	1.34	30430	
31215	N	US	5.0	10.0	854	303	3826984.	0484	2.68	30438	
31217	N	US	5.0	10.0	854	303	3823741.	0975	5.36	30446	
31302	N	US	5.0	10.0	853	303	3816623.	1463	8.04	30454	
25204	N	US	15.0	10.0	341	194	2421425.	0987	3.30	30462	
25205	N	US	15.0	10.0	341	194	2425459.	0494	1.65	30470	
25209	N	US	15.0	10.0	341	185	2423083.	1972	6.60	30478	
25214	N	US	15.0	10.0	852	297	3765532.	1990	10.72	30486	
25216	N	US	15.0	10.0	854	298	3731389.	1485	8.04	30494	
25301	N	US	15.0	10.0	854	298	3732775.	0244	1.34	30502	
25303	N	US	15.0	10.0	878	301	3952662.	0497	2.68	30510	
25311	N	US	15.0	10.0	878	301	3950602.	0994	5.36	30518	
25319	N	US	15.0	10.0	857	298	3697313.	1506	8.04	30526	
25210	N	US	15.0	10.0	852	297	3865306.	2013	10.72	30534	
25214	N	US	15.0	10.0	830	302	3726436.	0495	2.68	30542	
25216	N	US	15.0	10.0	830	302	3909711.	0986	5.36	30550	
25301	N	US	15.0	10.0	834	302	3903998.	0984	5.36	30558	
25303	N	US	15.0	10.0	855	303	3878688.	1962	10.72	30566	
25311	N	US	15.0	10.0	891	302	3852707.	0482	5.36	30574	
25319	N	US	15.0	10.0	891	302	3833693.	0980	5.36	30582	

ORIGINAL PAGE IS
OF POOR QUALITY

TABLE 11.- Continued.

(c) Concluded.

A	FRAME	TRIP	Y	N	UN	TYPE	AO	A1	Q	M	RE	K	FREQ	B
17200	N	UN	15.0	10.0	814	290	3702477.	.0999	5.24	22223				
21100	N	UN	15.0	10.0	.823	291	3718613.	.0099	.52	22300				
21107	N	UN	10.0	10.0	.857	299	3792469.	.0099	.53	22301				
21200	N	UN	10.0	5.0	.875	301	3932117.	.0098	.53	21201				
21208	N	UN	3.3	10.0	.892	302	3935549.	.0097	.53	21209				
21219	N	UN	6.5	10.0	.933	184	2455254.	.0099	.33	21220				
22023	N	UN	15.0	10.0	.827	293	3727453.	.0247	1.31	22202				
22103	N	UN	15.0	10.0	.837	294	3744490.	.0402	2.62	22104				
22201	N	UN	15.0	10.0	.795	285	3554419.	.1009	5.24	22202				
22206	N	UN	15.0	10.0	.754	279	3477029.	.1542	7.86	22207				
22209	N	UN	15.0	10.0	.763	281	3483672.	.0969	4.98	22209				
22216	N	UN	10.0	10.0	.875	302	3732711.	.0243	1.34	22202				
22218	N	UN	10.0	10.0	.852	300	3654371.	.0495	2.68	22202				
22219	N	UN	10.0	10.0	.825	294	3615534.	.0977	5.36	22209				
22307	N	UN	10.0	5.0	.875	301	3754397.	.0246	1.34	22223				
22308	N	UN	10.0	5.0	.830	303	3957224.	.0491	2.68	22300				
22309	N	UN	10.0	5.0	.891	303	3953241.	.0490	5.36	22301				
22311	N	UN	10.0	5.0	.877	302	3613799.	.1475	8.04	22302				
22312	N	UN	10.0	5.0	.882	303	3849072.	.1957	10.72	22303				
23021	N	UN	15.0	5.0	.851	297	3750472.	.0497	2.68	22302				
23023	N	UN	15.0	5.0	.840	295	3711331.	.1000	5.36	22303				
23100	N	UN	5.0	5.0	.822	292	3673934.	.1515	8.04	23108				
23107	N	UN	5.0	5.0	.867	300	3823826.	.0826	5.35	23110				
23109	N	UN	5.0	5.0	.867	300	3759174.	.1970	10.72	23118				
23117	N	UN	5.0	10.0	.869	300	3603440.	.0995	5.36	23202				
23201	N	UN	3.8	10.0	.865	293	3932310.	.1003	5.36	23207				
23206	N	UN	3.3	10.0	.865	294	3924045.	.0500	2.68	23210				
23208	N	UN	3.3	10.0	.871	300	3914465.	.0996	5.36	23212				
23211	N	UN	3.3	10.0	.870	300	3895319.	.1492	8.04	23220				
23219	N	UN	12.0	2.0	.844	299	3855609.	.1994	10.72	23306				
23305	N	UN	14.0	2.0	.853	299	3831711.	.1995	10.72	23311				
23310	N	UN	16.0	2.0	.859	294	3768792.	.2014	10.72	23306				
21112	N	UN	15.0	5.0	.873	301	3943131.	.0099	5.36	23311				
23101	N	UN	15.0	5.0	.800	287	3617353.	.2049	10.72	23311				

ORIGINAL PAGE IS
OF POOR QUALITY

TABLE 11.- Continued.

(d) Concluded.

A		B								
FRAME	TRIP	TYPE	AD	A1	Q	M	RE	K	FREQ	FRAME
39107	N	UN	11.0	5.0	.859	.299	3996897.	.0099	.53	
39115	N	UN	14.0	2.0	.865	.298	3838622.	.0100	.54	
38110	N	UN	16.0	2.0	.832	.293	3754517.	.2023	10.72	38111
39107	N	UN	10.0	5.0	.875	.300	3939495.	.0098	.53	

ORIGINAL PAGE IS
OF POOR QUALITY

TABLE 11.- Continued.
(e) Concluded.

A	TRIP	TYPE	AO	A1	G	M	PE	K	FREQ	B FRAME
44112	N	US	10.0	5.0	.880	.303	4003278.	.1989	10.72	44113
44118	N	US	10.0	5.0	.880	.302	4037690.	.0999	5.36	
44119	N	US	10.0	5.0	.876	.302	4019097.	.0250	1.34	
44120	N	US	10.0	5.0	.878	.302	4037236.	.1997	10.72	
44202	N	US	14.0	2.0	.875	.301	4004232.	.1001	5.36	44203
44204	N	US	14.0	2.0	.872	.301	3997136.	.2002	10.72	44205
44209	N	US	17.5	2.0	.773	.282	3756572.	.2132	10.72	
44212	N	US	15.5	2.0	.854	.297	3951107.	.0102	.54	
44214	N	US	15.5	2.0	.851	.297	3917470.	.0253	1.34	
44215	N	US	15.5	2.0	.849	.296	3904444.	.0506	2.68	
44216	N	US	15.5	2.0	.829	.293	3854681.	.1024	5.36	
44217	N	US	15.5	2.0	.820	.291	3826794.	.1545	8.04	
44218	N	US	15.5	2.0	.824	.292	3832243.	.2054	10.72	
44221	N	US	15.5	2.0	.821	.291	3955505.	.0101	.54	
44222	N	US	12.5	2.0	.871	.302	3943321.	.0248	1.34	
44223	N	US	12.5	2.0	.871	.301	3916390.	.0493	2.68	
44300	N	US	12.5	2.0	.874	.301	3933775.	.0994	5.36	
44303	N	US	12.5	2.0	.877	.302	3953217.	.1490	8.04	
44304	N	US	12.5	2.0	.878	.302	3945918.	.1984	10.72	
43308	N	US	15.0	5.0	.813	.290	3809287.	.1549	8.04	

ORIGINAL PAGE IS
OF POOR QUALITY

TABLE 11.- Continued.
(f) Concluded.

A	FRAME	TRIP	TYPE	AO	A1	Q	M	RE	K	FREQ	B
54216	N	UN	15.0	10.0	.340	.184	2547606.	.1514	4.95	54217	
49019	N	UN	4.1	10.0	.674	.296	4215503.	.0103	.54	48020	
48023	N	UN	4.1	10.0	.880	.300	4189935.	.0255	1.34	49100	
48101	N	UN	4.1	10.0	.877	.499	4160141.	.0509	2.68	48102	
48103	N	UN	4.1	10.0	.879	.300	4154411.	.1016	5.36	48124	
48116	N	UN	13.0	2.0	.878	.299	4054662.	.0253	1.34	48117	
48118	N	UN	13.0	2.0	.878	.299	4059323.	.0504	2.68	48119	
48122	N	UN	13.0	2.0	.876	.299	4057706.	.1010	5.36	48123	
48709	N	UN	16.0	2.0	.870	.298	4059728.	.2028	10.72	48211	
48215	N	UN	14.0	2.0	.877	.300	4057379.	.0504	2.68		
48216	N	UN	14.0	2.0	.879	.300	4047826.	.1005	5.36		
48217	N	UN	14.0	2.0	.879	.300	4030080.	.2009	10.72	48218	
48320	N	UN	12.5	2.0	.878	.300	4033369.	.0101	.54		
48301	N	UN	12.5	2.0	.878	.300	4011700.	.0251	1.34		
48302	N	UN	12.5	2.0	.831	.301	4009355.	.0500	2.68		
48303	N	UN	12.5	2.0	.874	.299	3936169.	.1004	5.36		
48324	N	UN	12.5	2.0	.873	.299	3930450.	.1505	8.04		
48308	N	UN	12.5	2.0	.875	.300	3999348.	.2007	10.72	48309	
49110	N	UN	15.0	10.0	.339	.182	2634238.	.0257	.83	49111	
49117	N	UN	15.0	10.0	.342	.185	2619356.	.0507	1.65	49118	
49120	N	UN	15.0	10.0	.340	.185	2599912.	.1014	3.30	49121	
49203	N	UN	15.0	10.0	.341	.185	2527337.	.1518	4.95	49204	
49206	N	UN	15.0	10.0	.341	.185	2545516.	.2020	6.80	49207	
49216	N	UN	4.7	10.0	.340	.182	2550479.	.0254	.83	49217	
49300	N	UN	4.7	10.0	.339	.184	2535455.	.1009	3.30	49301	
49207	N	UN	4.7	10.0	.342	.185	2548693.	.2005	6.60	49308	
49310	N	UN	4.7	10.0	.343	.185	2543519.	.2503	8.25	49311	
49323	N	UN	15.0	10.0	.338	.184	2543127.	.0101	.33	49100	
57018	N	UN	4.7	10.0	.339	.183	2531156.	.0101	.33	50117	
57018	N	UN	15.0	10.0	.340	.184	2555187.	.1516	4.95	57019	
58018	N	UN	15.0	10.0	.338	.183	2437793.	.1295	4.95	58019	
58102	N	UN	15.0	10.0	.121	.037	496703.	.0983	1.65	58103	
58111	N	UN	15.0	10.0	.121	.109	1528745.	.1010	1.96	58112	
58120	N	UN	15.0	10.0	.340	.184	2536174.	.1511	4.95		
58121	N	UN	15.0	10.0	.340	.184	2532330.	.1007	3.30		
47022	Y	UN	15.0	10.0	.841	.296	5990015.	.0501	2.62	47023	
48200	N	UN	13.0	2.0	.884	.301	4062447.	.2006	10.72	48201	

ORIGINAL PAGE IS
OF POOR QUALITY

TABLE 11.- Continued.
(g) Concluded.

A	FRAME	TRIP	TYPE	AD	AI	G	M	RE	K	FREQ	B
63320	N	US	2.5	10.0	.878	.303	3739575.	.0969	5.36	63321	
63323	N	US	2.7	10.0	.880	.303	3746774.	.0969	5.36	63400	
64019	Y	US	15.0	10.0	.844	.298	3865490.	.0247	1.31	64020	
64021	Y	US	15.0	10.0	.840	.292	3813267.	.0493	2.62	64022	
64023	Y	US	15.0	10.0	.821	.292	3752005.	.0997	5.24	64100	
64107	Y	US	15.0	10.0	.840	.185	2448919.	.0496	1.65	64108	
64109	Y	US	15.0	10.0	.840	.184	2439010.	.0991	3.30	64110	
64111	Y	US	15.0	10.0	.841	.185	2429226.	.1481	4.95	64112	
64119	Y	US	2.5	10.0	.876	.302	3823617.	.0099	.54	64119	
64121	Y	US	2.5	10.0	.875	.302	3785031.	.0244	1.34	64121	
64202	Y	US	2.3	10.0	.879	.303	3794315.	.0737	2.68	64202	
64204	Y	US	2.5	10.0	.879	.302	3774318.	.0974	5.36	64204	
64212	Y	US	2.0	10.0	.877	.302	3717936.	.0098	.54	64212	
64213	Y	US	2.0	10.0	.878	.303	3695424.	.0241	1.34	64213	
64214	Y	US	2.0	10.0	.880	.302	3685179.	.0482	2.68	64214	
65121	N	US	2.0	10.0	.869	.303	3683703.	.0963	5.36	65121	
65122	N	US	2.0	10.0	.873	.301	3700235.	.0243	1.34	65122	
65123	N	US	2.0	10.0	.877	.301	3694893.	.0485	2.68	65123	
65200	N	US	15.0	10.0	.845	.302	3694943.	.0968	5.36	65200	
65207	N	US	15.0	10.0	.829	.199	264668.	.0997	3.57	65207	
65209	N	US	15.0	10.0	.829	.292	3775170.	.1019	5.36	65209	
65223	N	US	7.0	5.0	.121	.109	1475386.	.0249	.49	65223	
65300	N	US	7.0	5.0	.121	.109	1472656.	.1996	3.92	65300	
65311	N	US	7.0	5.0	.879	.301	3862901.	.1969	10.72	65311	
65309	N	US	7.0	5.0	.876	.301	3889117.	.0100	.54	65309	
63222	N	US	15.0	2.0	.818	.291	3675798.	.2028	10.72	63223	

ORIGINAL PAGE IS
OF POOR QUALITY

TABLE 11.- Concluded.
(h) Concluded.

A	FRAME	TRIP	TYPE	AD	A1	Q	H	RE	K	B	FRQ	FRAME
69100	N	US	10.0	10.0	10.0	.873	300	3918788.	.0249	1.34	69101	
69102	N	US	10.0	10.0	10.0	.876	300	3900063.	.0295	2.68	69103	
69105	N	US	10.0	10.0	10.0	.877	301	3904033.	.0291	5.36	69106	
69107	N	US	10.0	10.0	10.0	.876	300	3884160.	.1484	8.04	69108	
69119	N	US	16.8	2.0	2.0	.727	273	3492462.	.0270	1.34	69120	
69121	N	US	16.8	2.0	2.0	.710	270	3433737.	.0546	2.68	69122	
69123	N	US	16.8	2.0	2.0	.700	268	3296634.	.1100	5.36	69200	
69201	N	US	16.9	2.0	2.0	.692	267	3346733.	.2208	10.72	69202	
69206	N	US	17.2	2.0	2.0	.734	275	3455551.	.0269	1.34	69207	
69208	N	US	17.2	2.0	2.0	.745	277	3468113.	.0530	2.68	69209	
69211	N	US	17.2	2.0	2.0	.709	270	3370449.	.1025	5.36	69212	
69213	N	US	17.2	2.0	2.0	.719	272	3357722.	.1616	8.04	69214	
69215	N	US	17.2	2.0	2.0	.755	279	3459727.	.2098	10.72	69216	
69221	N	US	17.5	2.0	2.0	.726	273	3404711.	.0536	2.68	69222	
69223	N	US	17.5	2.0	2.0	.694	265	3285912.	.2305	10.72	69300	
69304	N	US	18.5	2.0	2.0	.698	266	3258767.	.0549	2.68	69305	
69310	N	US	16.5	2.0	2.0	.671	252	3218073.	.0554	2.68	69311	
70019	N	US	9.4	10.0	10.0	.341	163	2344007.	.0245	83	70020	
70021	N	US	9.4	10.0	10.0	.340	185	2319519.	.0973	3.30	70022	
70023	N	US	9.4	10.0	10.0	.340	185	2316677.	.1948	6.60	70100	
70107	N	US	5.7	10.0	10.0	.676	301	3816444.	.0104	.56	70108	
70109	N	US	5.7	10.0	10.0	.676	301	3876178.	.0247	1.34	70110	
70113	N	US	5.7	10.0	10.0	.672	300	3841569.	.0495	2.68	70114	
70115	N	US	5.7	10.0	10.0	.675	301	3854554.	.0986	5.36	70116	
70117	N	US	5.7	10.0	10.0	.674	301	3842662.	.1479	8.04	70118	

TABLE 12.- LIST OF STATIC DATA

Airfoil ¹	M _∞	First frame	Last frame	No. of frames	α _{min}	α _{max}	Figure	Airfoil ²	M _∞	First frame	Last frame	No. of frames	α _{min}	α _{max}	Figure
N-0012	0.30	04019	04412	24	-5.0	20.0		FX-098T	0.30	17208	17314	8	0.0	20.0	
	.30	11018	11309	33	-5.0	30.0	9,12,16	FX-098T	.18	18019	18206	10	0.0	20.0	
	.30	12102	(quasi-steady)		-5.0	15.0	16	SC-1095	.30	35021	35214	17	-5.0	16.0	19
	.25	12109			-4.0	16.0		SC-1095	.25	35220	35401	20	-5.0	25.0	
	.26	13222			10.1	29.9		SC-1095	.18	36019	36120	10	-5.0	20.0	
	.27	12020			10.1	29.9		SC-1095T	.11	36202	36218	11	-5.0	20.0	
	.26	12118			10.1	29.9		SC-1095T	.30	34022	34115	8	0.0	16.0	
	.25	12208			-3.0	17.0		SC-1095T	.18	34200	34214	7	0.0	16.0	
	.25	13303			-3.0	17.0		HH-02	.30	40222	41103	20	-5.0	20.0	20
	.23	12203			10.1	29.9		HH-02	.25	41110	41215	20	-5.0	20.0	
	.22	13308			-3.0	17.0		HH-02	.18	40114	40215	10	-5.0	20.0	
	.22	13310			-3.0	17.0		HH-02	.11	40018	40108	11	-5.0	20.0	
	.20	12300			10.1	29.9		HH-02T	.30	41221	41314	8	0.0	16.0	
	.18	12310			-3.0	17.0		HH-02T	.18	41401	41419	10	0.0	16.0	
	.17	12305			10.1	29.9		VR-7	.30	46418	46615	18	-5.0	25.0	11,21
	.11	13021			-3.0	17.0		VR-7	.25	46307	46412	19	-5.0	25.0	
	.11	13107			10.1	29.9		VR-7	.18	46116	46301	13	-5.0	25.0	
	.07	13120			-3.0	17.0		VR-7	.11	46018	46110	13	-5.0	25.0	
	.07	13115			10.1	29.9		VR-7T	.30	46802	46823	10	0.0	20.0	
	.04	13205			-5.0	15.0		VR-7T	.18	46621	46718	10	0.0	20.0	
	.04	13217			10.1	29.9		NLR-1	.30	61407	61606	19	-5.0	25.0	22
N-0012T	.29	13321			-3.0	17.0		NLR-1	.25	61221	61401	19	-5.0	25.0	
N-0012T	.18	13313			-3.0	17.0		NLR-1	.18	61114	61215	10	-5.0	20.0	
Ames-01	.30	26020	26307	23	-5.0	25.0	17	NLR-1	.11	61018	61108	11	-5.0	20.0	
Ames-01	.25	26313	27117	22	-5.0	25.0		NLR-1T	.30	65019	65115	13	-11.0	16.0	
Ames-01	.18	27123	27318	22	-5.0	25.0		NLR-1T	.18	64221	64311	8	0.0	16.0	
Ames-01	.11	27400	28120	21	-5.0	25.0		NLR-7301	.30	66019	66209	17	-5.0	20.0	23
Ames-01T	.30	28312	28410	9	0.0	16.0		NLR-7301	.25	66214	66314	17	-5.0	25.0	
Ames-01T	.19	28207	28304	10	0.0	20.0		NLR-7301	.18	66320	66511	18	-5.0	25.0	
FX-098	.30	20118	20322	21	-5.0	25.0	18	NLR-7301T	.11	66516	66617	17	-5.0	25.0	
FX-098	.25	19314	20112	22	-5.0	25.0		NLR-7301T	.30	66810	66822	6	0.0	13.0	
FX-098	.18	19020	19508	23	-5.0	25.0		NLR-7301T	.18	66623	66802	13	0.0	25.0	
FX-098	.11	18215	18502	23	-5.0	25.0	10								

¹T = trip.

TABLE 13.- MACH NUMBER SWEEP AT $\alpha = 15^\circ + 10^\circ \sin \omega t$, $k = 0.10$

M_∞^α	NACA 0012	A-01	FX-098	SC-1095	HH-02	VR-7	NLR-1	NLR-7301
0.035	8102		16019			58102		
.07	8114	24323	16105	33022	42121	47123	62020	
.11	8214	24314	16114	33106	42321	{47206 58111	62104	67120
.18	8220	{24217 31209	16200	33110	42302	{47213 58121	62112	67220
.18T	{14021 14106	29117	17103	34321	42110	47112	64109	67021
.20							{62114 65207	
.22	9202	24209	16300	33205	42309	47217	62208	
.25	9203	24201	16308	33207	42313	47301	62210	67305
.28	9208	24117	22208	33215	42218	47305	62218	
.29	{9217 14220	24105	22201	33300	42210	45023	{62307 65209	
.29T	{14208 14210	29106	17200	34308	42100	47100	64023	

$\alpha_T = \text{trip.}$

TABLE 14.- FREQUENCY SWEEP AT $M_\infty = 0.29$, $\alpha = 15^\circ + 10^\circ \sin \omega t$

k^α	NACA 0012	A-01	FX-098	SC-1095	HH-02	VR-7	NLR-1	NLR-7301
0.01	9210	{30019 30020	21100	38300				
.025	{9213 14218	24022	22023	33217	42206	45019	62302	
.025T	{14117 14200	29023	17117		42019	47020	64019	
.05	{9214 14219	24100	22103	33222	42208	45021	62304	
.05T	{14119 14202	29101	17119	34306	42021	47022	64021	
.10	{9217 14220	24105	22201	33300	42210	45023	{62307 65209	
.10T	{14208 14210	29106	17200	34308	42100	47100	64023	
.15	9218	24109	22206	34409	{42212 42217	45101	62309	

$\alpha_T = \text{trip.}$

TABLE 15.- FREQUENCY SWEEP AT $M_\infty = 0.30$, $\alpha = 10^\circ + 10^\circ \sin \omega t$

k	NACA 0012	A-01	FX-098	SC-1095	HH-02	VR-7	NLR-1	NLR-7301
0.01	9221	30105	21107	38306	43019	45109	62317	69019
.025	9222	{25022 31102	22216	37023	43106	45111	62320	69100
.05	9223	{25102 31104	22217	37101	43108	45113	62322	69102
.10	9302	25104	22218	37107	43112	45117	62400	69105
.12							62403	
.15	9307	{25109 31110 31112	22219	37109	{43114 43117	45119	62405	69107

TABLE 16.- FREQUENCY SWEEP AT $M_\infty = 0.30$, $\alpha = 15^\circ + 5^\circ \sin \omega t$

k	NACA 0012	A-01	FX-098	SC-1095	HH-02	VR-7	NLR-1	NLR-7301
0.01	10113	30110	21112	39104		45203	63018	68019
.025	10114	25204	23021	38021	43303	45205	63019	68100
.05	10117	25205	23022	38022	43304	45207	63020	68102
.10	10118	25208	23023	38102	43305	45209	63021	68104
.12							63100	
.15	10120	25209	23100	38103	43308	45211	63101	68109
.20	10123	25210	23101	38104	43309	45213	63102	68111

TABLE 17.- FREQUENCY SWEEP AT $M_\infty = 0.30$, $\alpha = 10^\circ + 5^\circ \sin \omega t$

k	NACA 0012	A-01	FX-098	SC-1095	HH-02	VR-7	NLR-1	NLR-7301	NLR-7301T
0.01	10202	30119	21200	39107	44019			68119	
.025	{7112 10203	25117	22307	37207	{44021 44119	45221	63108	68121	67108
.05	{7222 10204	25118	22308	37208	44023	45223		68123	67110
.075	10207								
.10	{7113 10208	25119	22309	37210	{44104 44118	45300	63112	68201	67112
.15	{7300 10211	{25121 25122	22311	37213	44106	45302			
.20	{7114 10212	25123	22312	37215	{44112 44120	45303	63114	68203	

ORIGINAL PAGE IS
OF POOR QUALITY

TABLE 18.- STALL ONSET AT $M_\infty = 0.30$, $\alpha = \alpha_0 + 10^\circ \sin \omega t$, $k = 0.10$

NACA 0012, $\alpha_0 = 3.8^\circ$	A-01, $\alpha_0 = 5.5^\circ$	FX-098, $\alpha_0 = 3.8^\circ$	SC-1095, $\alpha_0 = 4.4^\circ$	HH-02, $\alpha_0 = 4.0^\circ$	VR-7, $\alpha_0 = 4.6^\circ$	NLR-1, $\alpha_0 = 2.7^\circ$	NLR-7301, $\alpha_0 = 5.7^\circ$
10305	25319	23201	34418	43219	63323	70115	

TABLE 19.- STALL SUPPRESSION AT $M_\infty = 0.30$, $\alpha = \alpha_0 + 10^\circ \sin \omega t$

k	NACA 0012 $\alpha_0 = 5.0^\circ$	A-01, $\alpha_0 = 5.0^\circ$	FX-098, $\alpha_0 = 3.3^\circ$	SC-1095, $\alpha_0 = 4.1^\circ$	HH-02, $\alpha_0 = 3.8^\circ$	VR-7, $\alpha_0 = 4.1^\circ$	NLR-1, $\alpha_0 = 2.5^\circ$	NLR-7301, $\alpha_0 = 5.7^\circ$
0.01	29205	21208	39021	43215	48019	63312	70107	
.025	31119			43202	48023	63314	70109	
.05	{29207 31121	23206	37119	43204	48101	63318	70113	
.10	{25311 29211 31123	23208	37121	43206	48103	63320	70115	
.15	{29213 29215 31201	23211	37123	43209			70117	

α See table 24.

TABLE 20.- STALL SUPPRESSION AT $M_\infty = 0.18$, $\alpha = \alpha_0 + 10^\circ \sin \omega t$

k	NACA 0012, $\alpha_0 = 8.0^\circ$	A-01, $\alpha_0 = 7.5^\circ$	FX-098, $\alpha_0 = 6.5^\circ$	SC-1095, $\alpha_0 = 6.2^\circ$	HH-02	VR-7, $\alpha_0 = 4.7^\circ$	NLR-1	NLR-7301, $\alpha_0 = 9.4^\circ$
0.01	9110	30215	21219			50116		70019
.025						49216		
.05	9112	{24302 31215	16213	33118				
.10						49300		70021
.20	9118	{24306 31217	16215	33121		49307		70023
.25						49310		

ORIGINAL PAGE IS
OF POOR QUALITY

TABLE 21.- PITCH DAMPING STUDIES AT $M_\infty = 0.30$, $\alpha = \alpha_0 + 2^\circ \sin \omega t$

NACA 0012	A-01	FX-098	SC-1095	HH-02	VR-7	NLR-1	NLR-7301 α
$k = 0.01$							
$\alpha_0 = 14.0^\circ$ 30206	$\alpha_0 = 14.0^\circ$ 39115	$\alpha_0 = 12.5^\circ$ 44221	$\alpha_0 = 12.5^\circ$ 48300				
		$\alpha_0 = 15.5^\circ$ 44212					
$k = 0.025$							
		$\alpha_0 = 12.5^\circ$ 44222	$\alpha_0 = 12.5^\circ$ 48301				$\alpha_0 = 16.8^\circ$ 69119
		$\alpha_0 = 15.5^\circ$ 44214	$\alpha_0 = 13.0^\circ$ 48116				$\alpha_0 = 17.2^\circ$ 69206
$k = 0.05$							
		$\alpha_0 = 12.5^\circ$ 44223	$\alpha_0 = 12.5^\circ$ 48302	$\alpha_0 = 11.1^\circ$ 63302			$\alpha_0 = 16.5^\circ$ 69310
		$\alpha_0 = 15.5^\circ$ 44215	$\alpha_0 = 13.0^\circ$ 48118	$\alpha_0 = 15.0^\circ$ 63220			$\alpha_0 = 16.8^\circ$ 69121
			$\alpha_0 = 14.0^\circ$ 48215	$\alpha_0 = 17.0^\circ$ 63213			$\alpha_0 = 17.2^\circ$ 69208
							$\alpha_0 = 17.5^\circ$ 69221
							$\alpha_0 = 18.5^\circ$ 69304
$k = 0.10$							
		$\alpha_0 = 12.5^\circ$ 44300	$\alpha_0 = 12.5^\circ$ 48303				$\alpha_0 = 16.8^\circ$ 69123
		$\alpha_0 = 14.0^\circ$ 44202	$\alpha_0 = 13.0^\circ$ 48122				$\alpha_0 = 17.2^\circ$ 69211
		$\alpha_0 = 15.5^\circ$ 44216	$\alpha_0 = 14.0^\circ$ 48216				

ORIGINAL PAGE IS
OF POOR QUALITY

Table 21.- Concluded.

NACA 0012	A-01	FX-098	SC-1095	HH-02	VR-7	NLR-1	NLR-7301 ^a
k = 0.15							
$\alpha_0 = 14.5^\circ$ 31310				$\alpha_0 = 12.5^\circ$ 44303	$\alpha_0 = 12.5^\circ$ 48304		$\alpha_0 = 17.2^\circ$ 69213
				$\alpha_0 = 15.5^\circ$ 44217			
k = 0.20							
$\alpha_0 = 13.5^\circ$ 29223	$\alpha_0 = 12.0^\circ$ 23219	$\alpha_0 = 12.3^\circ$ 38201	$\alpha_0 = 12.5^\circ$ 44304	$\alpha_0 = 12.5^\circ$ 48308	$\alpha_0 = 11.1^\circ$ 63304	$\alpha_0 = 16.8^\circ$ 69201	
$\alpha_0 = 14.5^\circ$ 29304	$\alpha_0 = 14.0^\circ$ 23305	$\alpha_0 = 14.0^\circ$ 38119	$\alpha_0 = 14.0^\circ$ 44204	$\alpha_0 = 13.0^\circ$ 48200	$\alpha_0 = 15.0^\circ$ 63222	$\alpha_0 = 17.2^\circ$ 69215	
$\alpha_0 = 16.0^\circ$ 31302	$\alpha_0 = 16.0^\circ$ 23310	$\alpha_0 = 16.0^\circ$ 38110	$\alpha_0 = 15.5^\circ$ 42218	$\alpha_0 = 14.0^\circ$ 48217	$\alpha_0 = 16.4^\circ$ 63208	$\alpha_0 = 17.5^\circ$ 69223	
$\alpha_0 = 16.5^\circ$ 29309			$\alpha_0 = 17.5^\circ$ 44209	$\alpha_0 = 16.0^\circ$ 48209	$\alpha_0 = 17.0^\circ$ 63215		

^aSee table 24.

TABLE 22.- NO SEPARATION: $M_\infty = 0.30$, $\alpha = 5^\circ + 5^\circ \sin \omega t$

k	NACA 0012	A-01	FX-098	SC-1095	HH-02	VR-7	NLR-1 ^a	NLR-7301 ^a
0.01	10218							
.10	10221	25301	23107					
.20	10222	25303	23109					68211

^aSee table 24.

TABLE 23.- DYNAMIC BOUNDARY-LAYER TRIP DATA

M_∞	k	NACA 0012	A-01	FX-098	SC-1095	HH-02	VR-7	NLR-1	NLR-7301
0.18	0.05	14019	29115	17100	34318	42108	47110	64107	67019
		14104							
.18	.10	14021	29117	17103	34321	42110	47112	64109	67021
		14106							
.18	.15	14023	29119	17109	34323	42113	47114	64111	
		14108							
.18	.20								67023
.30	.025	14117	29023	17117		42019	47020	64019 ^a	(a)
		14200							
.30	.05	14119	29101	17119	34306	42021	47022	64021 ^a	(a)
		14202							
.30	.10	14208	29106	17200	34308	42100	47100	64023 ^a	(a)
		14210							

^aSee table 24.

FOR BETTER QUALITY
USE REPRODUCED COPY

ORIGINAL PAGE IS
OF POOR QUALITY

TABLE 24.- MISCELLANEOUS DYNAMIC DATA

Airfoil	Frame	M_{∞}	α_0	α_1	k	Remarks
N-0012	8019	0.035	10.0	10.0	0.10	Low Reynolds number, 0.5×10^6
	8021	.035	10.0	10.0	.15	
	8023	.035	10.0	10.0	.25	
	8104	.035	15.0	10.0	.15	Match reference 3
	8106	.035	15.0	14.0	.10	
	8116	.07	15.0	10.0	.15	Match reference 3
	8118	.07	15.0	10.0	.25	
	8123	.07	15.0	14.0	.10	Match reference 3
	8203	.07	10.0	10.0	.25	
	8210	.11	10.0	10.0	.25	Match reference 3
	8222	.18	15.0	10.0	.15	
	8306	.18	15.0	14.0	.10	Match reference 3
	9022	.18	15.0	6.0	.24	
	9101	.18	15.0	5.0	.29	Match reference 3
	9106	.18	10.0	10.0	.25	
	7108	.30	8.0	5.0	.025	Variable α_0
	7110		8.0		.10	
	7111		8.0		.20	Variable α_0
	7216		8.8		.05	
	7214		8.8		.10	Variable α_0
	7212		8.8		.15	
	7104		9.0		.025	Variable α_0
	7019		9.0		.05	
	7021		9.0		.10	Variable α_0
	7101		9.0		.15	
	7023		9.0		.20	Variable α_0
			10.0		See table 17	
	7117		11.0		.025	Variable α_0
	7118		11.0		.05	
	7119		11.0		.10	Variable α_0
7120		11.0		.15		
7121		11.0		.20	Variable α_0	
7200		12.0		.025		
7202		12.0		.05	Variable α_0	
7205		12.0		.10		
7305		12.0		.15	Variable α_0	
7207		12.0		.20		
		15.0		See table 16	Variable α_0	
10309		2.8	10.0	.10		
10305		3.8			Variable α_0	
10303		5.0				
9302		10.0			Variable α_0	
10622		12.0				
9217	.29	15.0			Variable α_0	
14220	.29	15.0				
10101	.27	20.0			Variable α_0	
10104	.30	12.0	8.0	.05		
10105	.30	12.0	8.0	.10	Match reference 17	
10108	.30	12.0	8.0	.15		
15218	.29	15.0	10.0	.10	Pressure orifices closed	

TABLE 24.- Continued.

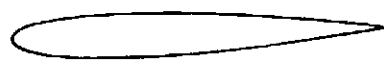
Airfoil	Frame	M_{∞}	α_0	α_1	k	Remarks
N-0012	Many	Variable	Variable	10.0	0.001	Quasi-static; see table 12
W-098	23117	0.30	5.0	10.0	.10	
Ames-01	30201		11.0	5.0	.01	
Ames-01	25214				.05	
Ames-01	25216				.10	
SC-1095	39110				.01	
	37219				.05	
	37221				.10	
	37304		12.0	8.0	.05	Match reference 18
	37305		12.0	8.0	.10	Match reference 18
	37306		12.0	8.0	.13	Match reference 18
HH-02	43314		11.0	5.0	.025	
HH-02	43315		11.0	5.0	.05	
HH-02	43316		11.0	5.0	.10	
VR-7	54019	.18	10.0	10.0	.025	
	54022		10.0		.05	
	54101		10.0		.10	
	54110		10.0		.15	
	54113		10.0		.20	
	54116		10.0		.25	
	49023		15.0		.01	
	49110				.025	
	49117				.05	
	49120				.10	
	58121				.10	
	49203				.15	
	54216				.15	
	57018				.15	
	58018				.15	
	58120				.15	
	49206				.20	
NLR-1	65223	.11	7.0	5.0	.025	No separation
	65300	.11	7.0	5.0	.20	No separation
	62114	.20	15.0	10.0	.10	
	65207	.20	15.0	10.0	.10	
	62121	.20	10.0	10.0	.17	Match reference 19
	62202	.20	15.0	5.0	.17	
	62201	.20	15.0	5.0	.28	
	62403	.30	10.0	10.0	.12	
	63100		15.0	5.0	.12	
	63122		12.0	8.0	.12	
	65309		7.0	5.0	.01	No separation
	65311		7.0	5.0	.20	No separation
	65121		-2.0	10.0	.01	Stall at negative α
	65122				.025	Stall at negative α
	65123				.05	Stall at negative α
	65200				.10	Stall at negative α
NLR-1T	64212				.01	Trip; stall at negative α
NLR-1T	64213				.025	Trip; stall at negative α
NLR-1T	64214				.05	Trip; stall at negative α

TABLE 24.- Concluded.

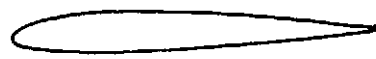
Airfoil	Frame	M_{∞}	α_0	α_1	k	Remarks
NLR-1T	64215	0.30	-2.0	10.0	0.10	Trip; stall at negative α
NLR-1T	64119	.30	2.5		.01	Trip; stall suppression
NLR-1T	64121	.30	2.5		.025	Trip; stall suppression
NLR-1T	64202	.30	2.5		.05	Trip; stall suppression
NLR-1T	64204	.30	2.5		.10	Trip; stall suppression
NLR-7	67201	.11	10.0		.10	
	67208	.18	10.0		.025	
	67210	.18	10.0		.10	
	67212	.18	10.0		.20	
	67218	.18	15.0		.025	
	67220	.18	15.0		.10	
	67222	.18	15.0		.20	
	67310	.25	10.0		.10	
	68219	.30	12.0	2.0	.05	No separation
	68221	.30	12.0	2.0	.10	No separation
	68304	.30	12.0	2.0	.20	No separation
NLR-7T	67108	.30	10.0	5.0	.025	Trip
NLR-7T	67110	.30	10.0	5.0	.05	Trip
NLR-7T	67112	.30	10.0	5.0	.10	Trip

TABLE 25.- TEST CASES FOR NUMERICAL ANALYSIS (ref. 1)

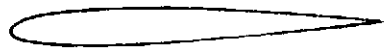
Case	Frame	Airfoil	α_0	α_1	k	Case	Frame	Airfoil	α_0	α_1	k
1	10222	NACA 0012	5	5	0.20	7	10212	NACA 0012	10	5	0.20
2	68211	NLR-7301	5			8	9302		10	10	.10
3	7111	NACA 0012	8			9	10113		15	5	.01
4	68203	NLR-7301	10				10114				.025
5	7023	NACA 0012	9				10117				.05
6	45221	VR-7	10		.025		10118				.10
	45223				.05		10120				.15
	45300				.10		10123				.20
	45302				.15	10	45203	VR-7			.01
	45303				.20		45205				.025
7	10202	NACA 0012			.01		45207				.05
	10203				.025		45209				.10
	10204				.05		45211				.15
	10208				.10		45213				.20
	10211				.15						



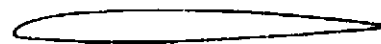
NACA 0012



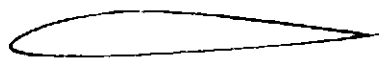
AMES-01



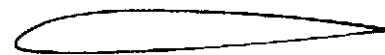
SIKORSKY SC-1095



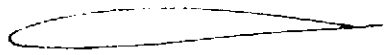
NLR-1



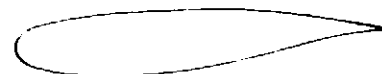
VERTOL VR 7



WORTMANN FX-098



HUGHES HH-02



NLR-7301 SUPERCRITICAL

Figure 1.- Airfoils tested in the experiment.

ORIGINAL PAGE IS
OF POOR QUALITY

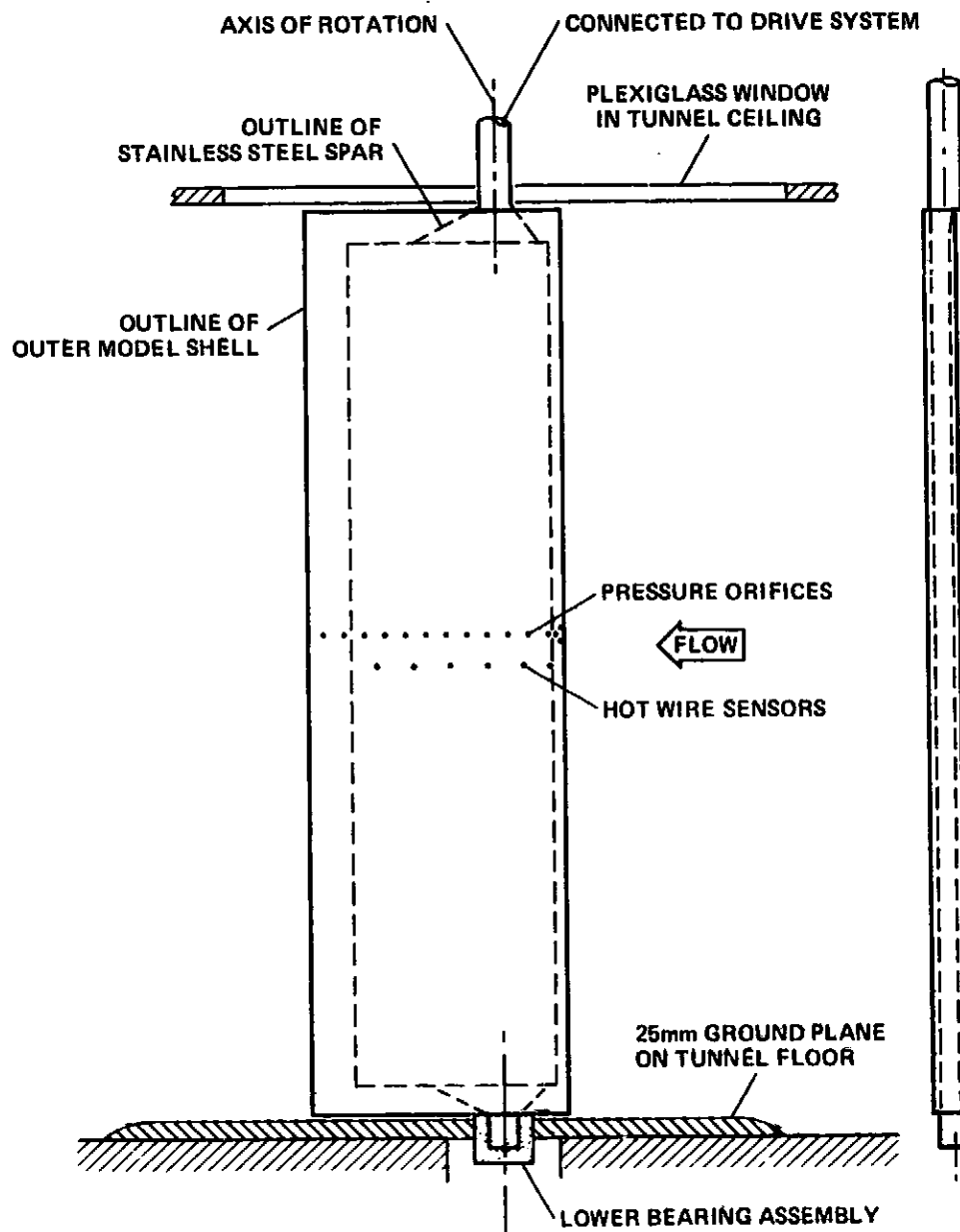


Figure 2.- Model installation in the test section.

ORIGINAL PAGE IS
OF POOR QUALITY

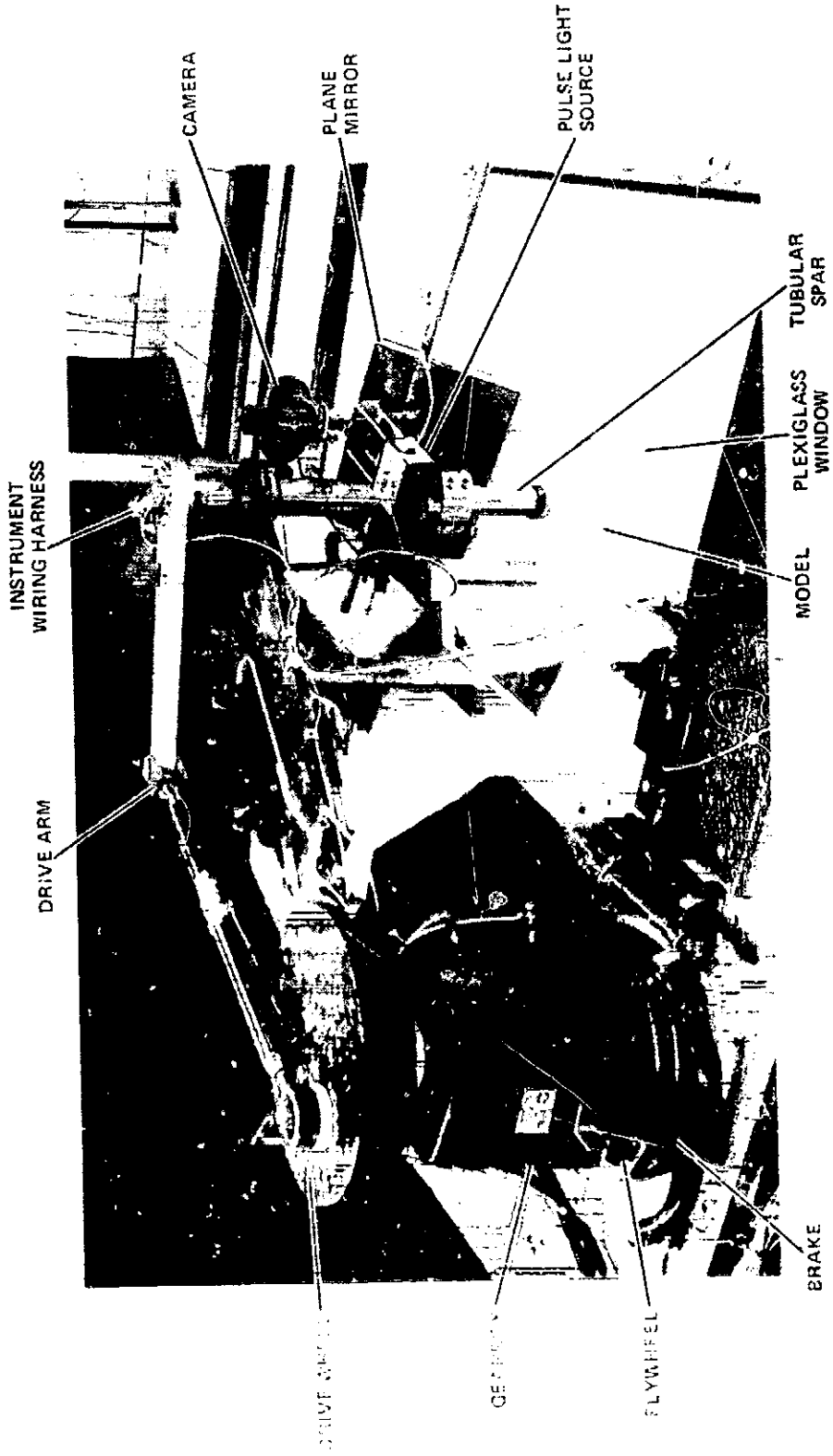
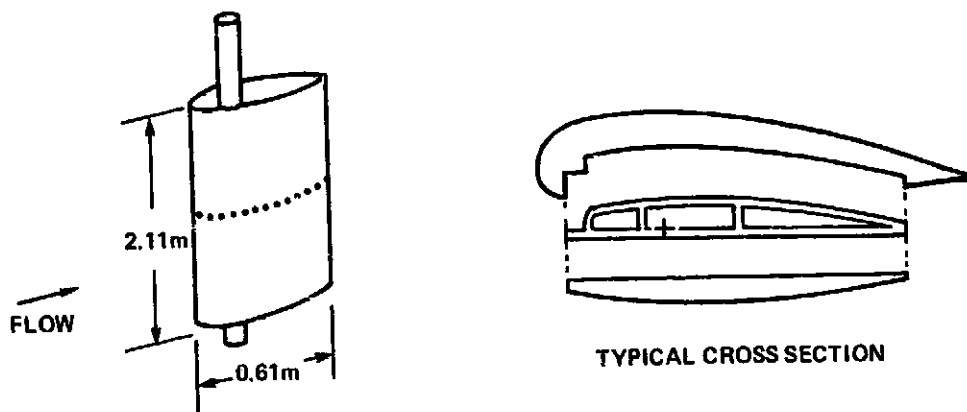


Figure 3.- Photograph of the oscillation mechanism.

ORIGINAL PAGE IS
OF POOR QUALITY



WOODEN UPPER SHELL
WITH FIBERGLASS SKIN

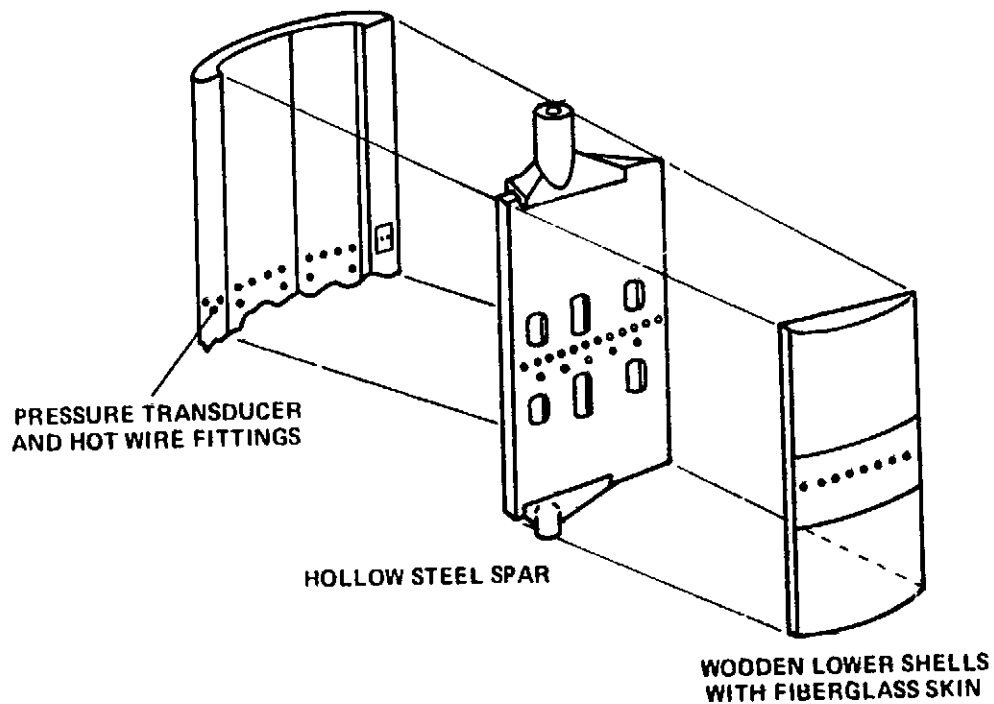


Figure 4.- Sketch of the wooden model shells surrounding the steel spar.

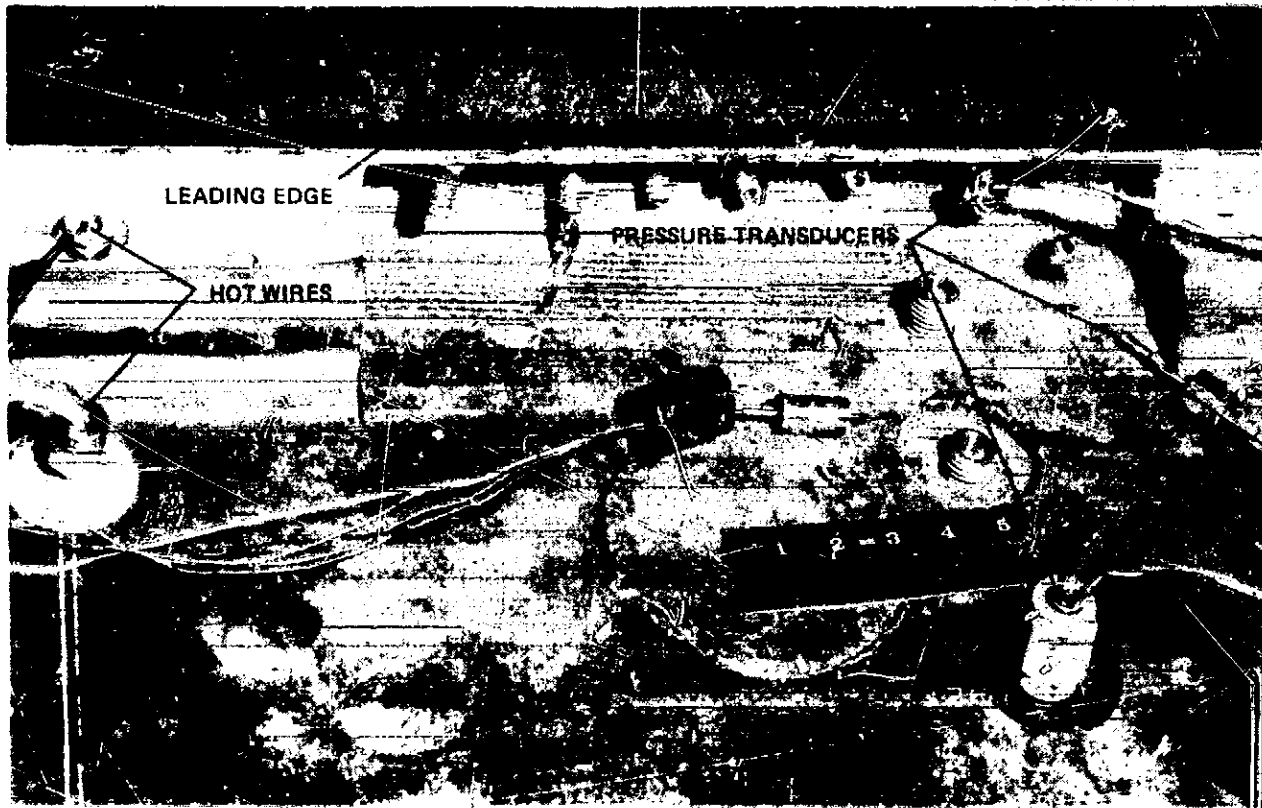


Figure 5.- Pressure transducer and hot-wire installation: view from inside the upper-surface shell.

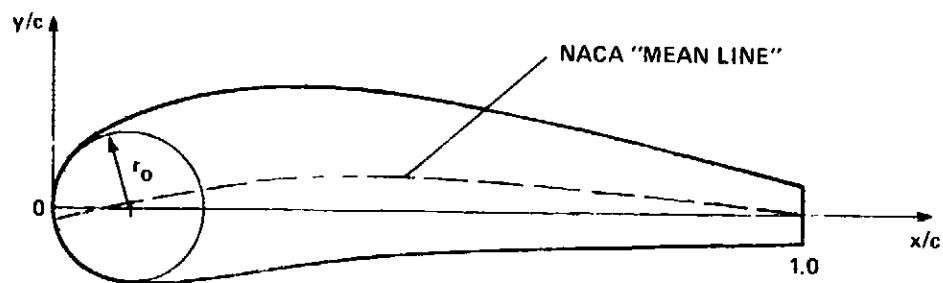


Figure 6.- Coordinate axes for the airfoils.

ORIGINAL PAGE
BLACK AND WHITE PHOTOGRAPH

ORIGINAL COPY
OF POOR QUALITY

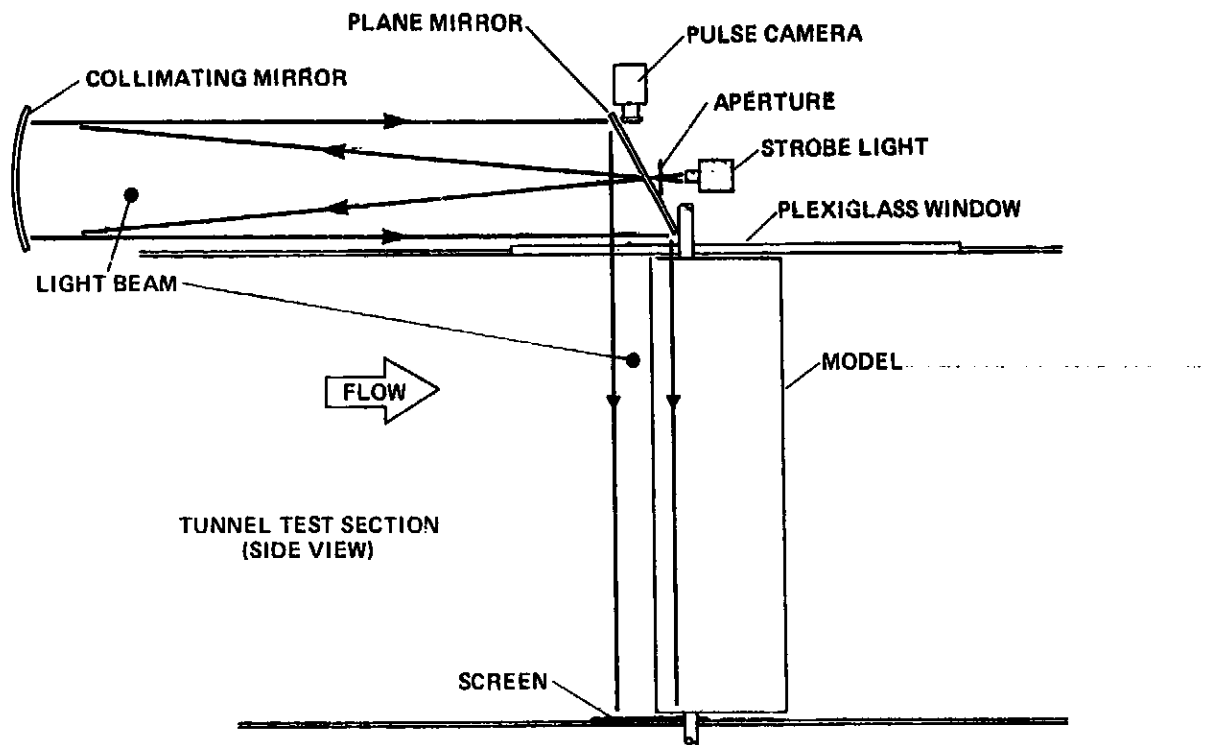


Figure 7.- Sketch of the shadowgraph system for visualizing the leading-edge region.

ORIGINAL PAGE
BLACK AND WHITE PHOTOGRAPH

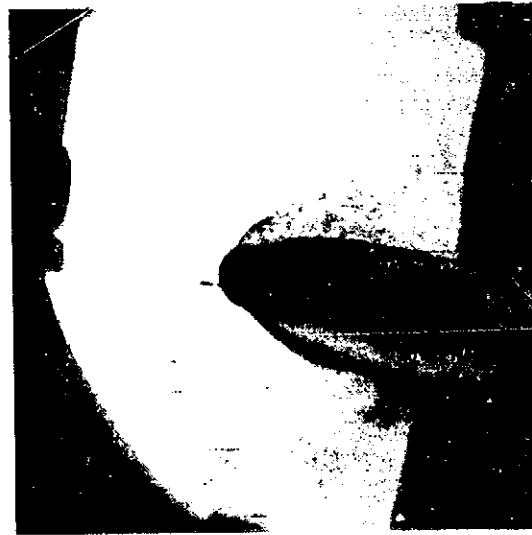
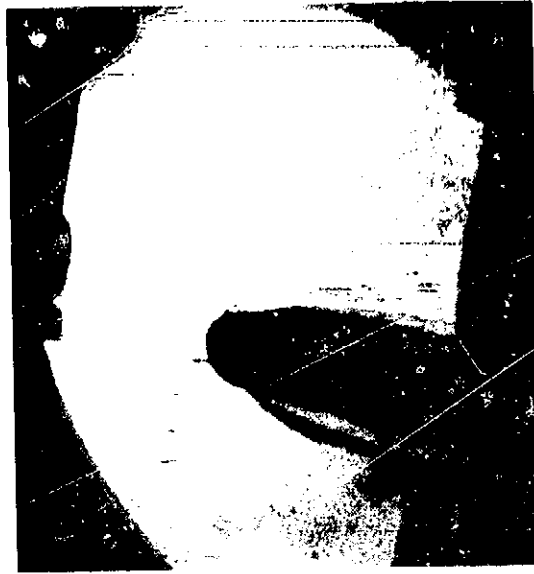


Figure 8.- Representative shadowgraphs before (upper) and during (lower) dynamic stall: Sikorsky SC-1095 airfoil, $M_{\infty} = 0.30$, $\alpha = 10^{\circ} + 10^{\circ} \sin \omega t$, $k = 0.10$.

ORIGINAL REPORT
OF POOR QUALITY

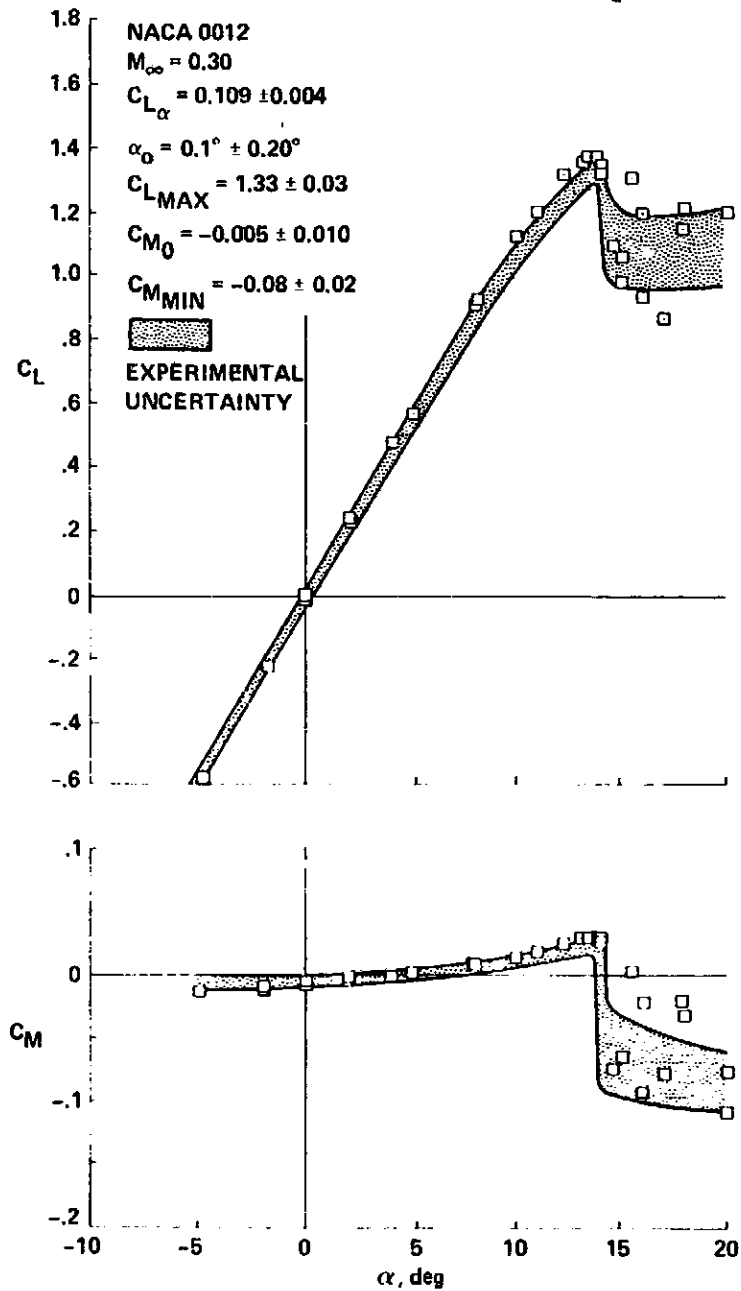


Figure 9.- Static lift and moment data on the NACA 0012 airfoil at $M_\infty = 0.3$; shaded bands represent uncertainty limits of data corrected for wind-tunnel-wall effects.

ORIGINAL PAGE IS
OF POOR QUALITY

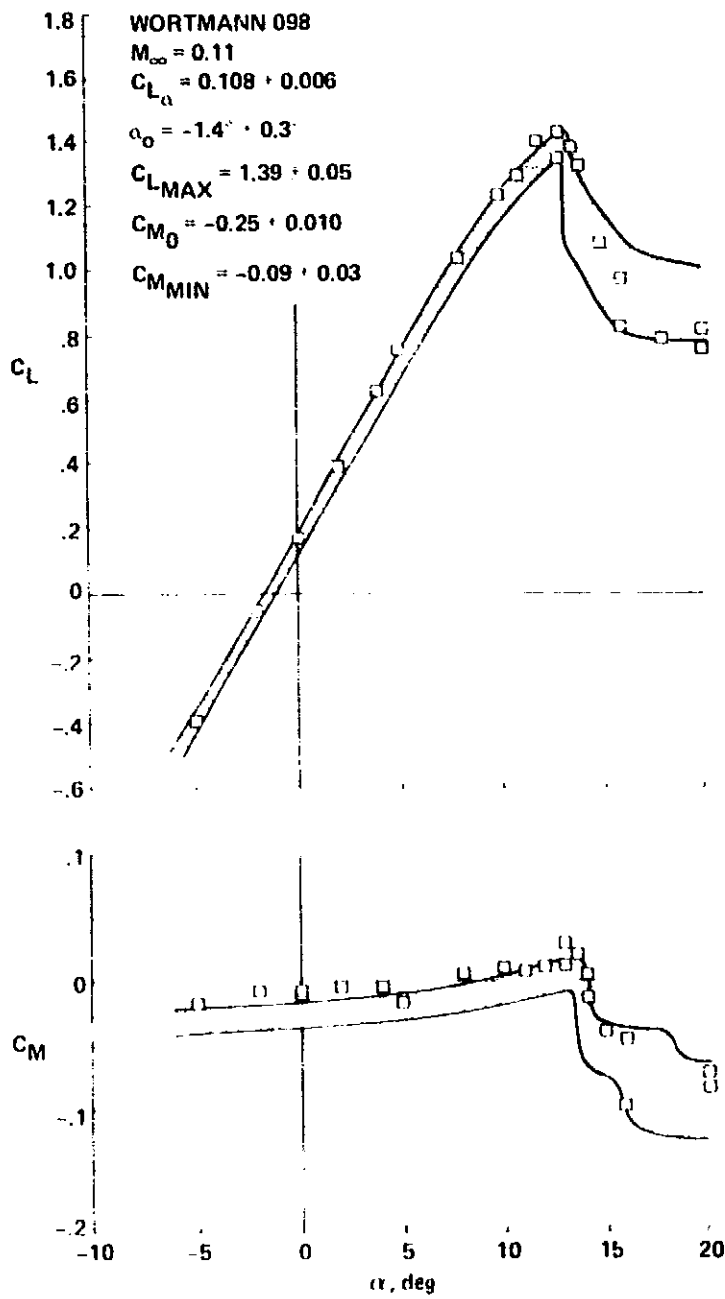


Figure 10.- Static lift and moment data on the Wortmann FX-098 airfoil
at $M_\infty = 0.11$.

ORIGINAL PAGE IS
OF POOR QUALITY

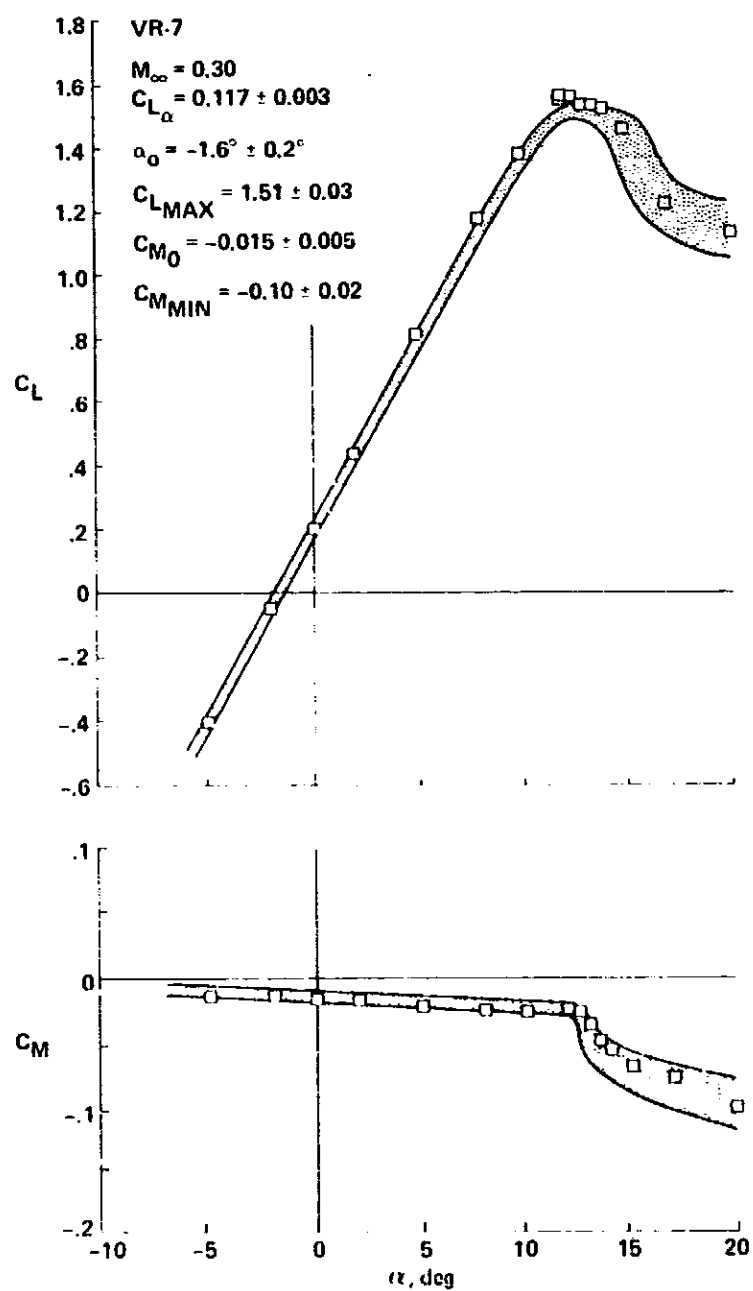


Figure 11.- Static lift and moment data on the Vertol VR-7 airfoil
at $M_{\infty} = 0.30$.

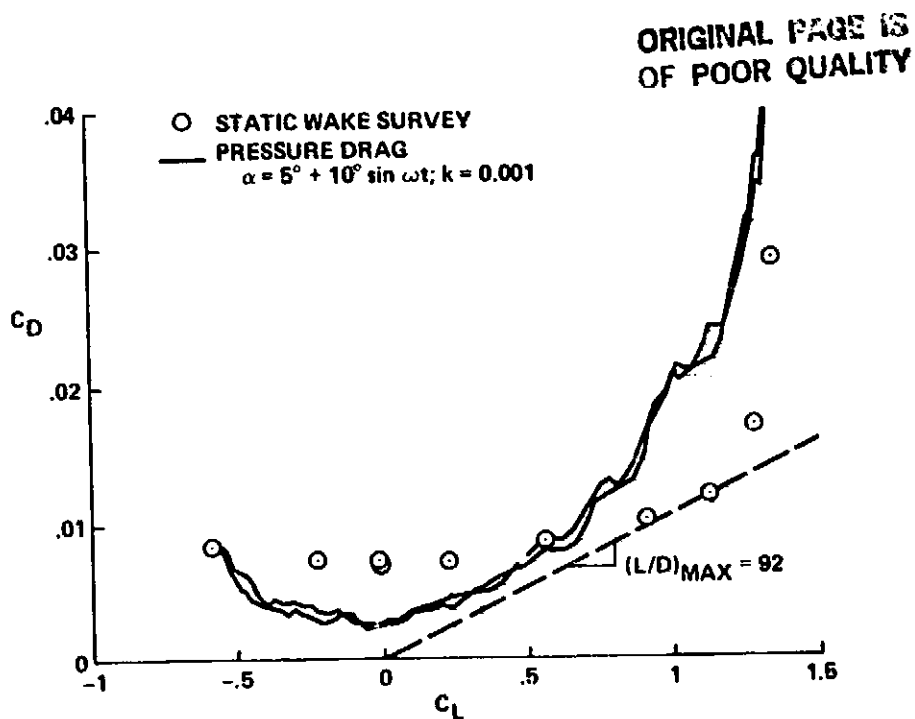


Figure 12.- Comparison of measured lift-drag polars for the NACA 0012 airfoil at $M_\infty = 0.30$, including wind-tunnel-wall corrections.

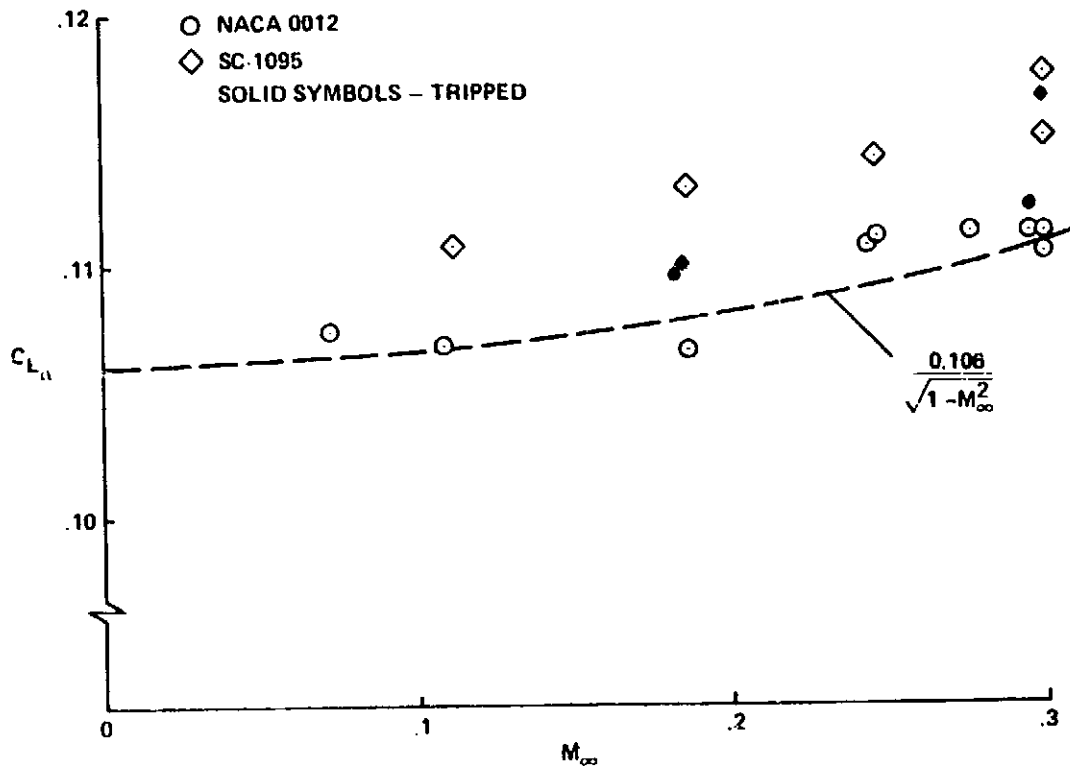


Figure 13.- Comparison of lift-curve slopes on the NACA 0012 and SC-1095 airfoils, including wind-tunnel-wall corrections.

ORIGINAL PAGE IS
OF POOR QUALITY

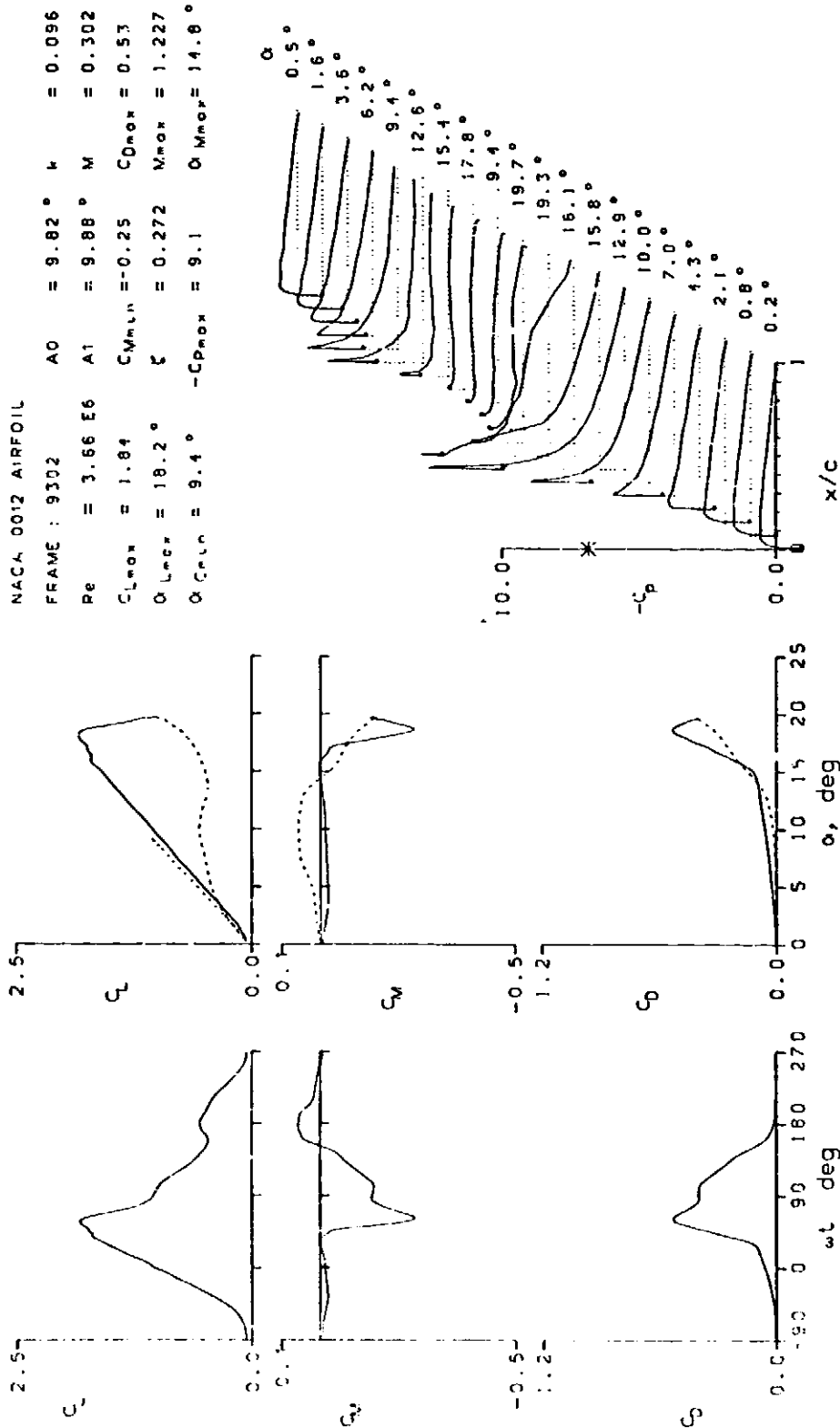


Figure 14.- Typical data presentation from volume 2; no wall corrections.

ORIGINAL PAGE IS
OF POOR QUALITY

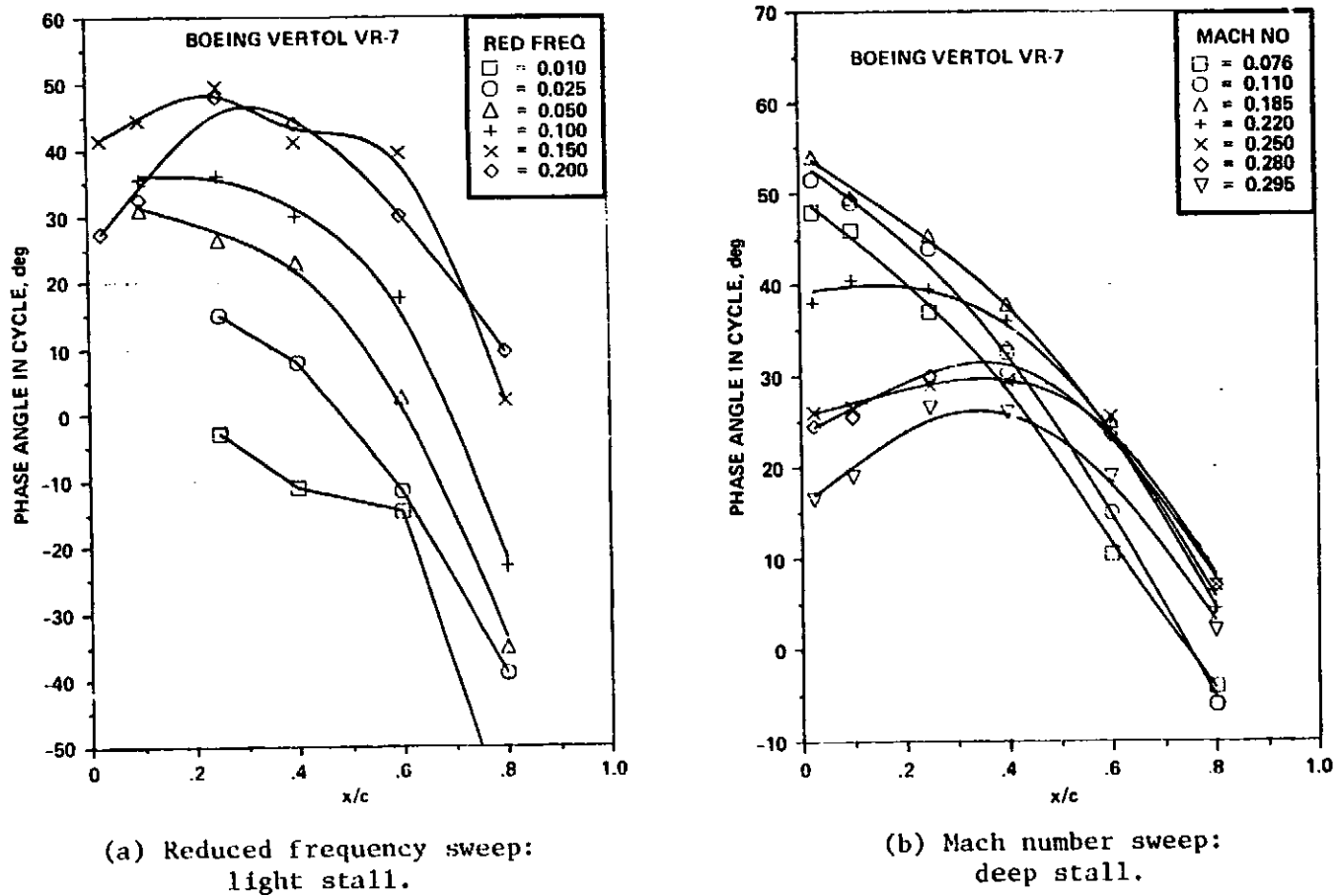


Figure 15.- Typical data presentation from volume 3.

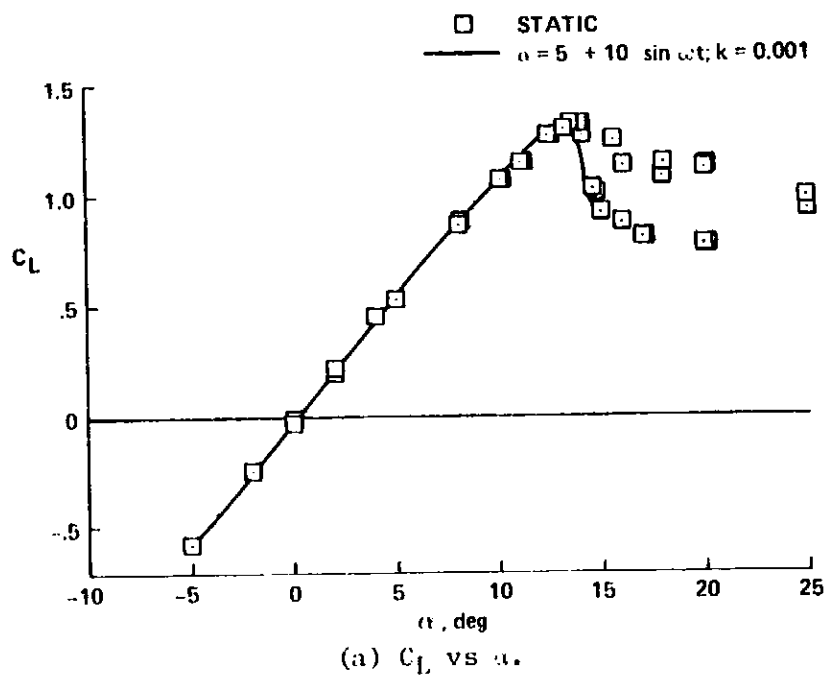
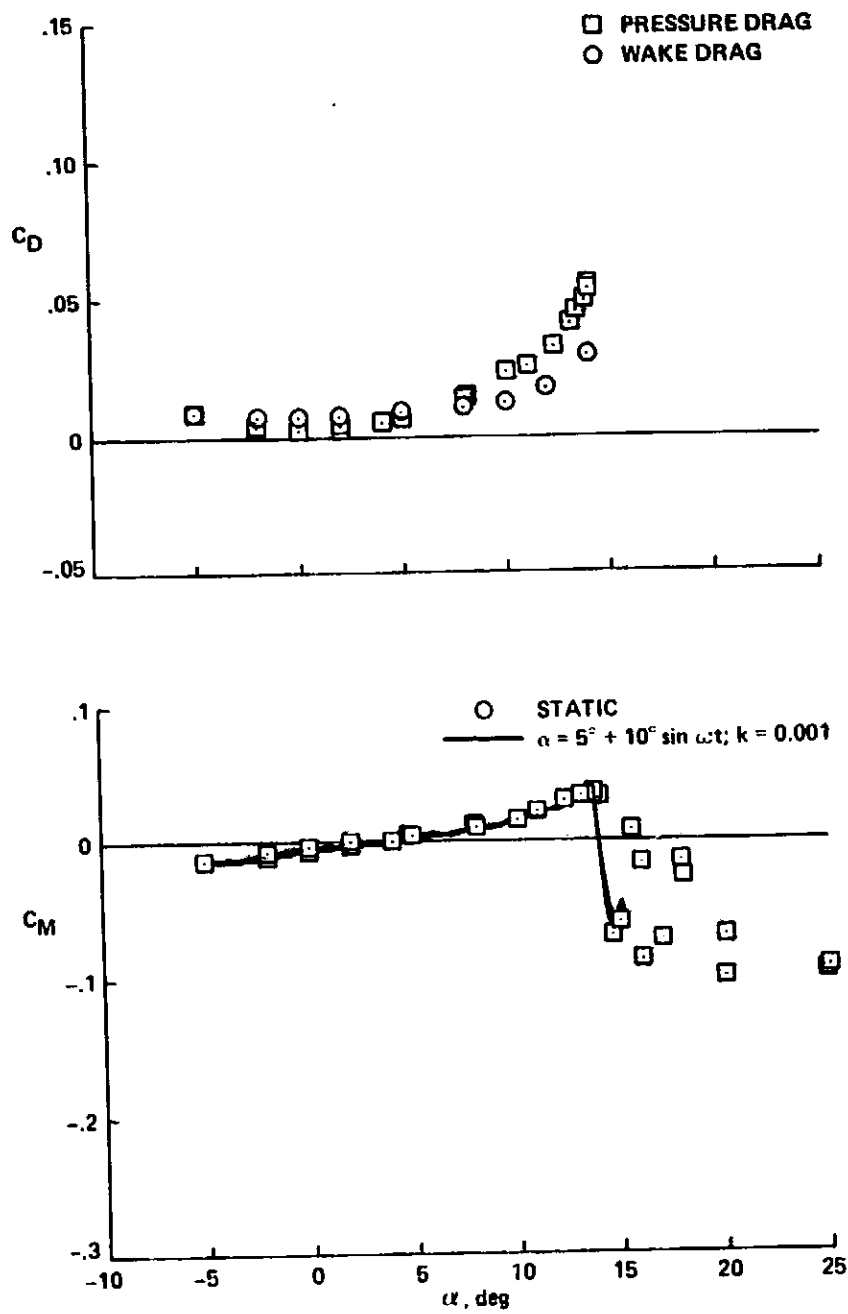


Figure 16.- Static characteristics of the NACA 0012 airfoil at $M_\infty = 0.30$, including wind-tunnel-wall corrections.

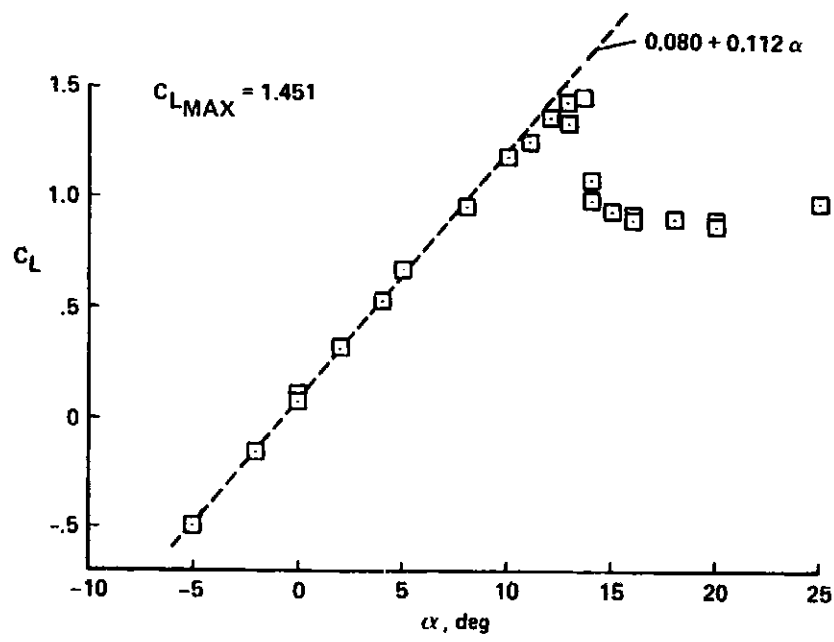
ORIGINAL PAGE IS
OF POOR QUALITY



(b) C_D and C_M vs α .

Figure 16.- Concluded.

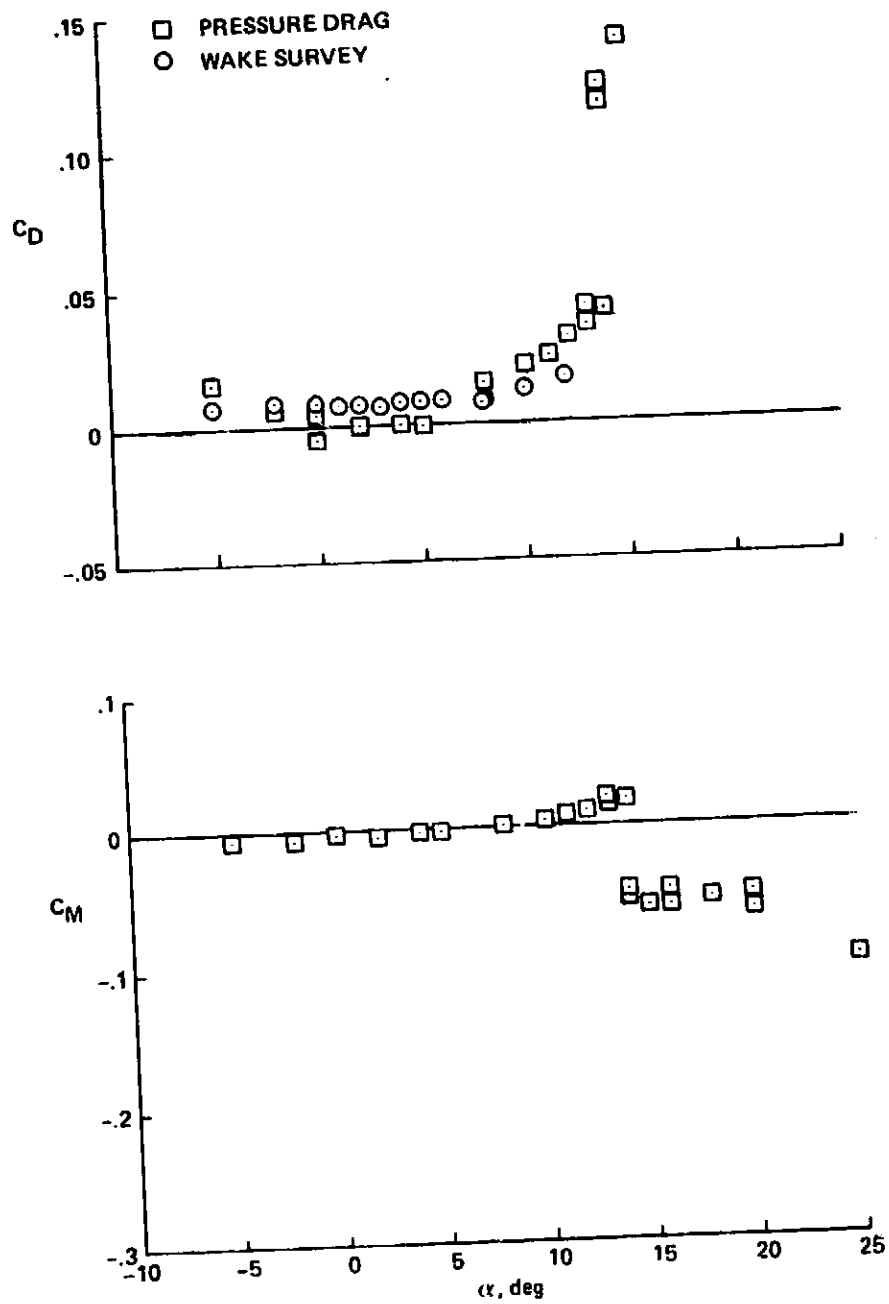
ORIGINAL PAGE IS
OF POOR QUALITY



(a) C_L vs α .

Figure 17.- Static characteristics of the Ames A-01 airfoil at $M_\infty = 0.30$, including wind-tunnel-wall corrections.

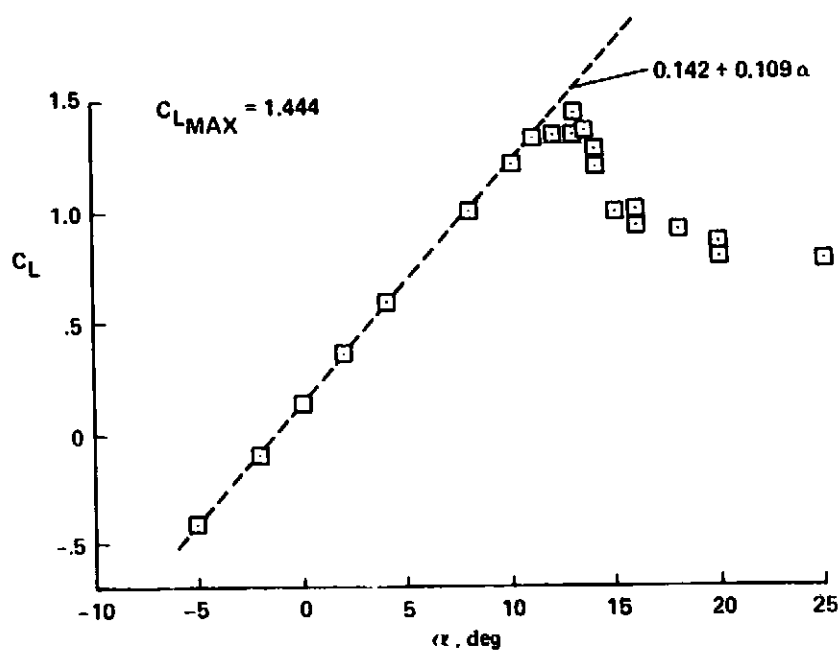
ORIGINAL PAGE IS
OF POOR QUALITY



(b) C_D and C_M vs α .

Figure 17.- Concluded.

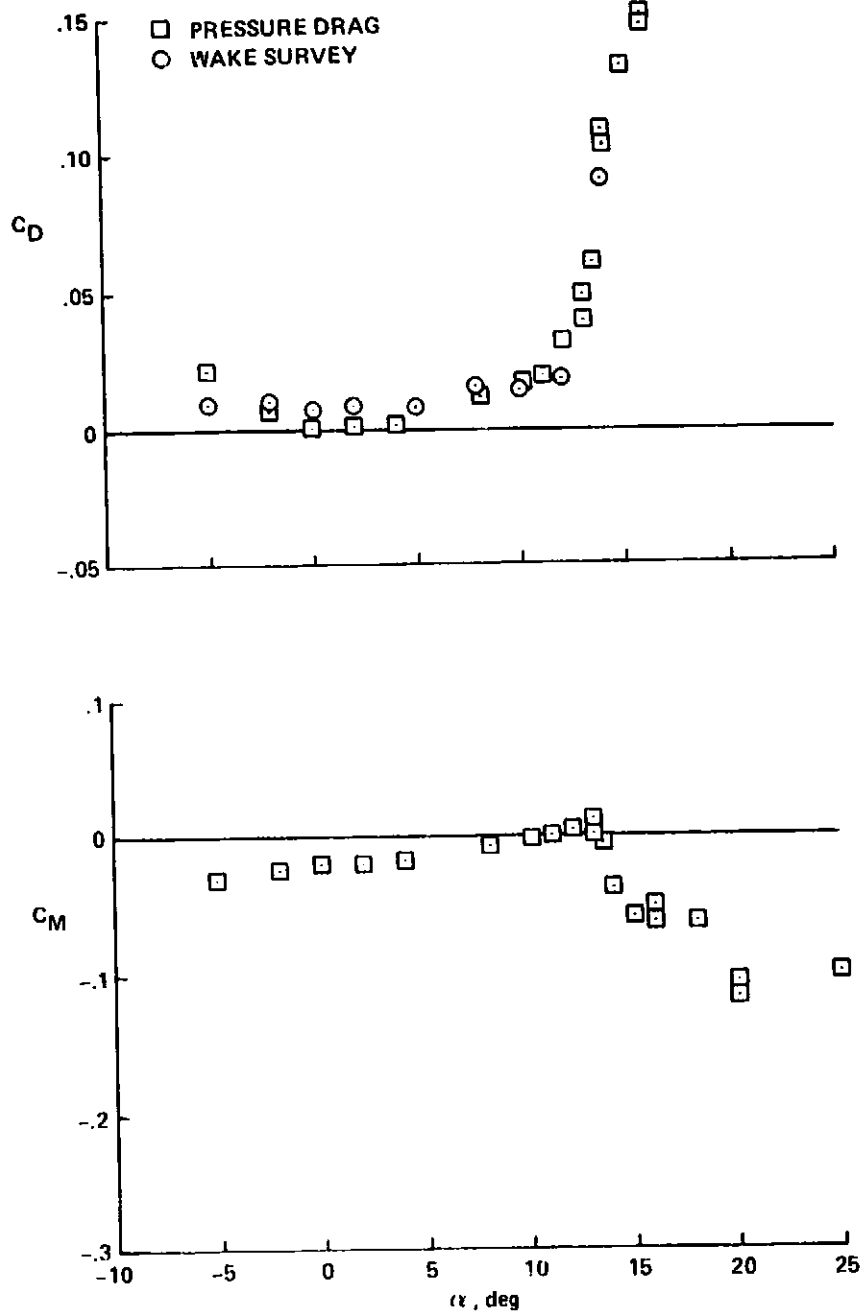
ORIGINAL PAGE IS
OF POOR QUALITY



(a) C_L vs α .

Figure 18.- Static characteristics of the Wortmann FX-098 airfoil at $M_\infty = 0.30$, including wind-tunnel-wall corrections.

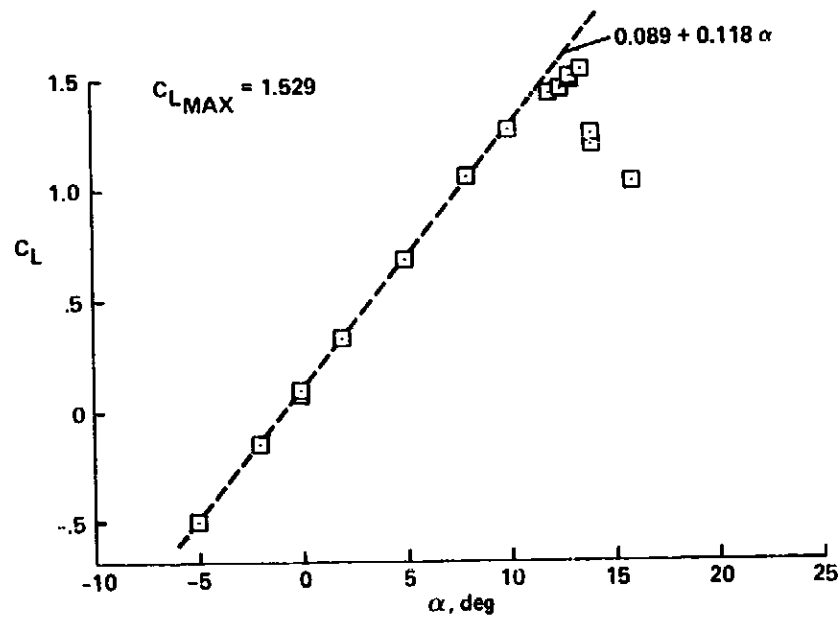
ORIGINAL PAGE IS
OF POOR QUALITY



(b) C_n and C_M vs α .

Figure 18.- Concluded.

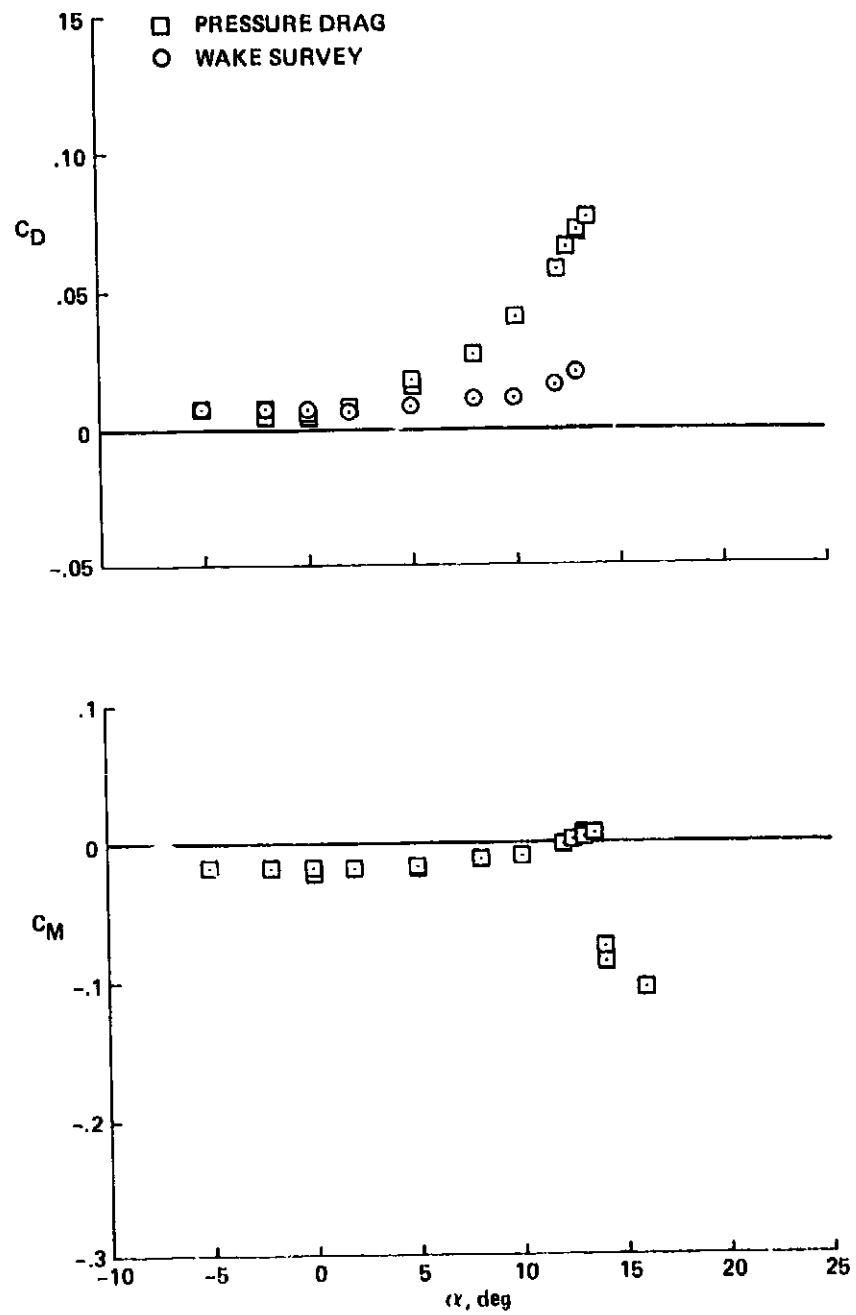
ORIGINAL PAGE IS
OF POOR QUALITY



(a) C_L vs α .

Figure 19.- Static characteristics of the Sikorsky SC-1095 airfoil at $M_\infty = 0.30$, including wind-tunnel-wall corrections.

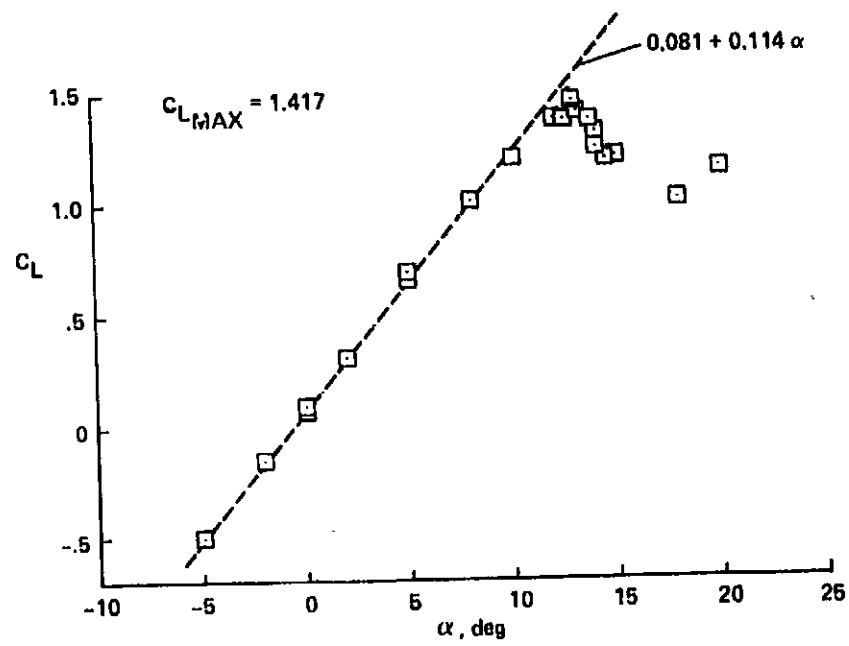
ORIGINAL PAGE 13
OF POOR QUALITY



(b) C_D and C_M vs α .

Figure 19.- Concluded.

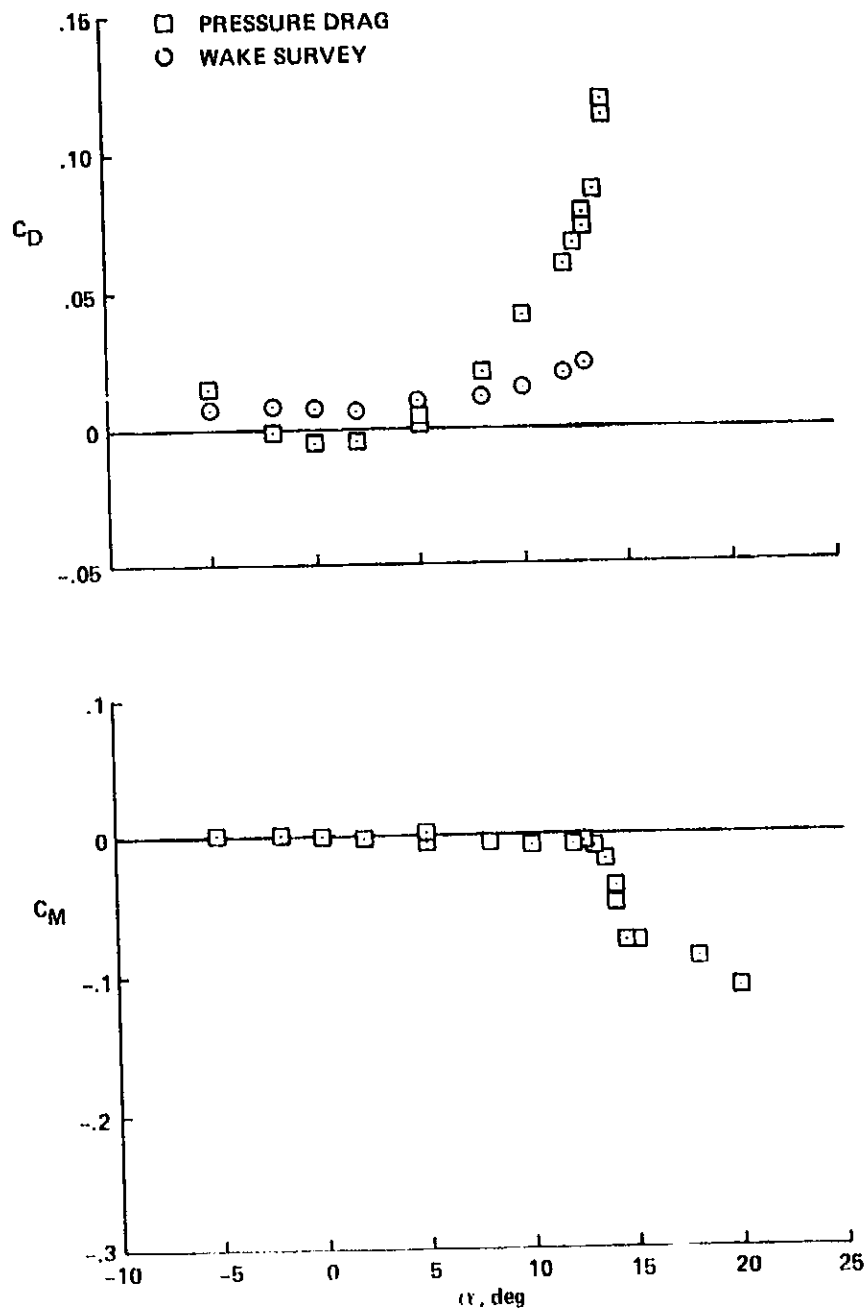
ORIGINAL PAGE IS
OF POOR QUALITY



(a) C_L vs α .

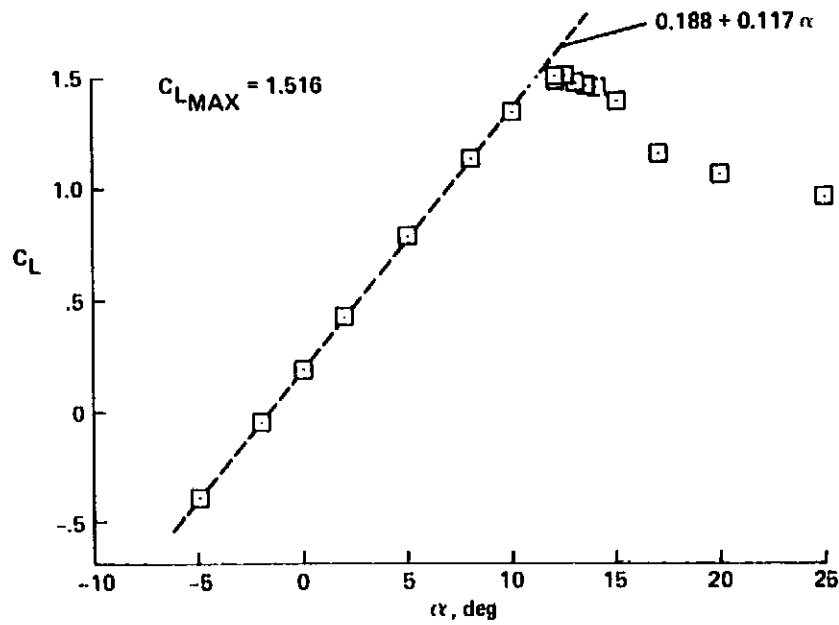
Figure 20.- Static characteristics of the Hughes HH-02 airfoil at $M_\infty = 0.30$, including wind-tunnel-wall corrections.

ORIGINAL PAGE IS
OF POOR QUALITY



(b) C_D and C_M vs α .
Figure 20.- Concluded.

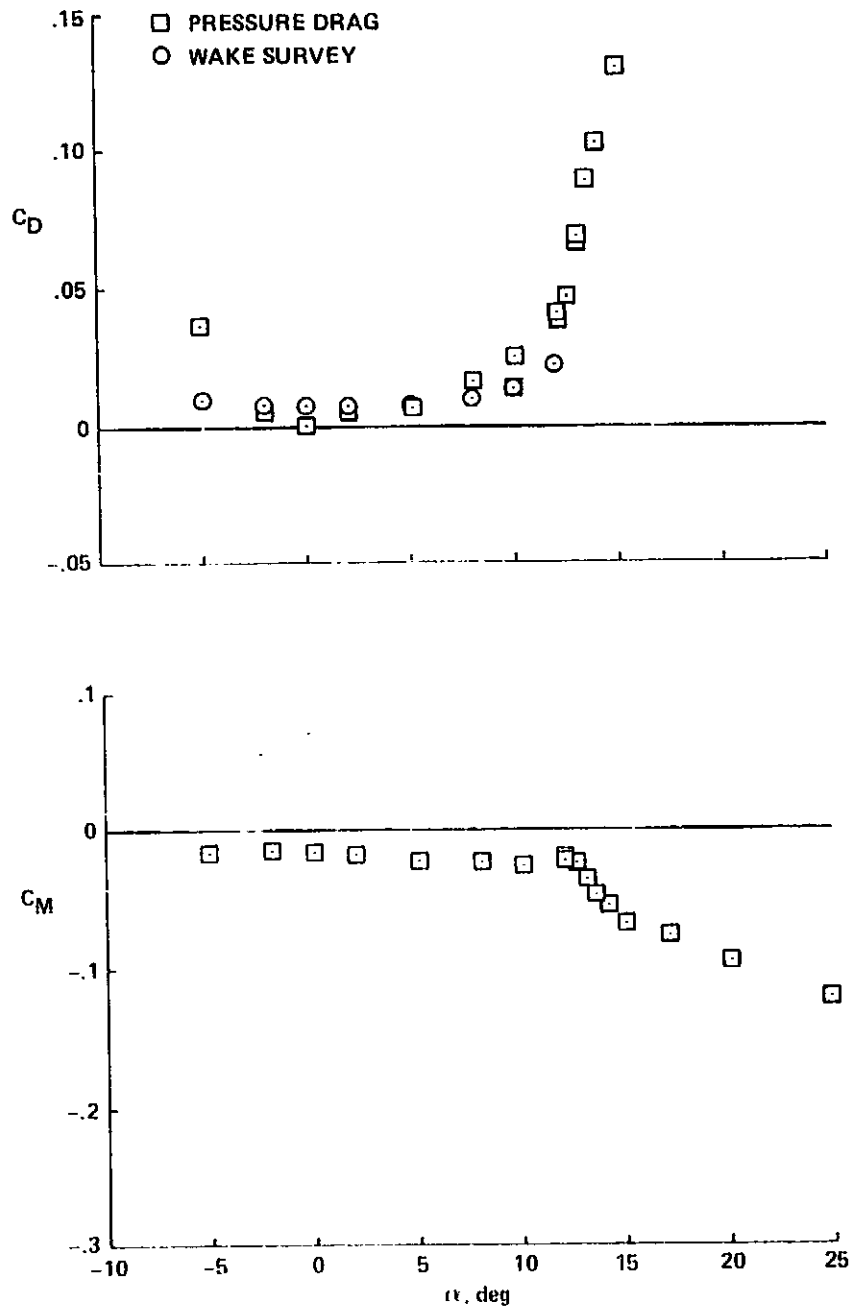
ORIGINAL PAGE IS
OF POOR QUALITY



(a) C_L vs α .

Figure 21.- Static characteristics of the Vertol VR-7 airfoil at $M_\infty = 0.30$, including wind-tunnel-wall corrections.

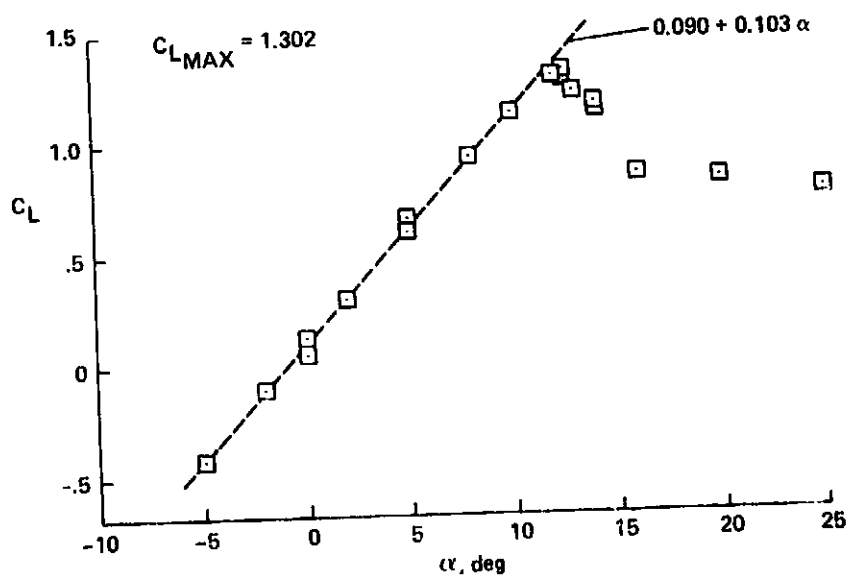
ORIGINAL SOURCE
BY THE NATIONAL



(b) C_D and C_M vs α .

Figure 21.- Concluded.

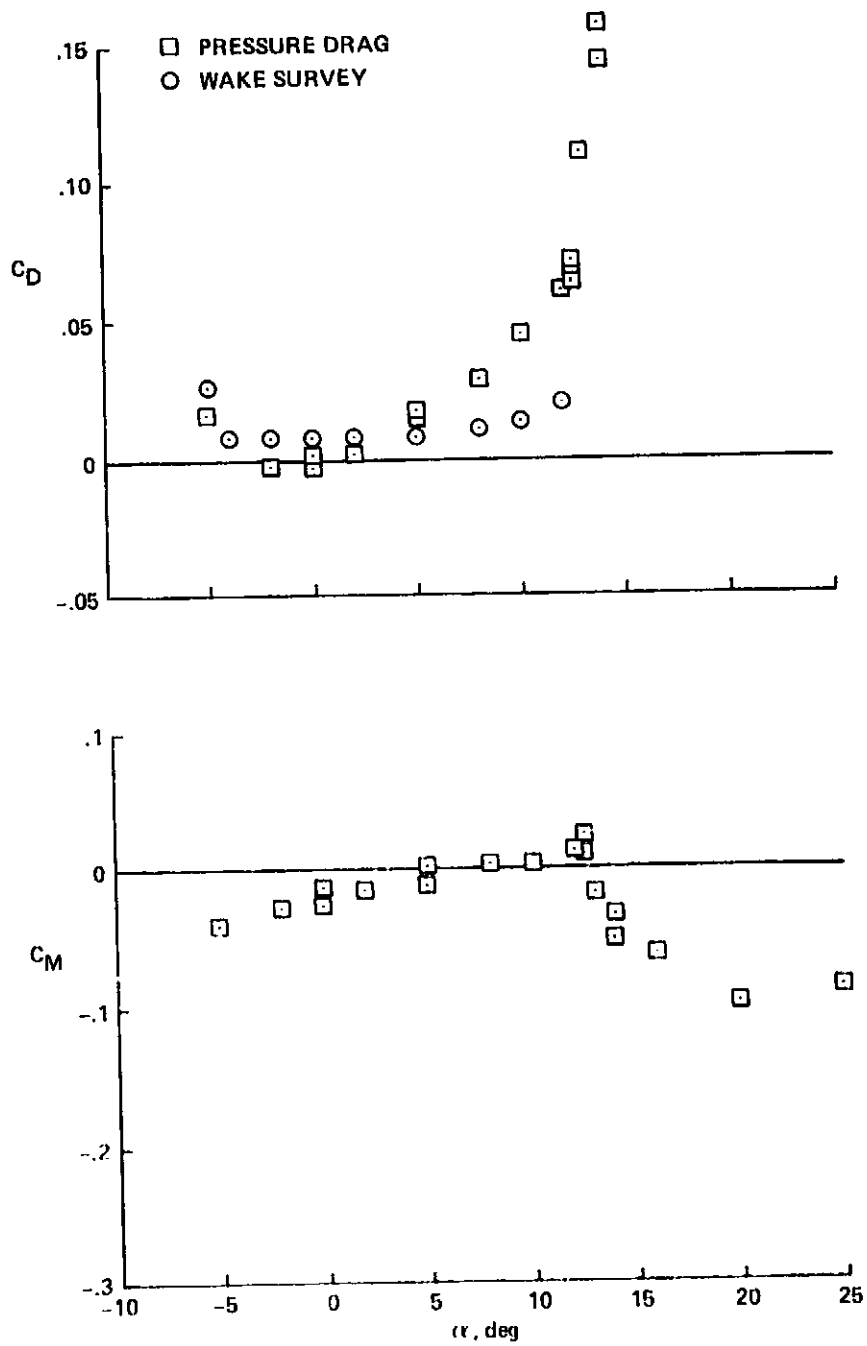
REPRODUCED FROM
OF POOR QUALITY



(a) C_L vs α .

Figure 22.- Static characteristics of the NLR-1 airfoil at $M_\infty = 0.30$, including wind-tunnel-wall corrections.

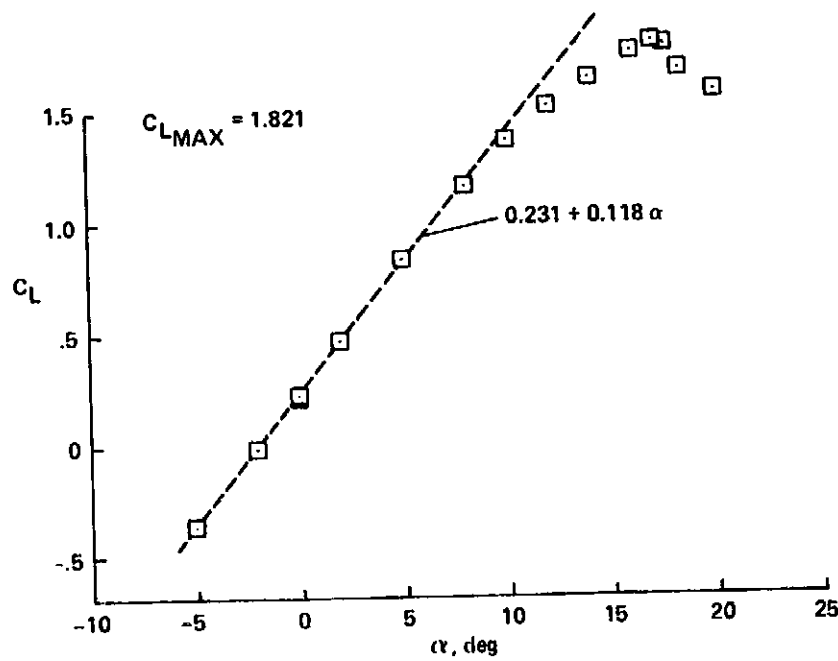
ORIGINAL PAGE IS
OF POOR QUALITY



(b) C_D and C_M vs α .

Figure 22.- Concluded.

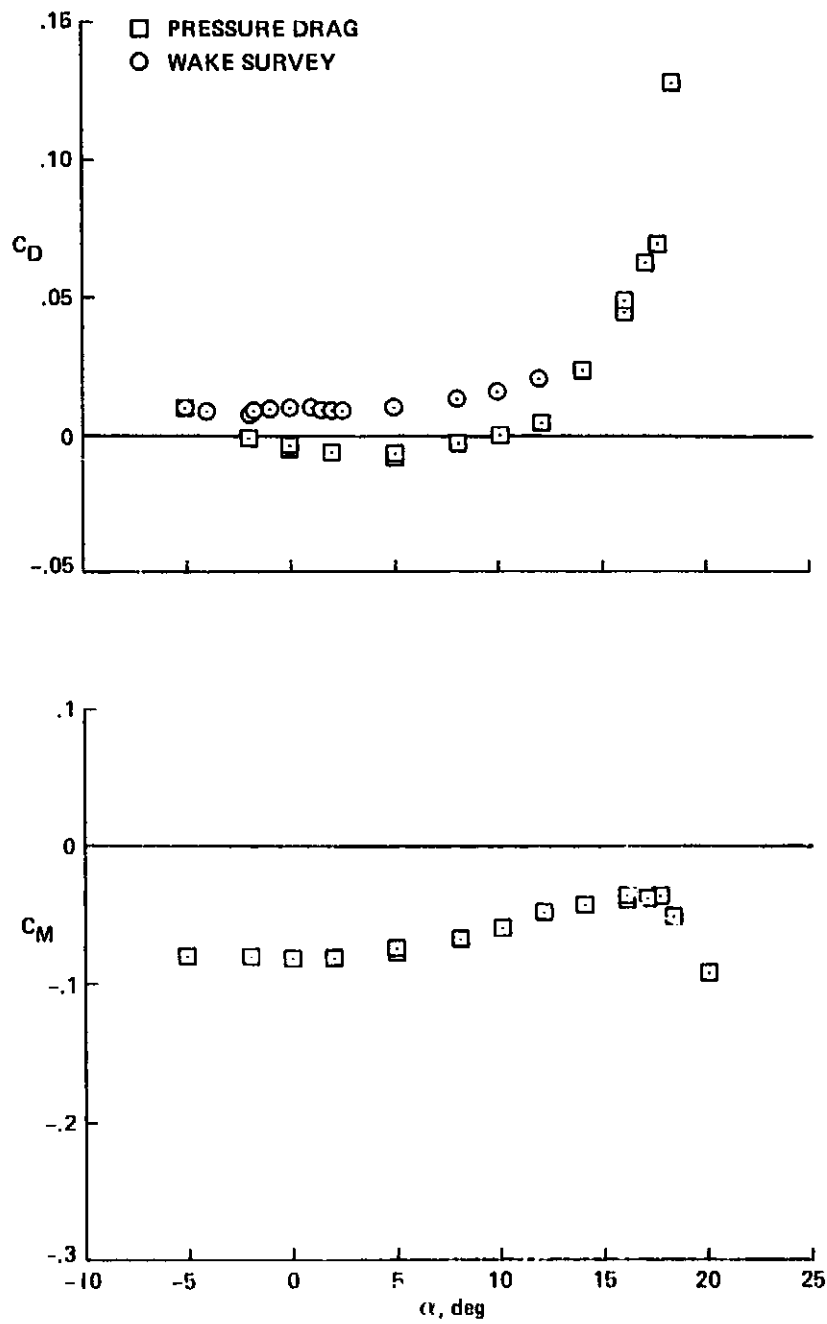
ORIGINAL PAGE IS
OF POOR QUALITY



(a) C_L vs α .

Figure 23.- Static characteristics of the NLR-7301 airfoil at $M_\infty = 0.30$, including wind-tunnel-wall corrections.

ORIGINAL PAGE IS
OF POOR QUALITY



(b) C_D and C_M vs α .

Figure 23.- Concluded.

ORIGINAL PAGE IS
OF POOR QUALITY

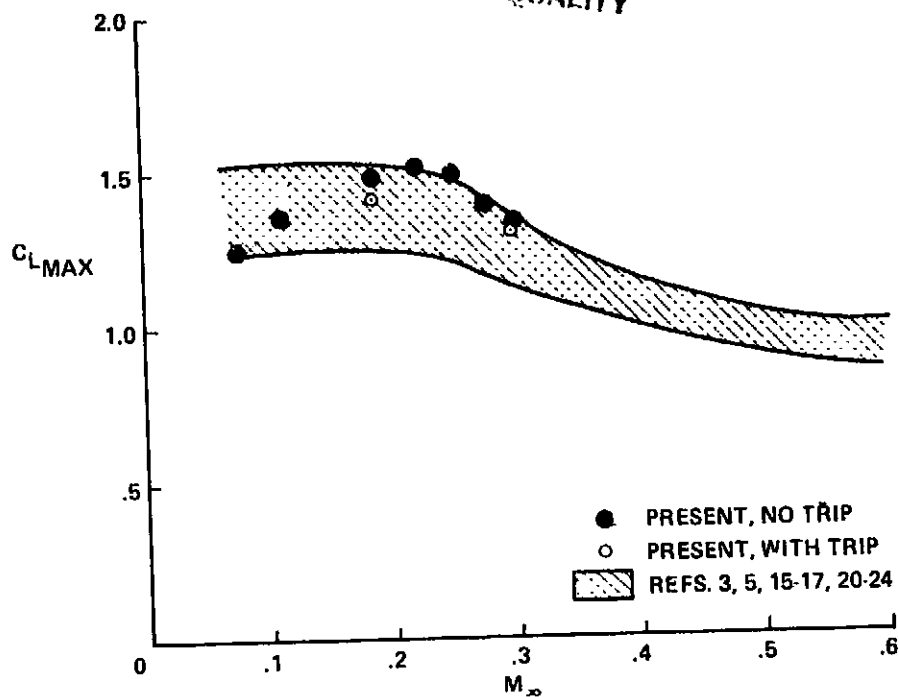


Figure 24.- Comparison of maximum static lift on the NACA 0012 airfoil.

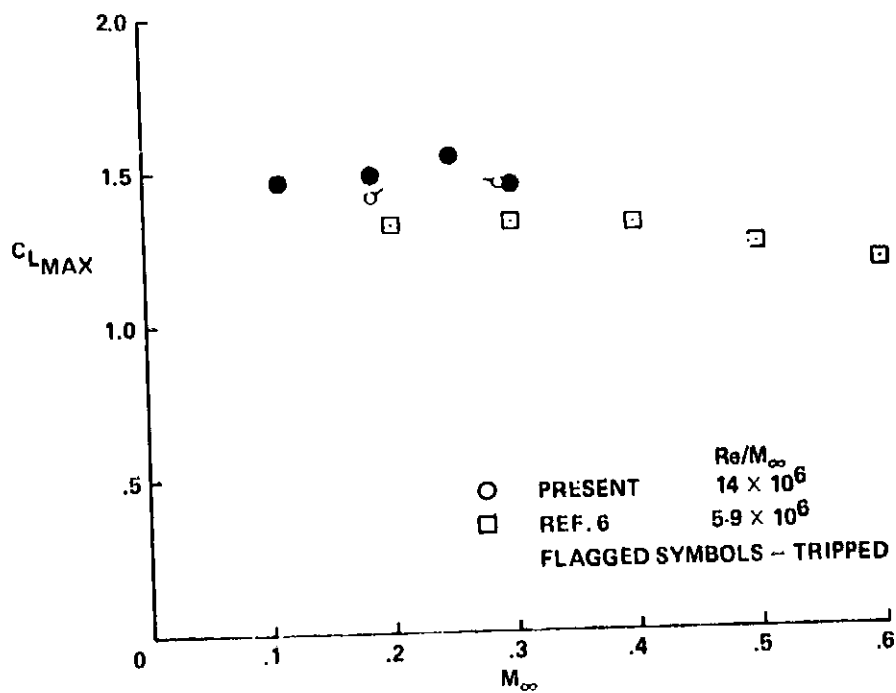


Figure 25.- Comparison of maximum static lift on the Ames A-01 airfoil.

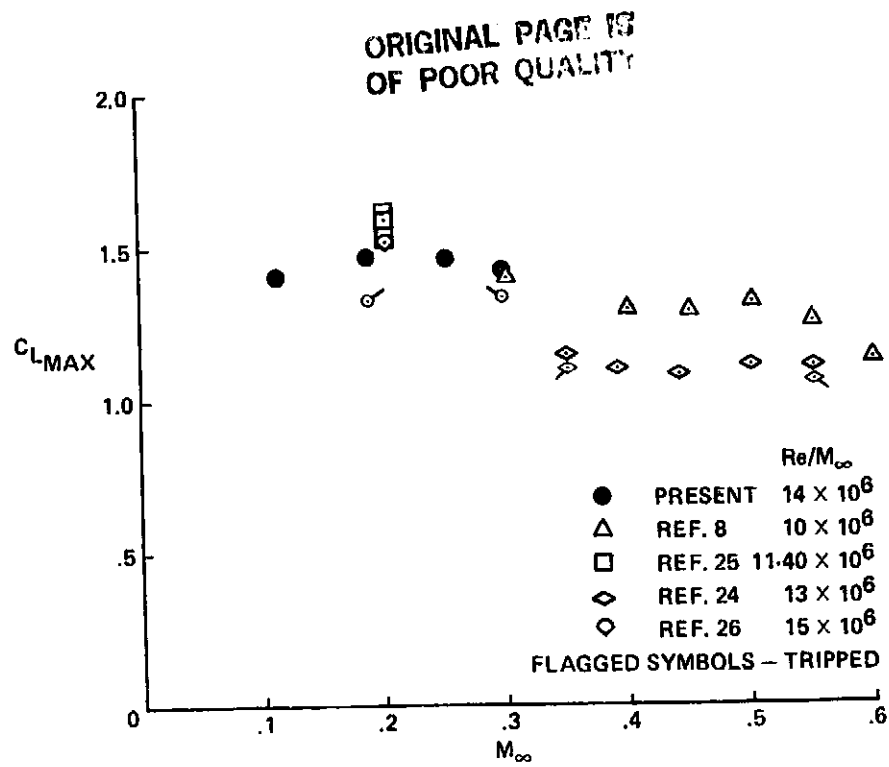


Figure 26.- Comparison of maximum static lift on the Wortmann FX-098 airfoil.

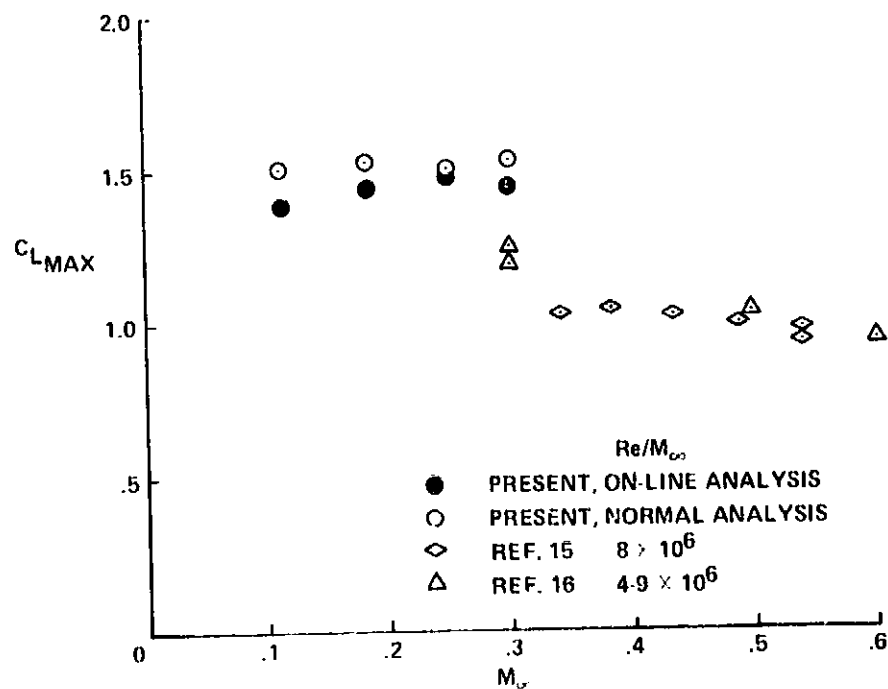


Figure 27.- Comparison of maximum static lift on the Sikorsky SC-1095 airfoil.

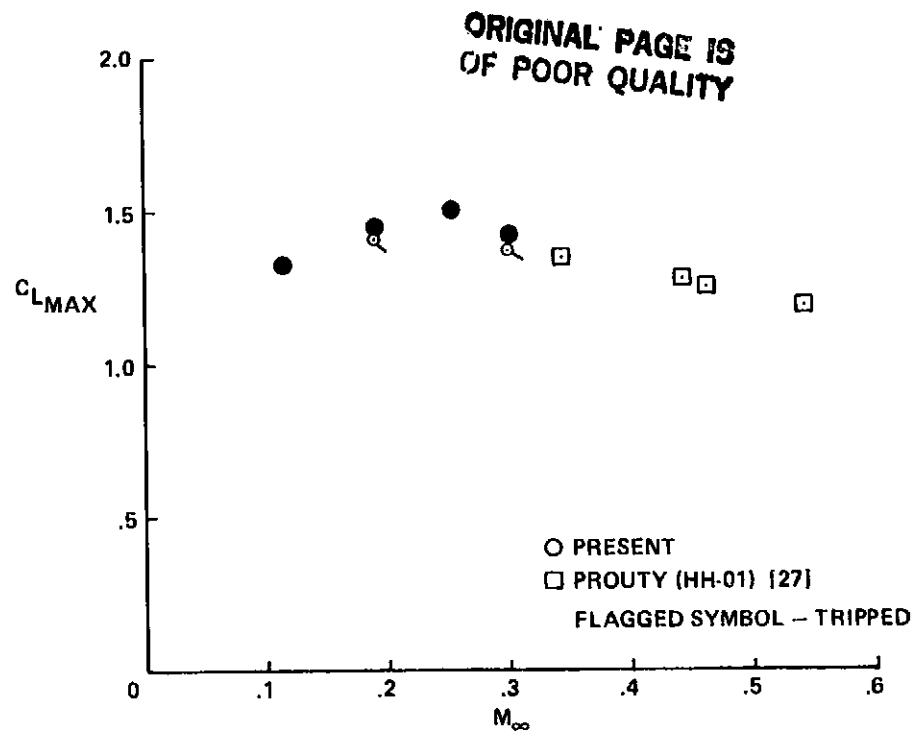


Figure 28.- Comparison of maximum static lift on the Hughes HH-02 airfoil.

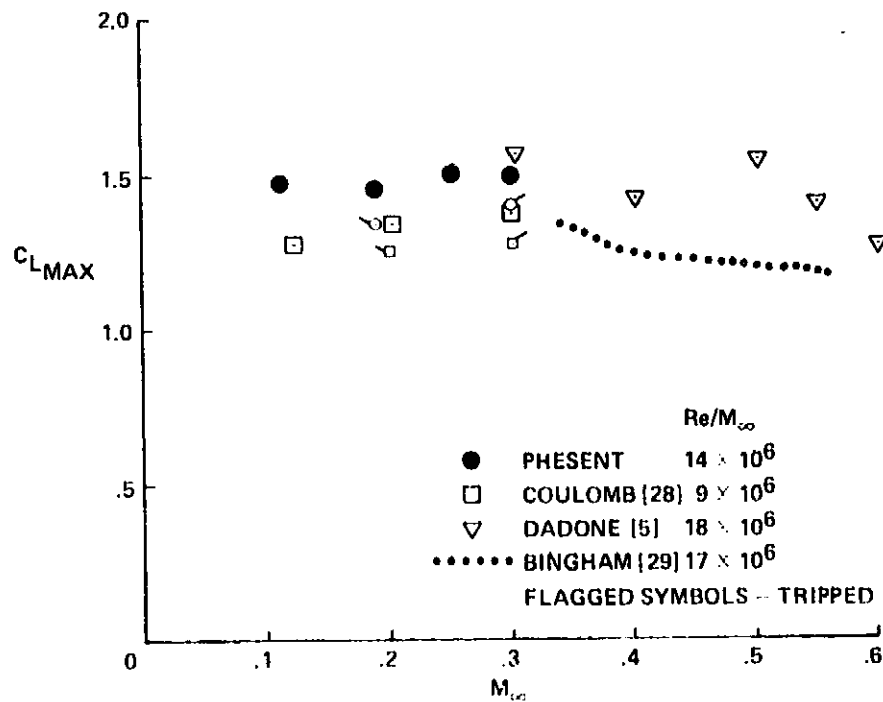


Figure 29.- Comparison of maximum static lift on the Vertol VR-7 airfoil.

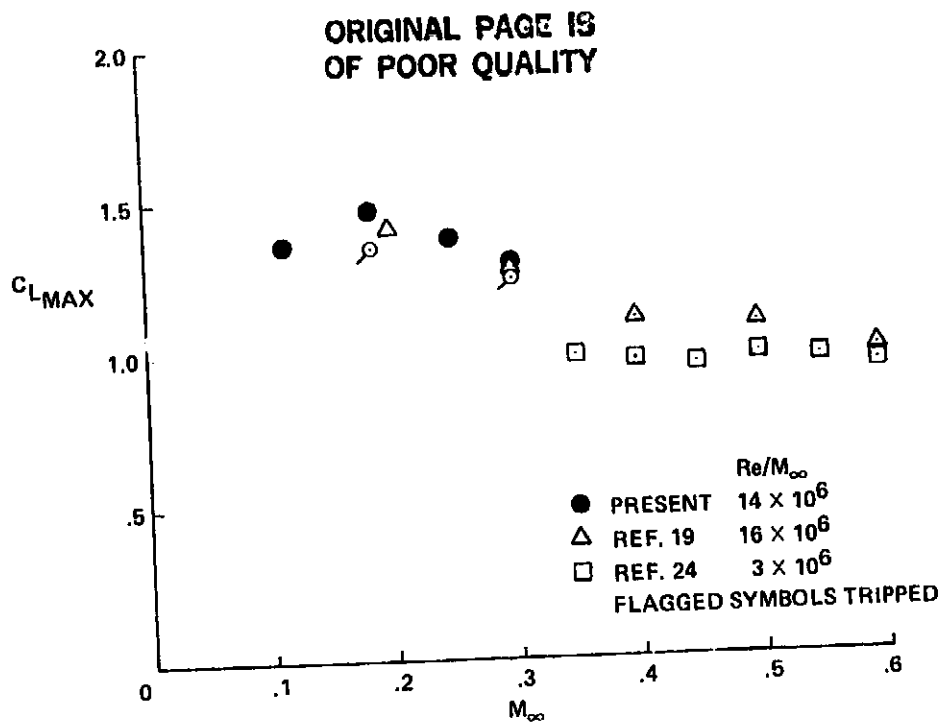


Figure 30.- Comparison of maximum static lift on the NLR-1 airfoil.

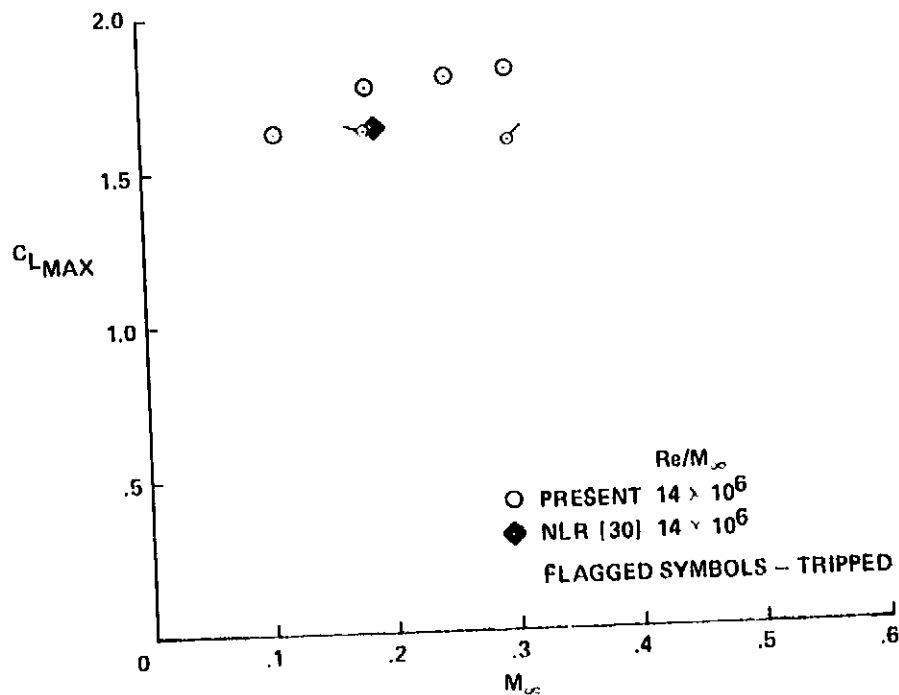


Figure 31.- Comparison of maximum static lift on the NLR-7301 airfoil.

ORIGINAL PAGE IS
OF POOR QUALITY

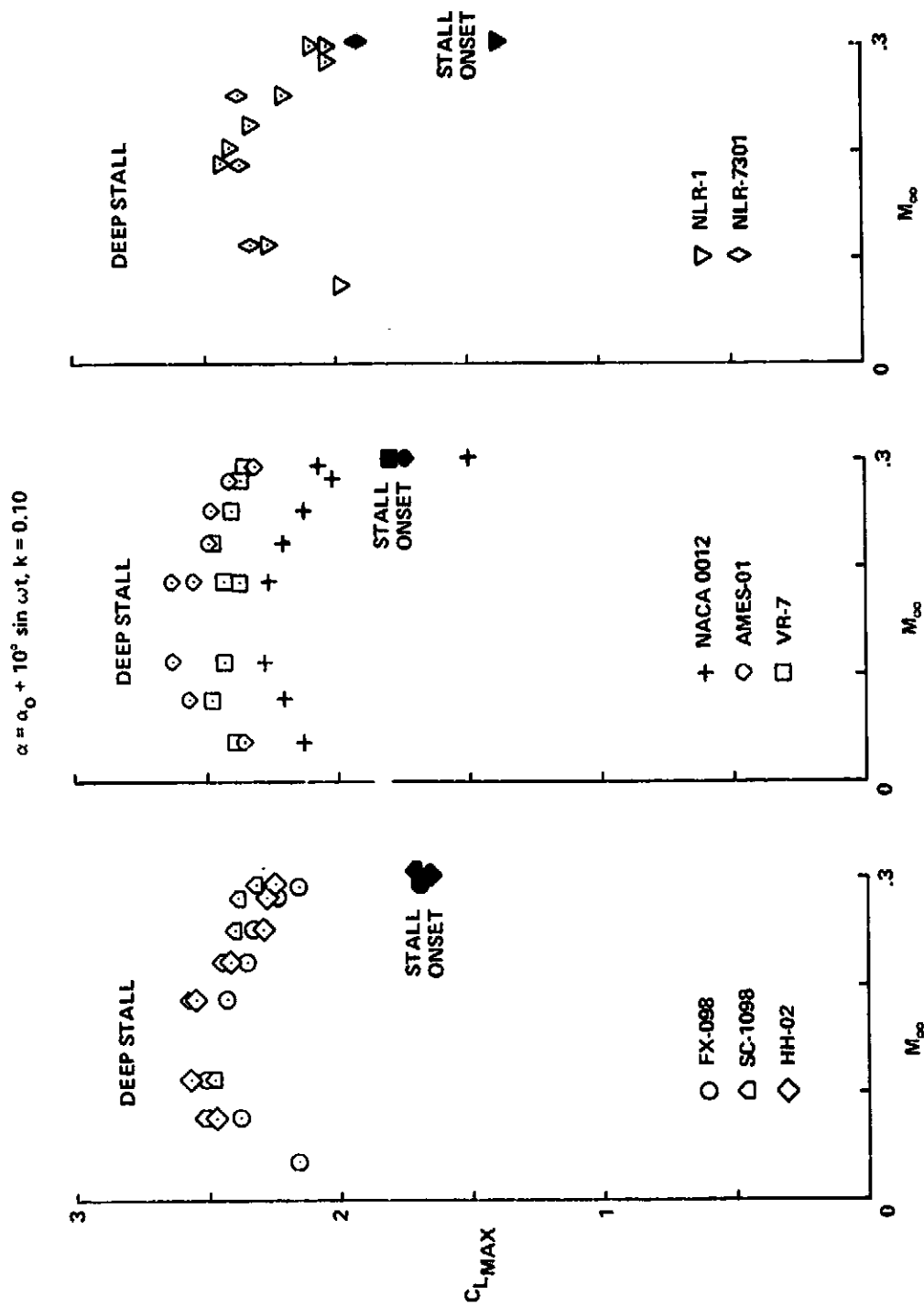


Figure 32.- Maximum unsteady lift on the eight airfoils: solid symbols = stall onset;
open symbols = deep stall.

ORIGINAL PAGE IS
OF POOR QUALITY

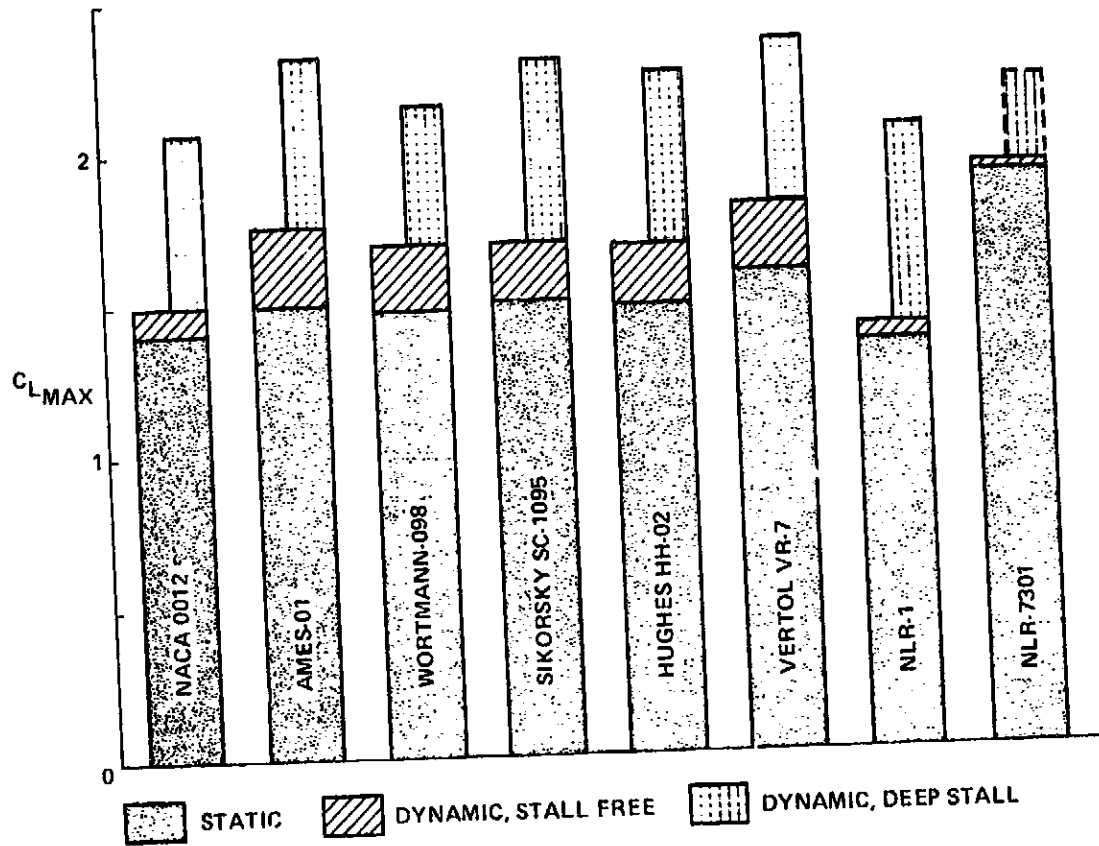


Figure 33.- Comparison of maximum lift on the eight airfoils at $M_\infty = 0.30$.

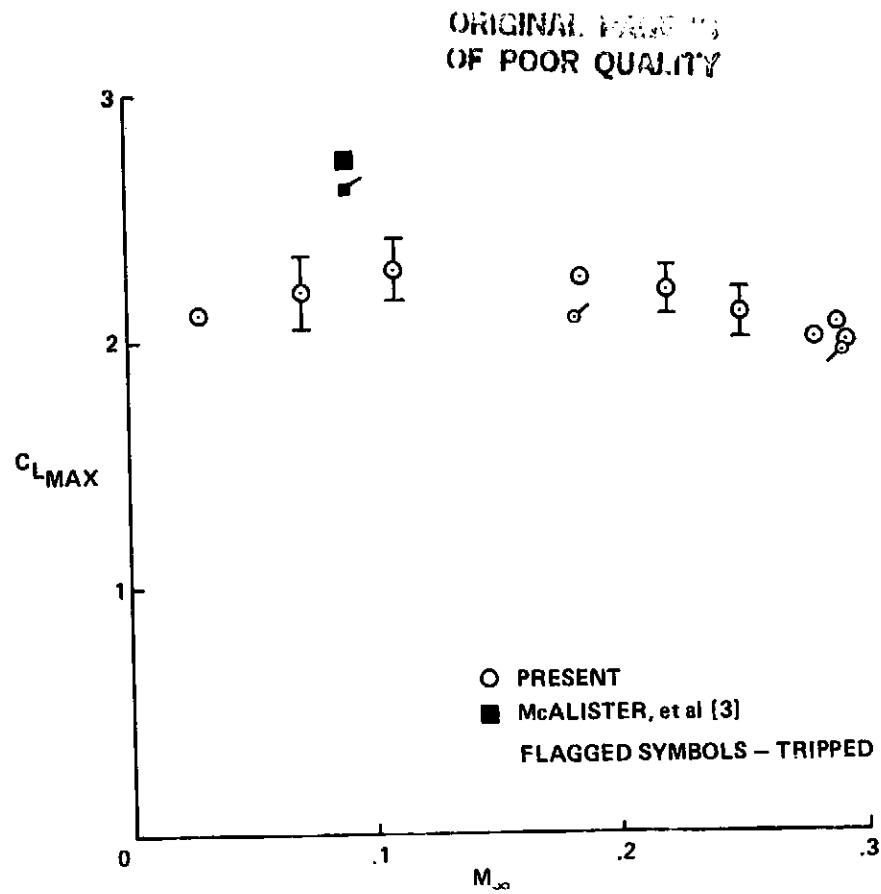


Figure 34.- Comparison of maximum lift on the NACA 0012 airfoil under deep-dynamic-stall conditions: $\alpha = 15^\circ + 10^\circ \sin \omega t$, $k = 0.10$.

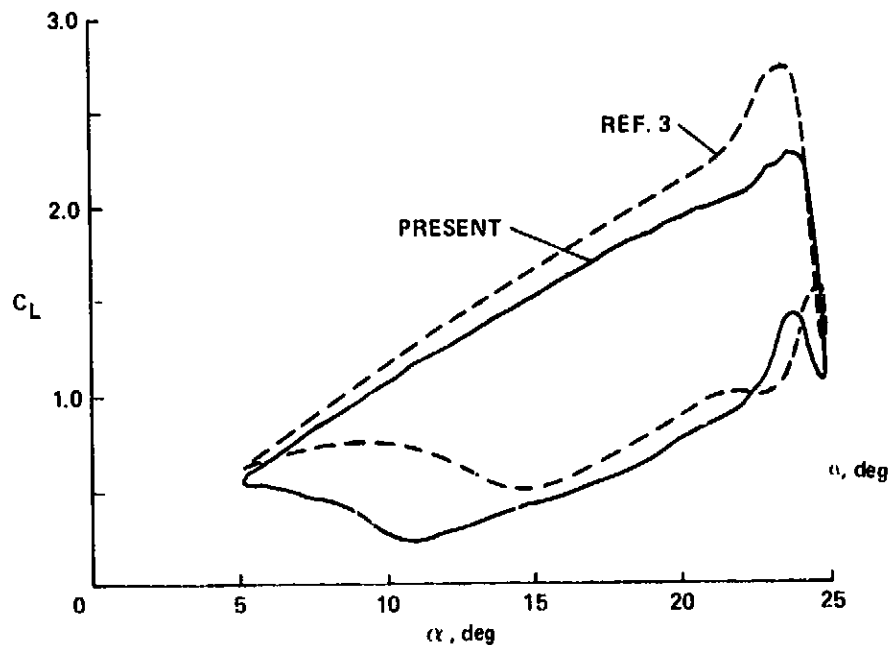


Figure 35.- Comparison of the lift hysteresis on the NACA 0012 airfoil:
 $M_{\infty} = 0.1$, $\alpha = 15^\circ + 10^\circ \sin \omega t$, $k = 0.10$.

ORIGINAL COPY
OF POOR QUALITY

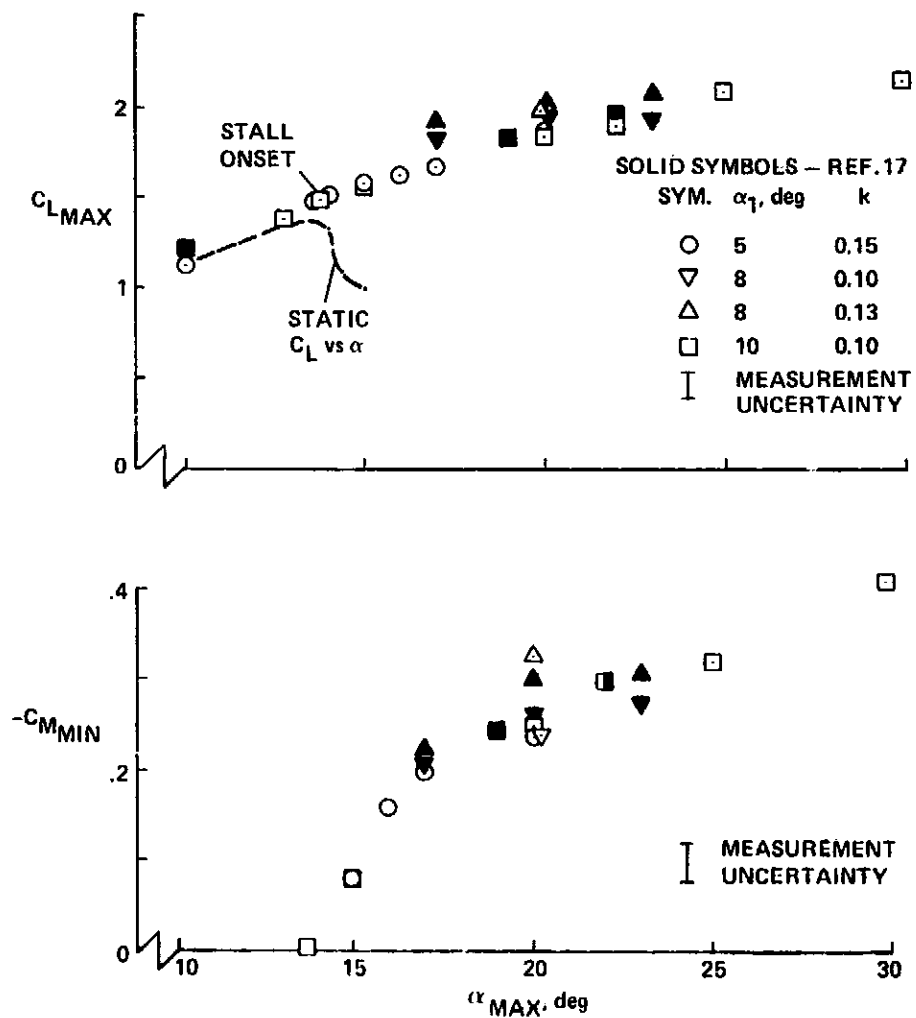


Figure 36.- Comparison of maximum airloads on the NACA 0012 airfoil at $M_{\infty} = 0.30$ and $\alpha_1 k^2 \approx \text{constant}$.

ORIGINAL PAGE IS
OF POOR QUALITY

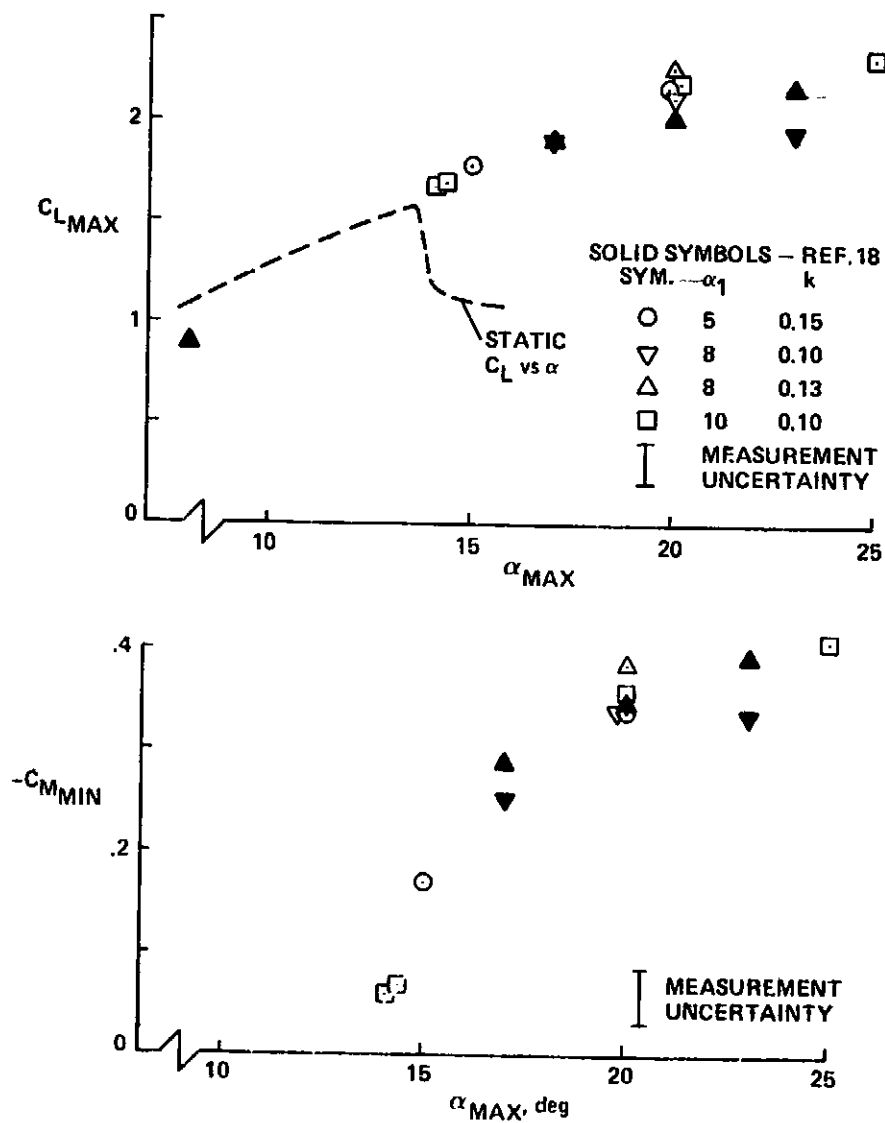


Figure 37.- Comparison of maximum airloads on the Sikorsky SC-1095 airfoil at $M_\infty = 0.30$ and $\alpha_1 k^2 \cong \text{constant}$.

ORIGINAL PAGE IS
OF POOR QUALITY.

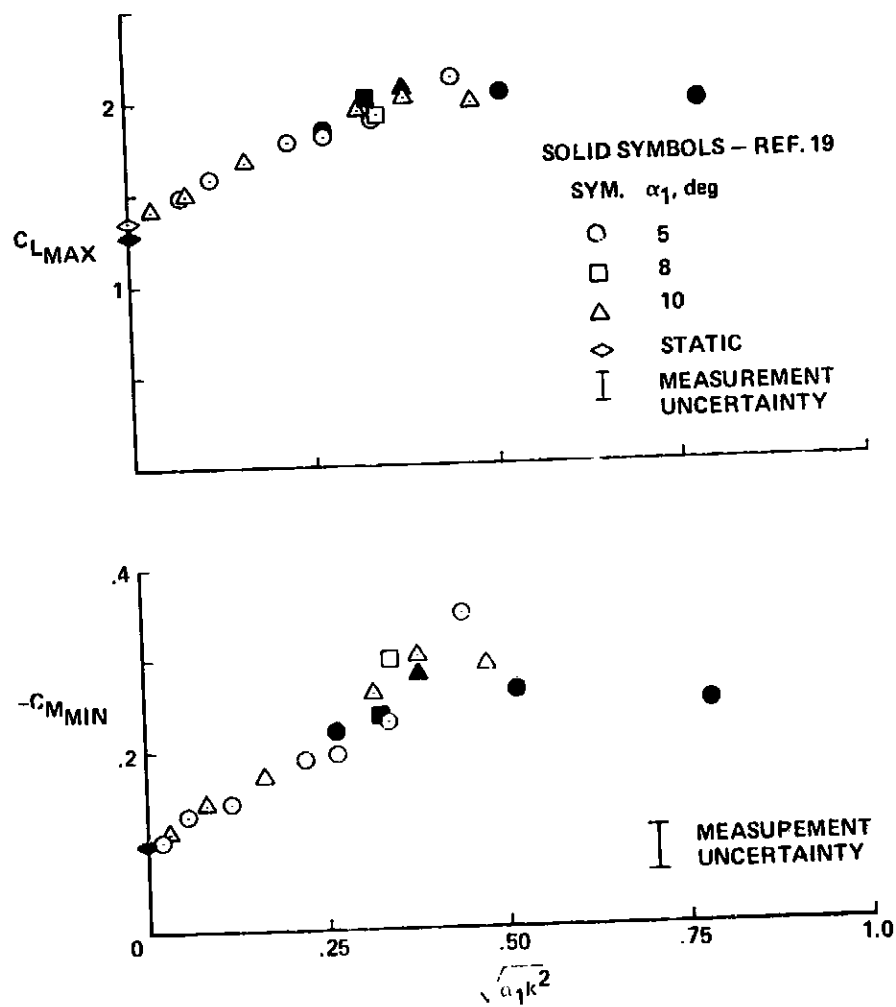


Figure 38.- Comparison of maximum airloads on the NLR-1 airfoil at $M_{\infty} = 0.3$ and $\alpha_{max} = 20^\circ$.